CHARACTERIZATION OF THE NEURAL MECHANISMS SUPPORTING THE IMPLEMENTATION OF COGNITIVE CONTROL IN HUMAN DECISION MAKING

Thesis by
Shabnam Hakimi

In Partial Fulfillment of the Requirements
for the Degree of
Doctor of Philosophy

CALIFORNIA INSTITUTE OF TECHNOLOGY
Pasadena, California
2014
(Defended 14 August 2013)

ACKNOWLEDGEMENTS

During my time at Caltech I have been the lucky recipient of a great deal of kindness and support. John O'Doherty gave me a home, and for his time, expertise, and understanding I am inexpressibly grateful. I am also lucky to have had the mentorship of Ralph Adolphs, who has been a constant source of sage advice. (The first piece of advice Ralph gave me was at S*f*N in 2007. Rather than approach him to introduce myself, I cowered behind a poster for twenty minutes, totally awestruck. When I finally got up the courage to be late to our appointment, he immediately put me in my place, telling me that I was being ridiculous.)

I must also thank the other members of my committee, Colin Camerer, Pietro Perona, and Shin Shimojo, for their advice, support, and availability. I must also thank Associate Dean of Graduate Studies Felicia Hunt, without whom I would not have made it through graduate school. Thank you, Felicia, for your incredible kindness and for believing in me when I did not.

I would not have survived without my Caltech family, who helped keep me excited about science while gifting me with laughs along the way. Many thanks to my officemates – Alice Lin, Vanessa Janowski, and Cendri Hutcherson – who made living in the lab worthwhile. More thanks to Damian Stanley, whose encouragement and playlist crafting skills helped me to smile when neither of us wanted to. Thank you to Catherine Holcomb for being dedicated as both collaborator and friend. And boundless gratitude to my patient collaborator Todd Hare, who kindly indulged my many questions as we tried to make sense of experiments that didn't go as planned… Science!

I want to thank Cendri once more. Apart from always being enormously generous with her time, she has often been the one who has kept me connected to the things I love about science. Our conversations, even when focused on the most complex, seemingly unsolvable issues, have

motivated me to work smarter, harder. I am fortunate to know her as a scientist, collaborator, and friend.

To my family and friends: thank you for understanding when weeks passed without a phone call, and for offering kindness and support when I did finally pick up the phone. To my parents: I promise to call and visit more now that this thesis is complete. My mother and father have always been my most ardent supporters, and this Ph.D. belongs as much to them as it does to me.

Last, but certainly not least, I must acknowledge my partner in all things, Kyle Woodward. He has enjoyed the dubious honor of being my on-demand math tutor and code debugger. Without his love, unwavering support, and expert singing, this thesis would not be.

ABSTRACT

Humans are particularly adept at modifying their behavior in accordance with changing environmental demands. Through various mechanisms of cognitive control, individuals are able to tailor actions to fit complex short- and long-term goals. The research described in this thesis uses functional magnetic resonance imaging to characterize the neural correlates of cognitive control at two levels of complexity: response inhibition and self-control in intertemporal choice. First, we examined changes in neural response associated with increased experience and skill in response inhibition; successful response inhibition was associated with decreased neural response over time in the right ventrolateral prefrontal cortex, a region widely implicated in cognitive control, providing evidence for increased neural efficiency with learned automaticity. We also examined a more abstract form of cognitive control using intertemporal choice. In two experiments, we identified putative neural substrates for individual differences in temporal discounting, or the tendency to prefer immediate to delayed rewards. Using dynamic causal models, we characterized the neural circuit between ventromedial prefrontal cortex, an area involved in valuation, and dorsolateral prefrontal cortex, a region implicated in self-control in intertemporal and dietary choice, and found that connectivity from dorsolateral prefrontal cortex to ventromedial prefrontal cortex increases at the time of choice, particularly when delayed rewards are chosen. Moreover, estimates of the strength of connectivity predicted out-of-sample individual rates of temporal discounting, suggesting a neurocomputational mechanism for variation in the ability to delay gratification. Next, we interrogated the hypothesis that individual differences in temporal discounting are in part explained by the ability to imagine future reward outcomes. Using a novel paradigm, we imaged neural response during the imagining of primary rewards, and identified negative correlations between activity in regions associated the processing of both real and imagined rewards (lateral orbitofrontal cortex and ventromedial prefrontal cortex, respectively) and

the individual temporal discounting parameters estimated in the previous experiment. These data suggest that individuals who are better able to represent reward outcomes neurally are less susceptible to temporal discounting. Together, these findings provide further insight into role of the prefrontal cortex in implementing cognitive control, and propose neurobiological substrates for individual variation.

TABLE OF CONTENTS

LIST OF FIGURES AND TABLES

NOMENCLATURE

AC-PC line	*anterior commissure - posterior commissure line*
BA	*Brodmann area*
BOLD signal	*blood oxygen level-dependent signal*
dlPFC	*dorsolateral prefrontal cortex*
EPI	*echoplanar imaging*
fMRI	*functional magnetic resonance imaging*
GLM	*general linear model*
ITC	*intertemporal choice*
OFC	*orbitofrontal cortex*
PFC	*prefrontal cortex*
ROI	*region of interest*
vlPFC	*ventrolateral prefrontal cortex*
vmPFC	*ventromedial prefrontal cortex*
voxel	*3-D pixel*

C h a p t e r 1

INTRODUCTION

"Like the entomologist in pursuit of brightly coloured butterflies, my attention hunted, in the flower garden of the gray matter, cells with delicate and elegant forms, the mysterious butterflies of the soul, the beating of whose wings may some day – who knows? – clarify the secret of mental life."

– Santiago Ramón y Cajal[1]

Preamble

Like many before me, I find myself obsessed by a single cell: the neuron. How is it that the entirety of the human experience can be defined by a network of tiny cells and their hundreds of trillions of connections to one another? Human behaviors are immensely complex, and each individual is exceedingly different. Evolution has imagined the brain as a structure stereotyped yet plastic, incredibly robust to the unique path navigated by an individual through the series of decisions that make up her life.

When Nobel laureate Ramón y Cajal first began to consider the nervous system in the late nineteenth century, neuroscience was energized by a fierce debate over the nature of these cells, with some contending that they were part of a continuous mesh while others maintained that the cells were discrete units. Cajal's exquisite drawings of the cells he imaged bolstered the argument of the latter camp, cementing the definition of the neuron as the fundamental unit of the nervous system. At the same time, a debate over the nature of the psyche raged in philosophy and, by extension, psychology. Functionalism, a theory espoused by William James, author of the seminal text *Principles of Psychology*, was in the process of supplanting the introspective psychology that had dominated previous theories of the mind. At its core, functionalism posited that mental states could be defined by their functional roles – their causal interactions with other components of the system, such as sensory inputs, other mental states, and behavioral output. In many ways, cognitive

neuroscience is the natural convergence of these theories. Cognitive neuroscientists look to the brain as the mediator between mind and behavior, localizing psychological processes to brain regions and neural networks.

Cognitive neuroscience witnessed a revolution[2] with Ogawa and colleagues' discovery of the BOLD signal in 1990[3]; inquisitive scientists were provided unparalleled access into the world of the behaving mind. Changes in the BOLD response are now imaged as individuals engage in actions that mirror the complexity of their everyday decisions. Neuroimaging studies of cognitive control have provided critical insight into the neurobiological mechanisms of some of the most pervasive actions in human life. Cognitive control processes – ranging from suppression of a motor action in response to an environmental change to self-regulation that sustains long-term wellness goals – allow individuals to do more than just respond reflexively to their immediate environment, enabling more complex behaviors directed by often-distant future goals[4]. Studying behaviors so fundamental to the human condition brings us ever closer to understanding how and why we do the things we do, questions that have long driven philosophical thought. Ramón y Cajal could hardly have imagined how close we could be to glimpsing those "mysterious butterflies of the soul."

Inhibition and cognitive control

The ability to navigate a changing world requires the ability to detect such changes and adjust behavior accordingly. At the same time, the environment can remain unchanged for long periods of time, rendering active behavior adjustment unnecessarily costly and facilitating more automatic and efficient learned responses. Response inhibition, through suppression of inappropriate behaviors, enables optimal behaviors in this kind of unpredictable setting, and is a crucial component of cognitive control.

Research on the cognitive neuroscience of inhibition has been marked by disagreement over the meaning of the term. In neuroscience, the contextual meaning of inhibition is clear at multiple levels of analysis, as it is observable either in neurophysiological measures or in behavior. In psychology, inhibition is less clearly defined, and has been used to describe components of myriad processes[5]. Unsurprisingly, the marriage of neuroscience and psychology of inhibition lacks this kind of clarity, and studies of the neural underpinnings of inhibition and, more generally, cognitive control encompass many potentially distinct processes, spanning motor inhibition, attentional inhibition of distracting stimuli, emotion regulation, and self-control[5]. Despite this lack of clear operationalization, all these processes seem to involve a single substrate: a cognitive signal issued in response to an environmental change that has rendered current behavior sub-optimal. It is this constituent process that will be examined in this thesis.

Because of its unique pattern of connectivity, which facilitates both internal links and external connections to other cortical regions and subcortical structures[6-9], the PFC is well positioned to issue such a signal[4,10,11]. The vlPFC has been consistently implicated in response inhibition by lesion[12] and functional neuroimaging[5,13-15] studies, and is thought to support response inhibition through maintenance of stimulus-response associations[16,17]. More dorsal regions of lateral PFC have also been implicated in the maintenance of information relevant to response selection[18-20] and response inhibition[21-23]. Furthermore, apart from representing value (e.g., [24]), the vmPFC/OFC may mediate the effects of emotion on response selection[25-27].

Activations in these prefrontocortical regions are reported by many neuroimaging studies of response inhibition[28]. The go/no-go task[29], which measures ability to withhold a motor response, is perhaps the most prominent paradigm in this literature. Also common is the stop signal task, which measures a slightly different construct than the go/no-go paradigm: instead of merely examining

what is needed to withhold an action, the stop-signal task assays the ability to abort a prepared action that is no longer required[30,31], and poor performance in this task is thought to reflect impulsivity[32]. Recent work[33] suggests that the action cancelation needed to perform in the stop signal task is a late-emerging subcomponent of response inhibition. Importantly, while action withholding (as in go/no-go) begins earlier, both processes seem to engage the same network of fronto-parietal-pre-motor regions.

Sebastian and colleagues' findings[33] align well with an influential neurocomputational model of action selection that maps onto the direct, indirect, and hyperdirect pathways from the cortex to the basal ganglia. In this model, the direct pathway facilitates the implementation of the appropriate action, while the indirect pathway suppresses any actions that are inappropriate given the current state; the hyperdirect pathway functions as a global inhibitor of action[34-36]. This so-called basal ganglia go/no-go (BG-GNG) model[37] accounts for the balance of signaling between the direct (go), indirect (no-go), and hyperdirect (global no-go) pathways, providing a neuroanatomical[38] and neurochemical (i.e., dopaminergic)[39] basis for response inhibition. This model, which has been shown to provide a good fit for experimental data[40-42], has also been used to examine aberrant response inhibition in the underlying cortico-basal ganglia-thalamo-cortical circuitry in disorders including Parkinson's disease, Tourette's syndrome, attention deficit/hyperactivity disorder, drug addiction, and schizophrenia[43].

ITC as a model for self-control

Studies of self-control have commonly defined self-control as a preference for larger, delayed relative to smaller, immediate rewards[44-53]. The tasks implemented in this paradigm involve ITCs, or decisions whose outcomes occur at some point in the future. Such decisions are ubiquitous outside the laboratory, and have important consequences for individuals as well as policy-making bodies[54-57].

Temporal discounting is antithetical to this definition of self-control, and describes the opposite tendency to value immediate gains over future gains[58,59]; this phenomenon has been observed in a variety of species, including pigeons[60-62], rats[60,63], macaques[64-66], and humans[67-69]. While multiple frameworks for ITC have been proposed[70], two models are generally used to describe these behaviors. The first, which is based on the standard discounted utility model in economics[71], assumes a constant rate of discounting over time. The second assumes a hyperbolic relationship between value and delay (to the reward)[72] – meaning that discounting is steeper for values nearer in the future – and tends to provide a better fit for observed behavior[54,73].

As such, the hyperbolic discounting function is commonly used to model human choice data in neuroimaging studies. The work of Kable and Glimcher (2007) has been particularly influential, and provided the first fMRI evidence of the neural correlates of subjective desirability for choice preferences in intertemporal decision making[74]; they demonstrated that activity in ventral striatum, medial PFC – a region critical for valuation[75] – and posterior cingulate track subjective value. Others have replicated and extended this work using a variety of methodological parameters[70]. Despite these advances, however, the neural circuitry mediating ITC remains poorly understood. Consistent with other theories of cognitive control (e.g., [10]), the fronto-cortico-striatal circuitry is thought to be involved[76-81]. Human[82] and non-human primate[66,83,84] research has specifically implicated the dlPFC, which is thought to maintain context and goal information over time[85-87] and has been shown to be important for self-control in dietary choice[88,89].

Individual differences in ITC

Individuals vary widely in their ability to delay gratification[49,59,90], and temporal discounting is thought to be another key correlate of trait impulsivity[91-93]. Because temporal discounting behavior is similar to the clinical phenomenology seen in disorders of impulse control, it has further been used to study impairment in conditions including substance abuse, pathological gambling, and

attention deficit/hyperactivity disorder, and may serve as an important target for therapeutic intervention[28,94-97]. Understanding the continuum of ITC behavior and its underlying neurobiology can therefore have significant implications for the treatment of psychological disorders.

Theories addressing the psychological basis of temporal discounting have often dealt with varying conceptions of the self. Some[44,52,53,72] have proposed that ITC can be thought of as "intrapersonal bargaining among multiple 'selves'"[98]. In this model, an individual evaluates how outcomes will affect future selves relative to the present self; the distance between an individual and his or her future self – or, rather, the extent to which the future self is viewed as a distinct entity – is reflected in shortsighted decision making[99,100]. This theory is consistent with the idea that humans are particularly adept at "mental time travel"[101], and that this ability to represent the future has played a direct role in human success as a species[101,102]. Specifically, the representation of future outcomes at the time of decision facilitates goal-directed planning that can help overcome a tendency for impulsive, myopic decision making shaped only by the demands of the moment. Indeed, vividness of representation of the future self is linked to mitigated temporal discounting[55,103,104] and reduced delinquency[105].

Recent neuroimaging research has begun to characterize the role of self-referential processing and "mental time travel" on the neural correlates of temporal discounting. In 2011, Mitchell and others found evidence of decreased self-referential processing in vmPFC when short-sighted monetary decisions were made[98]. Two other recent studies have focused on the role of episodic imagery on discounting behavior. Peters and Büchel (2010) found that when ITCs were associated with cues to generate imagery, temporal discounting was reduced and neural response was enhanced in a network of regions implicated in episodic thinking, including medial PFC. Moreover, the strength of functional coupling between anterior cingulate cortex and subcortical regions predicted the extent

to which temporal discounting was attenuated[77]. Benoit and colleagues (2011) also cued specific episodic imagery during an ITC task and demonstrated strong, imagery-related medial PFC response in association with reduced temporal discounting[106]. A separate line of research has implicated the vmPFC in envisioning positive future events[107], suggesting that emotional salience affects the vividness of imagery.

Contributions of this thesis

Increased experience with environmental stimuli facilitates the development of automaticity, leading to enhanced efficiency in both behavioral and neural responding. While the neural correlates of learning for frequent stimulus-response associations over time has been well described[26], learning for infrequent stimuli – particularly if their appearance requires cognitive control – is less well understood. The work described in Chapter 2 examines whether learned automaticity in cognitive control behavior for such infrequent events is associated with concomitant changes in neural response.

In Chapter 3, we interrogate the neurobiology of a more abstract form of cognitive control using an ITC task. We combine research on the neural correlates of self-control in dietary choice[88,89] and ITC (especially [82]) to test a neurocomputational model of self-control that posits that control is implemented through modulation of vmPFC by dlPFC. We apply this model further, examining the relationship between the strength of these connections and individual temporal discounting behavior. We examine another potential source of individual differences in ITC in Chapter 4, testing the hypothesis that behavioral variation in ITC is related to the ability to imagine and neurally represent rewards.

These experiments provide new insight into the neuroscience of cognitive control, advancing understanding of the function of PFC, especially the dorsal and ventral aspects of lateral PFC, in

driving goal-directed behavior. Moreover, the research presented in this thesis underscores the importance of studying the neural basis of individual variation, demonstrating the inferential power of individual differences-based approaches.

Chapter 2

NEURAL CHANGES ASSOCIATED WITH LEARNED COGNITIVE CONTROL*

Learned automaticity allows organisms to take advantage of environmental stability, enabling the efficient deployment of well-learned responses to common stimuli. Nonetheless, organisms must be prepared for the occurrence of infrequent events, since optimal outcomes in new conditions may require the deployment cognitive control processes to affect a change in behavior. A growing literature suggests that cognitive control can also benefit from experience-dependent automaticity, yet the neural correlates supporting this effect remain unclear. We used fMRI to examine the neural correlates of learning associated with enhanced cognitive control ability over time in a speeded response inhibition task with motivationally salient incentives for performance, where trials requiring inhibition were relatively infrequent. We found both behavioral and neural evidence of automaticity in frequent trials, replicating and extending previous work. Moreover, our data show that performance improvements in infrequent trials requiring control are supported by concomitant neural changes, with the right vlPFC, a region thought to be necessary for response inhibition, demonstrating linear decreases in BOLD response over time. These findings are consistent with the theory that learning of promotes both behavioral and neural efficiency in both frequent and infrequent environmental conditions.

Introduction

A dynamic environment necessitates the ability to adapt one's behavior to the demands of the situation. More often than not, however, the environment is relatively unchanging. During these stable periods, automaticity emerges; such automaticity may be adaptive, ensuring that responses to frequently occurring events are deployed efficiently and effectively[108,109]. Nonetheless, one must

* Work done in collaboration with Antonio Rangel.

still be prepared to act appropriately should a rare, unexpected event take place. For example, suppose you have sleepily entered a hotel shower and turned the right knob on the faucet only to find that scalding hot water is released. Even though the vast majority of faucet knobs map cold water to the right – including the one you're used to at home – you had still better be prepared to jump back to avoid a burn. Learning when to be prepared for such a behavioral change is equally important. The challenge, therefore, is to learn the appropriate balance between the efficiency of learned automaticity and vigilance, so that automatic responses can be inhibited should goals change.

Effective response inhibition is critical to maintaining this balance. Functional neuroimaging studies have often utilized two paradigms, go/no-go and stop signal, to examine how the human brain accomplishes this cognitive process. The go/no-go task[29] presents participants with a series of stimuli, most of which are 'go' cues, indicating that a response should be made as quickly as possible. Interspersed between 'go' stimuli are the less-frequent 'no-go' cues, which indicate that a response should be withheld. The number of errors made of on 'no-go' trials (i.e., 'go'ing when no response should have been made) is the index of inhibitory control. The stop signal paradigm[110] also creates a speeded environment for responding to a sequence of stimuli; in this task, however, an additional stimulus is presented after some short – and often variable – delay on a small fraction of trials. This stop signal indicates that a response should be withheld on the trial as well as the duration of the stopping process is the measure of inhibitory control for the task. While the inhibitory processes (i.e., responses to successful 'no-go' and 'stop' trials) examined in the two paradigms are not fully equivalent[111-113], they do elicit similar neural responses, particularly in right vlPFC (e.g., [21,114-122]). Other related paradigms have also provided insight into the neural architecture required to inhibit a response process that has already begun. Task switching paradigms[123,124], which measure the "cost" of switching from one task to another by indexing the

additional time required[125-127], and reversal learning tasks, which require the abandonment of a well-learned response for a new one when stimulus-response contingencies reverse[98,128,129], have also suggested a role for the vlPFC. Other regions implicated more generally in these tasks include the anterior cingulate cortex[130-134] (ACC), vmPFC/OFC[135,136], (medial) pre-supplementary motor area[122,137-139] (preSMA), inferior parietal cortex[15,130], posterior parietal cortex[134,140], insula[116,141,142], striatum[98,138,142-144], and subthalamic nucleus/ventral tegmental area[145,146] (STN/VTA).

One important characteristic of such paradigms is the relative infrequency of events that require inhibition. Indeed, vlPFC[147-150], OFC[151,152], and striatum[153,154] are also implicated in the detection of infrequent, yet salient targets. What remains unclear, however, is how the response in these regions and in this larger network for behavioral control changes with exposure to these infrequent events over time. Does automaticity develop in these regions as practice with cognitive control increases? Recent work from Chiu and colleagues (2012) has shown that practice with 'no-go' stimuli can lead to automaticity in suppressing the 'go' response (as measured by motor evoked potentials) for those events. Interestingly, this automatic inhibition effect "wears off" as performance asymptotes, ostensibly because less inhibitory control is needed, since an incorrect motor response is less likely to be triggered. The authors suggest that automatic response inhibition is facilitated by the formation and subsequent retrieval of stimulus-stop associations[155]. Such automatic activation of an inhibitory control network would be consistent, for example, with evidence showing that right vlPFC activity can be elicited by stimuli that were previously associated with stopping[156]. Nonetheless, the link between automaticity in these regions and learned success in response inhibition remains poorly defined.

Here, we introduce a novel paradigm for the study of cognitive control in the face of an emergent automatic response. While undergoing functional neuroimaging, participants learned to rapidly

associate particular motor responses to different visual stimuli; the appearance of relatively infrequent cues signaled a reversal of the appropriate response to a particular visual stimulus. In order to study how learning impacts both automaticity and cognitive control, we examined changes in response to frequent (i.e., most susceptible to automaticity) and infrequent (i.e., requiring control) cues over the course of several hundred trials. We hypothesized that (1) increasing experience with frequent trials will encourage automaticity, as evidenced through improved accuracy in these trials over time; (2) learning (as evidenced by changes over time in response) in frequent trials will engage regions associated with response automaticity, including premotor areas[157,158]; (3) correct responses to infrequent events will require cognitive control and will therefore necessitate the recruitment of brain areas that have been implicated in response inhibition and cognitive control, specifically vlPFC; and (4) in contrast to learning in frequent trials, learning in the context of increased experience with response inhibition in infrequent trials will be associated with changes in vlPFC or other regions involved in cognitive control.

Methods

Participants. 24 healthy, right-handed male individuals (age = 23 ± 4.0 years) completed the study. All participants had normal or corrected-to-normal vision, no history of neurological, psychiatric, or metabolic illness, and were not taking any medications that interfere with the BOLD signal at the time of scanning. The institutional review board at the California Institute of Technology (Pasadena, CA) approved the study.

Task. Upon arriving for the experiment, participants were shown four fractal cues (matched for visual complexity) and their associated behavioral responses (i.e., the association between a particular fractal and a left or right button press). They were allowed to study these relationships for as long as was necessary to feel comfortable with the associations (mean = 49.7 ± 30.9 s). The associations between cues and responses were randomized across participants. After studying the

responses associated with each cue, the participant was told that, most of the time, the fractal would have a white circle at its center (normal contingency, or normal, trials) and they should respond according to the associations they had just seen. Participants were also told that occasionally the fractal cue would have a white triangle at its center instead of the circle (reversed contingency, or reversal, trials). On these trials, participants were instructed to respond to the cue using the *opposite* hand. For example, if the normal response to the fractal (with the circle in the center) was a right thumb button press, a triangle in the center would instead cue a reversal trial and thus, a left thumb button press.

Each trial was initiated by the appearance of one of the four fractals, with either a circle or triangle at its center. Each cue appeared onscreen for 600 ms, and participants were told that any response made outside this time period would be recorded as incorrect. A correct response resulted in a gain of one point, while an incorrect response resulted in the loss of a point. A feedback screen with a duration of 1 s indicated the outcome of the trial. Feedback was immediately followed by a fixation period, during which participants were instructed to attend to a white cross at the center of the screen. The duration of fixation varied between 3 and 7 s (mean 5 s). A single trial is diagrammed in Figure 2.1A and a sample sequence of trials is shown in Figure 2.1C.

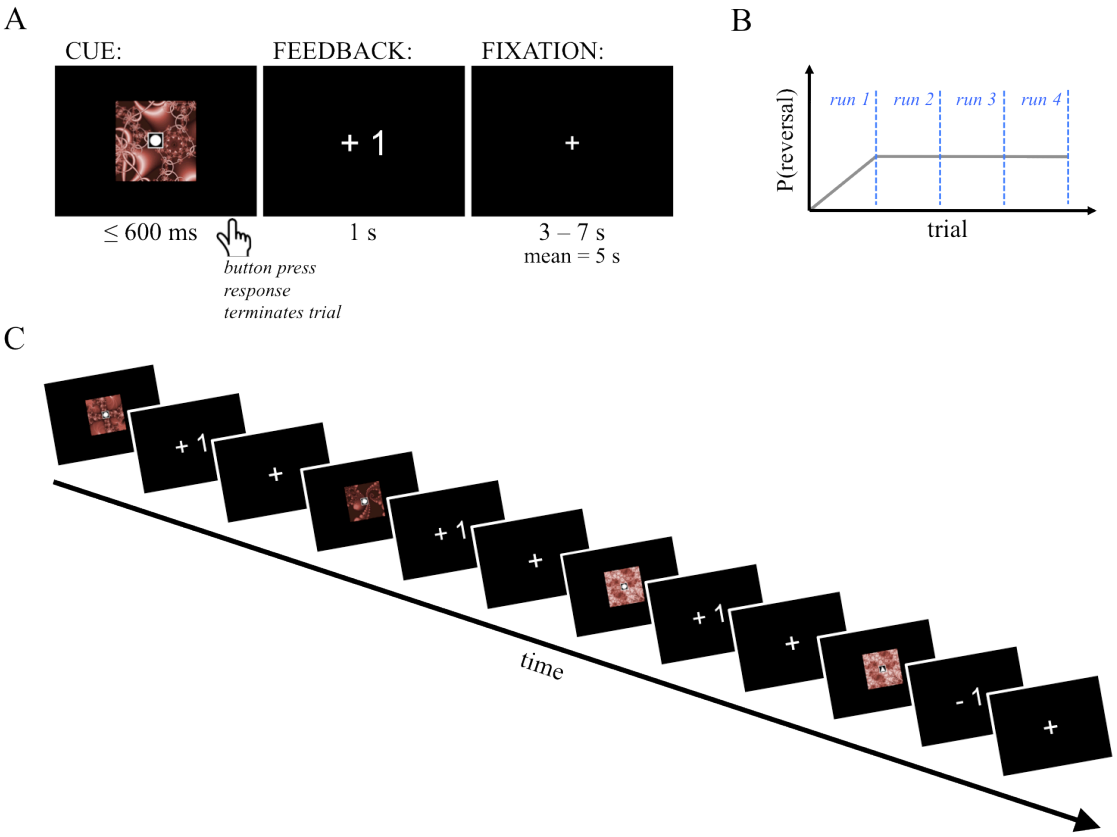

Figure 2.1. Task design. A) Single-trial schematic. B) Graphic depicting temporal evolution of reversal trial probability. C) Sample sequence of events.

The task was divided into four experimental runs, each comprised of 120 trials. Twenty percent of the trials were reversal trials (96 total). In order to solidify automatic responding to the fractal cues, the probability of the reversal event increased linearly over the first 120 trials to reach a stable, uniform probability of 20% over the last 360 trials (see Figure 2.1B). Participants were instructed to respond as quickly and accurately as possible to each trial. Importantly, their payment outcome for the study was directly related to their performance on the task. At the end of the task, the total points earned over all 480 trials were summed and multiplied by a conversion factor of 0.05 to determine an individual's dollar payout. (Complete task instructions are included in Appendix A.)

After finishing the experiment, all participants completed a battery of questionnaires designed to assess the effect of individual differences on the behavioral and neural responses to the task. The results of these analyses will be discussed in a separate manuscript.

Error analysis. Two types of errors are possible on reversal trials: an error of commission, in which the response is consistent with that fractal's associated response in normal contingency trials, or an error of omission, in which the participant failed to enter any response during the allotted time. Because participants rarely made this second type of error, all incorrect trials were binned together for subsequent analysis. Errors on reversal trials, therefore, serve as our index of inhibitory control. Moreover, since there were no behavioral differences in performance by fractal identity (normal contingency performance x fractal identity ANOVA, $p > 0.05$), trials were grouped by condition for all subsequent behavioral and neural analyses. (A subsequent, *post hoc* analysis revealed no significant effect of fractal identity on neural response to either normal contingency or reversal cues.) These and other behavioral analyses were done using the Statistics Toolbox in MATLAB (Version 8.0.0.783, The MathWorks, Inc., Natick, Massachusetts).

Imaging data acquisition. Whole-brain functional imaging data were collected using a Siemens (Erlangen, Germany) 3.0 Tesla Trio MRI scanner. Using an eight-channel, phased array head coil, we collected gradient echo, T2*-weighted EPI images with BOLD contrast. In order to optimize BOLD sensitivity, we used a tilted acquisition in an orientation 30^{o} oblique to the anterior-posterior commissure line[159]. The imaging parameters were as follows: TR = 2750 ms; TE = 30 ms; flip angle = 80^{o}; FOV = 192 mm; in-plane resolution = 3 mm x 3 mm; and 44 3 mm slices with interleaved, bottom-up acquisition. Each of the four experimental runs corresponded to a scanning session with 304 EPI volumes. The first four volumes of each run were discarded to allow for sufficient time for the magnetic field to achieve steady-state magnetization. High-resolution, whole-brain, T1-

weighted structural images (TR = 1500 ms; TE = 3.05 ms; flip angle = 10^{o}; voxel resolution = 1 mm^3; single-shot, ascending acquisition) were also collected for each of the participants. These images were coregistered with the their respective EPI images to assist with the anatomical localization of the functional activations.

fMRI data preprocessing and statistical analysis. Imaging data analysis was performed using SPM5 (Wellcome Department of Imaging Neuroscience, Institute of Neurology, London, UK). Preprocessing of functional data consisted of correction for slice-time acquisition, motion correction and realignment to the mean image, spatial normalization to the Montreal Neurological Institute EPI template, and spatial smoothing using a Gaussian kernel with a full-width-half-maximum at 8 mm. Intensity filtering and high-pass temporal filtering (using a filter width of 128 s) were also applied to the data. All images were visualized using MRIcron software (http://www.sph.sc.edu/comd/rorden/mricron/).

We estimated two GLMs of the BOLD responses with first-order autoregression and convolution of regressors of interest to the canonical form of the hemodynamic response. Model 1 included two regressors of interest to examine brain regions generally associated with the processing of the two trial types: (1) an indicator function for the onset of all normal contingency trials and (2) an indicator for the onset of all reversal trials; all events were of duration 0 s. (An alternate GLM using RT for the event duration and as a parametric modulator showed qualitatively the same results as Model 1 and hence the results from this alternative model are not presented in more detail.) Four session constants and six motion parameters were included as regressors of no interest. For each participant, we computed the following contrasts at the first level: all normal contingency trials > all reversal trials and its reverse, and, to examine possible learning, a linear increase over the four sessions for both normal and reversal trials (separately) as well as the concomitant linear decrease.

To test for linear effects over time, we specified first-level contrasts separately for both normal contingency and reversal trials of the form [-0.75 -0.25 0.25 0.75] to test for linear increases in response and [0.75 0.25 -0.25 -0.75] to test for linear decreases in response over the four runs.

In order to address directly effects of performance on neural response for the two trial types, we estimated Model 2 with the following regressors of interest: (1) an indicator function for normal contingency trials where the correct response was entered (NormalCorrect, or NC), (2) an indicator for incorrect normal contingency trials (NormalIncorrect, or NI), (3) an indicator for correct reversal trials (ReversalCorrect, or RC), and (4) an indicator for incorrect reversal trials (ReversalIncorrect, or RI). All events were modeled with a duration of 0 s. Note that, as in the behavioral analysis, incorrect reversal trials were primarily errors of commission. The following first-level contrasts were computed for each individual: [NC - NI], [NI - NC], [RC-RI], [RI - RC], [NC - NI - RC + RI], [RC - RI - NC + NI], and [NC - NI + RC - RI]. (The final contrast identifies regions involved in processing correct responses relative to incorrect ones, while controlling for incorrect reversal responses, which were hypothesized to be similar to correct normal contingency responses.)

For each model, we evaluated effects on the group level by computing one-sample t-tests on the single-subject contrasts. We corrected for multiple comparisons at the whole-brain cluster level (denoted subsequently by WBC), using an individual voxel threshold of $p < 0.001$. (The minimum cluster extent was determined by the model and specific contrast; these values are noted in the table legends.) For completeness, we also report any clusters with extent greater than 10 voxels. Furthermore, we used small volume correction (SVC) to examine *a priori* areas of interest. Specifically, we used WFU PickAtlas software[160] (version 3.04) to create anatomically-defined masks [161] of the left and right vlPFC (Talairach Daemon label: “inferior frontal gyrus”).

Results

Behavioral results. Across all trials, participants responded with significantly greater accuracy on normal contingency trials (mean fraction correct = 0.68 ± 0.12) compared to reversal trials (mean fraction correct = 0.31 ± 0.096; $t_{23} = 12.4$, $p < 0.001$). Incorrect responses in reversal trials were primarily the button presses typically associated with the fractal cue (i.e., in normal contingency trials; mean fraction correct = 0.74 ± 0.14) rather than errors of omission. Since trials were also classified as incorrect if responses were entered after 600 ms (i.e., the subject received negative feedback at the end of the trial), we examined the accuracy of the button presses entered after the 600 ms period. For both trial types, performance was improved slightly for responses entered during the requisite window (normal: mean fraction correct = 0.80 ± 0.111; reversal: mean fraction correct = 0.56 ± 0.21), indicating that a longer response window would have improved accuracy.

We hypothesized that increasing experience with frequent trials would lead to automaticity, and we tested for improved accuracy as evidence of such an effect. We computed a 2x4 ANOVA where the within-subjects factors were task condition (normal or reversal) and time (i.e., run 1-4). Specifically, we were interested in possible learning of stimulus-response relationships over time, and whether this learning differed by condition. While main effects of condition ($F_{1,184} = 437$, $p < 0.001$) and time ($F_{3,184} = 4.89$, $p < 0.005$) were found, there was no significant interaction between the factors. These findings indicate that participants were more accurate for normal trials than reversal trials, and that their performance in both frequent and infrequent trials improved over the course of the experiment, with no interaction between conditions (Figure 2.2).

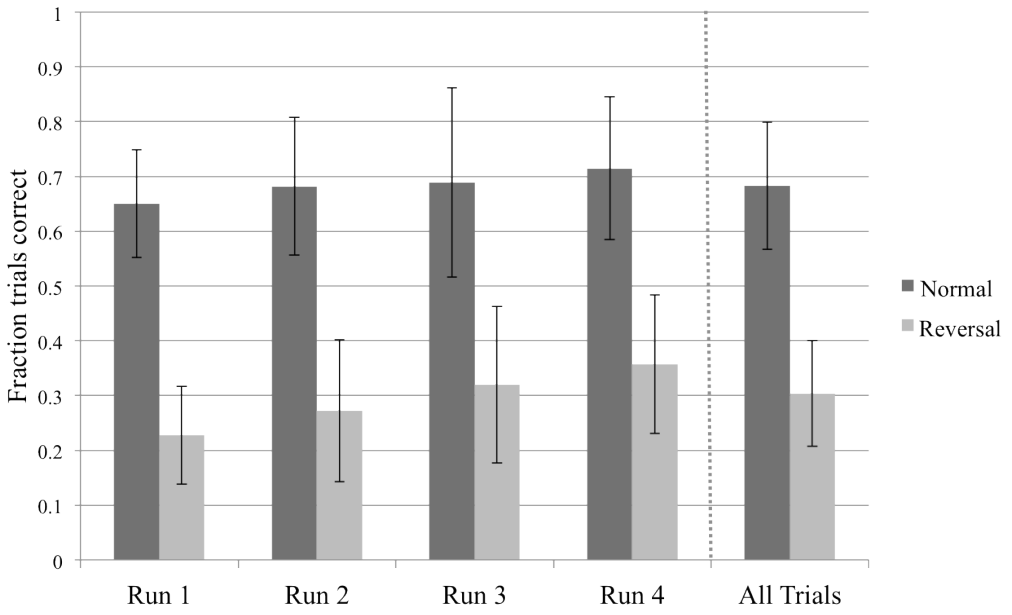

Figure 2.2. Behavioral performance by condition across time. Rightmost panel shows performance averaged across all four runs.

A *post hoc* examination verified a significant linear trend over time for both normal trial ($t_{23} = 2.78$, $p < 0.05$) and reversal trial accuracy ($t_{1,23} = 4.62$, $p < 0.001$).

To further examine evidence for automaticity, we also analyzed the relationships between reaction time (RT) and condition, accuracy, and time. Using log-transformed RT values, we computed a 2x2x4 ANOVA where the factors were condition (normal or reversal), performance (correct or incorrect), and time (i.e., run 1-4). The analysis revealed main effects of condition ($F_{1,367} = 26.5$, $p < 0.001$) and performance ($F_{1,367} = 6.97$, $p < 0.01$), but not time ($p = 0.98$); none of the interaction terms were statistically significant ($p > 0.05$); in summary, normal contingency trials were associated with comparatively shorter response latencies and RTs were longer for correct compared to incorrect trials.

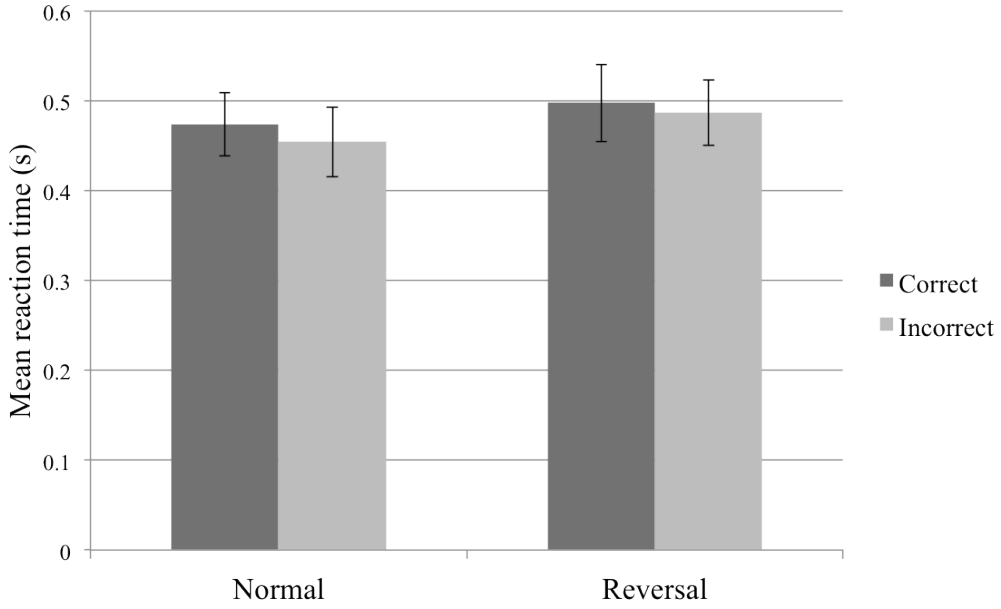

Figure 2.3. Reaction time by performance across conditions.

Figure 2.3 illustrates the reaction times over all trials for correct and incorrect trials in both conditions; values are listed in Table 2.1.

		Performance	
		Correct	Incorrect
Condition	Normal	0.474 ± 0.035	0.454 ± 0.039
	Reversal	0.497 ± 0.043	0.487 ± 0.037

Table 2.1. Mean reaction time by condition and performance. Mean (s) ± standard deviation.

Neuroimaging results. Model 1 tested for differences in neural response to normal contingency and reversal trials. As visualized in Figure 2.4, compared to reversal trials, normal contingency trials showed stronger BOLD response in vmPFC (including subgenual ACC and OFC), left superior temporal gyrus, and right insula extending into the putamen ($p < 0.05$, WBC; Table 2.2).

Region	k	BA	x	y	z	Peak Z score
Right insula, putamen	740		33	-12	-6	5.23*
Left superior temporal gyrus	570	42	-63	-3	18	5.03*
Ventromedial prefrontal cortex	337	25/11	3	18	-12	4.79*
Left putamen	69		-24	-3	-9	4.26
Left cuneus	35	19	-6	-93	33	4.09
Right postcentral gyrus	125	5/7	18	-54	63	3.90
Right anterior caudate	23		21	36	-3	3.90
Left caudate	31		-18	21	15	3.89
Right caudate	27		18	21	15	3.87
Posterior cingulate gyrus	24	31	-9	-18	51	3.83
Right middle occipital gyrus, cuneus	33	18/19	15	-93	33	3.78
Right cuneus	31	17	24	-90	15	3.76
Left precuneus	36	5	-18	-45	63	3.59
Left postcentral gyrus	11	3	-45	-27	60	3.28

Table 2.2. Regions showing greater response for normal contingency compared to reversal trials. All results are reported at $p < 0.001$, uncorrected, with cluster extent ≥ 10 voxels.
* Whole-brain corrected for multiple comparisons ($p < 0.05$) at the cluster level (minimum cluster size = 194 voxels).
k = cluster size. Coordinates reported in MNI space.

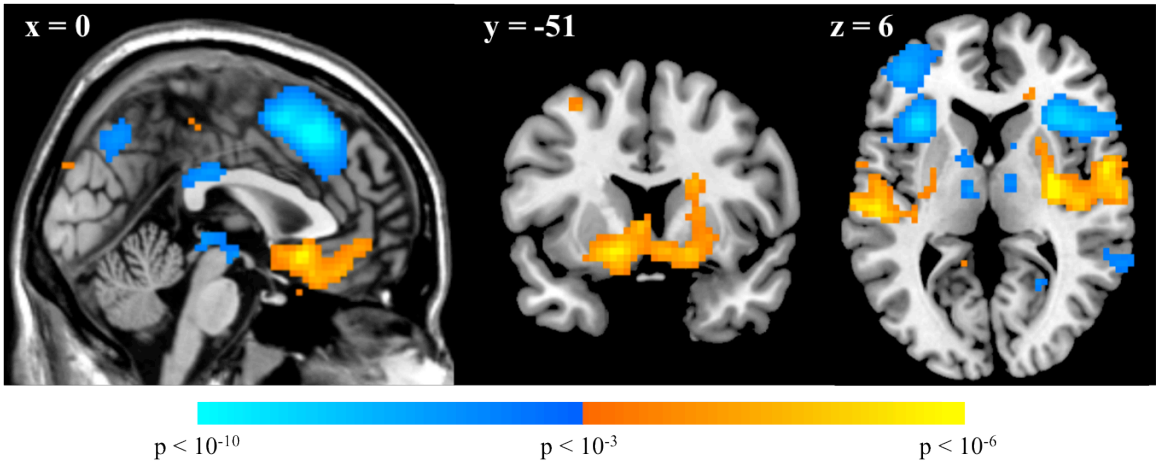

Figure 2.4. Voxels showing differential effects by condition. The warm color scale reflects regions more active for normal contingency than reversal trials, while the cool color scale reflects regions more active for the opposite contrast, reversal > normal.

In contrast, stronger response in reversal trials was observed in a large cluster encompassing medial preSMA, bilateral ventrolateral, right insular, and left insular cortices (including left vlPFC). Other regions demonstrating higher neural response for reversal compared to normal contingency trials included bilateral inferior parietal lobule, bilateral precuneus, left fusiform gyrus, and midbrain ($p < 0.05$, WBC; Table 2.3).

Region	k	BA	x	y	z	Peak Z score
Medial pre-supplementary motor area, bilateral dorsolateral prefrontal cortex bilateral anterior insula, bilateral ventrolateral prefrontal cortex	5004	6/8/9/10/47	0	24	48	6.89*
Left inferior parietal lobule, precuneus	1192	40/7	-30	-51	45	6.54*
Right inferior parietal lobule, precuneus	1564	40/7	42	-54	48	6.45*
Left fusiform gyrus	535	37	-42	-60	-12	5.83*
Midbrain	251		6	-24	-3	5.61*
Right fusiform gyrus, parahippocampal gyrus	73	20/36	30	-33	-24	5.08
Right cerebellum	24		12	-75	-30	4.47
Posterior cingulate cortex	83	23	3	-24	30	4.33
Right lateral prefrontal cortex	18	10	36	51	18	4.23
Left caudate	17		-12	3	6	3.70
Right caudate	12		12	3	15	3.64

Table 2.3. Regions showing greater response for reversal compared to normal contingency trials. All results are reported at $p < 0.001$, uncorrected, with cluster extent ≥ 10 voxels.
* Whole-brain corrected for multiple comparisons ($p < 0.05$) at the cluster level (minimum cluster size = 194 voxels).
k = cluster size. Coordinates reported in MNI space.

In order to test our second hypothesis, that learning in both frequent and infrequent trials will engage brain regions associated with response automaticity, we also evaluated Model 1 for linear changes in neural response over time.

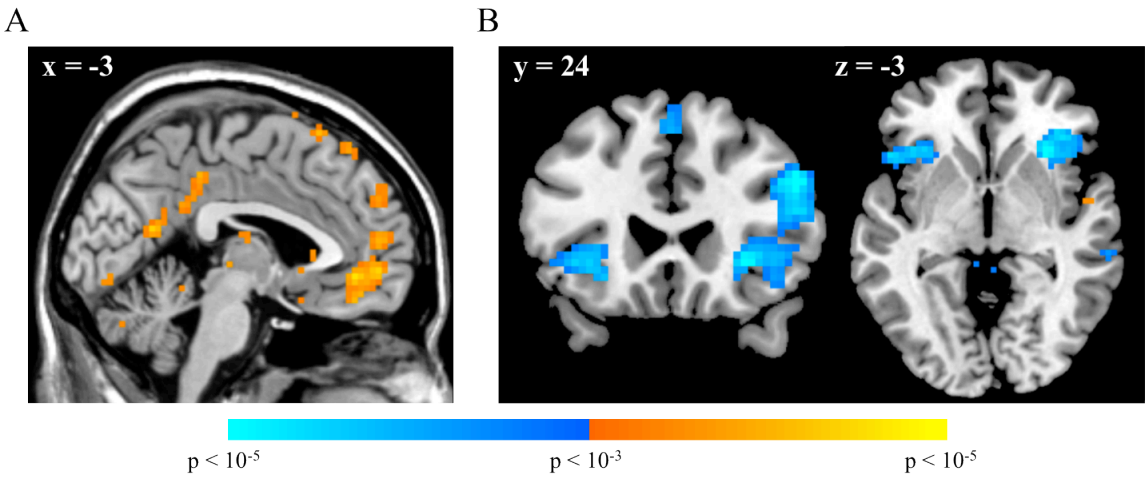

Figure 2.5. Voxels showing linear effects of time for each condition. A) Regions showing a positive linear effect in normal contingency trials. B) Regions showing a negative linear effect in reversal trials. The warm color scale reflects linear increases in response over time, while the cool color scale reflects linear decreases in response over time.

Neural response to normal trials increased over time in many areas, including right caudate and right cerebellum ($p < 0.05$, WBC), as well as vmPFC and PCC ($p < 0.001$, uncorrected; Figure 2.5A); no regions showed significant linear decreases in response over the runs during normal contingency trials (Table 2.4).

Region	k	BA	x	y	z	Peak Z score
Left angular gyrus, precuneus	156	39/19	-42	-81	36	4.73
Dorsomedial prefrontal cortex	42	9	15	36	33	4.63
Right cerebellum	220		39	-45	-36	4.54*
Left premotor cortex	155	6/8	-12	30	63	4.41
Right inferior temporal gyrus	30	20	57	-6	-27	4.37
Left cerebellum	128		-27	-72	-39	4.34
Right premotor cortex	29	8	27	42	51	4.30
Left caudate	68		-18	27	9	4.29
Right precentral gyrus	50	4	15	-24	54	4.28
Precuneus, posterior cingulate cortex	166	23/31	3	-54	24	4.36
Right caudate	194		24	33	3	4.22*
Ventromedial prefrontal cortex	127	10/11	-3	42	-6	4.05
Left posterior insula	55	13	-39	-48	21	4.02
Left precuneus	14	7	-15	-57	39	3.96
Left lingual gyrus, fusiform gyrus	44	18/19	-6	-81	-6	3.93
Right fusiform gyrus	19	18	27	-72	-12	3.79
Dorsomedial prefrontal cortex	121	10	-12	60	24	3.77
Left lateral prefrontal cortex	11	10	-30	57	6	3.76
Subgenual anterior cingulate cortex	12	25	3	15	-18	3.74
Right angular gyrus	19	39	54	-72	36	3.72
Left inferior temporal, middle temporal gyri	46	20/21	-57	-3	-27	3.69
Medial prefrontal cortex	33	10	-6	54	12	3.67
Posterior cingulate cortex	19	30	-21	-57	9	3.66
Right premotor cortex	13	6	12	27	63	3.66
Left putamen	40		-21	6	-3	3.64
Right superior frontal gyrus	29	10	21	51	33	3.58
Right insula	15	13	51	-15	9	3.51
Left cerebellum	16		-42	-51	-30	3.46
Left amygdala	12		-18	-6	-18	3.46
Left inferior frontal gyrus	16	47	-48	45	-3	3.45
Left extrastriate cortex	18	18	-12	-99	3	3.42

Table 2.4. Regions showing positive linear effects of time in normal contingency trials
All results are reported at $p < 0.001$, uncorrected, with cluster extent ≥ 10 voxels. * Whole-brain corrected for multiple comparisons ($p < 0.05$) at the cluster level (minimum cluster size = 174 voxels).
k = cluster size. Coordinates reported in MNI space.

In contrast, only a negative linear effect was evident in reversal trials, with premotor cortex and right lateral PFC extending into insula showing particularly strong decreases in neural response over time ($p < 0.05$, WBC; Figure 2.5B, Table 2.5).

Region	k	BA	x	y	z	Peak Z score
Right middle frontal gyrus	381	6	39	3	57	4.53*
Retrosplenial cortex	31	29	6	-39	6	4.53
Right lateral prefrontal cortex, anterior insula	323	45	51	24	30	4.52*
Right inferior parietal lobule	141	40	36	-51	42	4.31
Left anterior insula	107		-42	18	-9	4.25
Premotor cortex	63	6/8	0	27	51	3.95
Left inferior parietal lobule	16	40	-30	-60	39	3.74
Right middle temporal gyrus	15	21	51	-9	-15	3.61
Left lateral prefrontal cortex	14	46	-48	21	30	3.52

Table 2.5. Regions showing negative linear effects of time in reversal trials.
All results are reported at $p < 0.001$, uncorrected, with cluster extent ≥ 10 voxels.
* Whole-brain corrected for multiple comparisons ($p < 0.05$) at the cluster level (minimum cluster size = 173 voxels).
k = cluster size. Coordinates reported in MNI space.

Direct contrasts between normal and reversal for both the positive linear and negative linear effects confirmed that changes over time were unique to each condition (all $p < 0.01$, uncorrected).

With Model 2, we tested for effects of response accuracy. In Normal trials, correct compared to incorrect responses were associated with particularly heightened BOLD signal in PCC extending through striatum and into vmPFC/OFC, primary visual and extrastriate cortices, and right premotor areas ($p < 0.05$, WBC). The reverse contrast showed greater activations in medial preSMA extending into right supplementary motor cortex ($p < 0.05$, WBC), as well as bilateral anterior insula and dorsolateral prefrontal cortex ($p < 0.001$, uncorrected; Figure 2.6, Table 2.6).

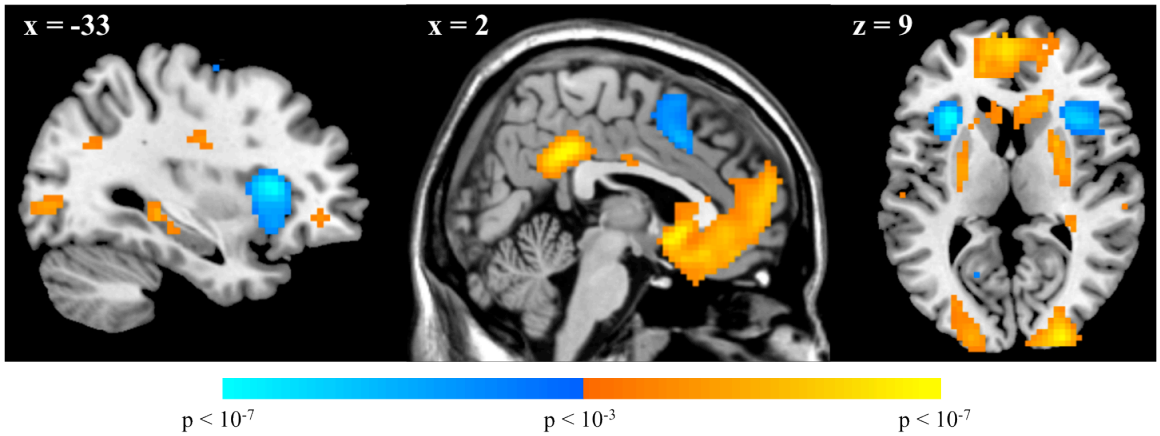

Figure 2.6. Neural main effects of accuracy in normal contingency trials. The warm color scale reflects regions more active for correct trials, while the cool color scale reflects regions more active for the incorrect trials.

Contrast	Region	k	BA	x	y	z	Peak Z score
NC - NI							
	Posterior cingulate cortex, striatum, ventromedial prefrontal cortex	3768	31	3	-42	36	5.28*
	Left premotor cortex	261	8/6	-18	30	54	5.27
	Right extrastriate cortex, cuneus, lingual gyrus	293	18	27	-96	9	5.17*
	Left primary visual cortex	275	17	-21	-96	6	4.55*
	Left precuneus, angular gyrus	62	39	-36	-66	30	4.32
	Right superior temporal gyrus	36	22	57	-9	-3	4.30
	Right premotor cortex	280	8/6	24	24	57	4.24*
	Right inferior temporal gyrus	67	20	60	-9	-24	4.10
	Left hippocampus	27		-30	-33	-3	4.00
	Left superior temporal gyrus	18	22	-54	-9	-3	3.98
	Right angular gyrus	32	39	48	-72	36	3.84
	Left middle temporal gyrus	16	41	-54	-45	-9	3.59
	Dorsomedial cingulate cortex	13	32	3	-9	30	3.39
NI - NC							
	Left anterior insula	229		-33	21	9	5.39
	Right anterior insula	190		36	18	9	4.64
	Medial premotor cortex, right supplementary motor cortex	299	32/6	6	15	42	4.40*
	Right supramarginal gyrus	75	40	63	-45	27	4.31
	Right dorsolateral prefrontal cortex	46	9	42	6	33	4.15
	Left dorsolateral prefrontal cortex	42	9	-42	15	33	4.00
	Left superior parietal lobule	29	7	-27	-60	42	3.75
	Precuneus	23	31	-9	-69	18	3.64
	Left supplementary motor cortex	17	6	-9	-9	72	3.64
	Right parahippocampal gyrus	10	30	18	-54	0	3.37
	Left parahippocampal gyrus	11	30	-18	-60	0	3.33

Table 2.6. Regions showing differential effects for correct and incorrect normal trials.
All results are reported at $p < 0.001$, uncorrected, with cluster extent ≥ 10 voxels.
* Whole-brain corrected for multiple comparisons ($p < 0.05$) at the cluster level (minimum cluster size = 257 voxels).
k = cluster size. Coordinates reported in MNI space.

We examined our third hypothesis by testing specifically for the involvement of cognitive control regions in trials for correct reversal responses. Significant effects for reversal trials were only found for correct > incorrect trials; correct responses in these trials were associated with activity in right supplementary motor areas ($p < 0.05$, WBC) and left vlPFC ($p < 0.05$, SVC), among others (Figure 2.7, Table 2.7).

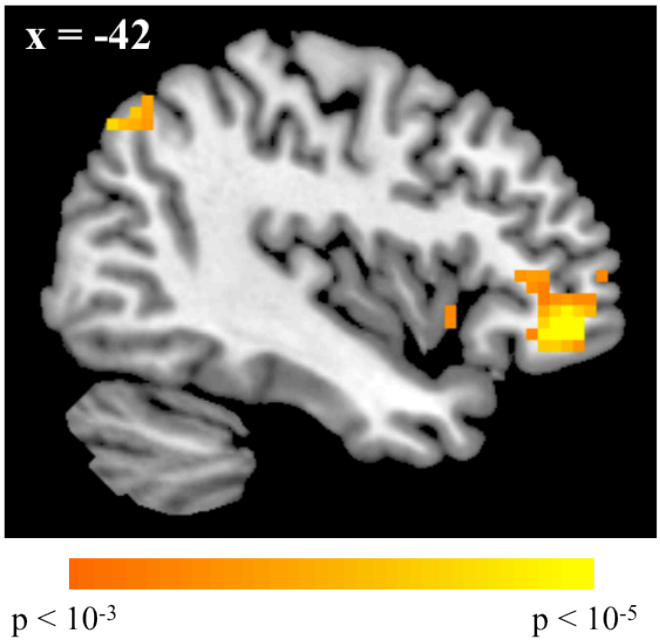

Figure 2.7. Voxels more active in correct reversal trials.

Contrast	Region	k	BA	x	y	z	Peak Z score
RC - RI							
	Right supplementary motor cortex	333	6/8	21	24	63	4.72*
	Left ventrolateral prefrontal cortex	127	11	-42	42	-9	4.64
	Right angular gyrus	138	7/40	51	-63	51	4.49
	Left supplementary motor cortex	121	6	-30	18	60	4.46
	Left ventral striatum	98		-12	6	-9	4.42
	Left angular gyrus	50	7	-39	-72	45	4.08
	Left anterior insula	28		-36	15	-6	3.88
	Anterior cingular gyrus	36	32	3	39	-3	3.87
	Right anterior insula	57		45	30	-9	3.74
	Medial prefrontal cortex	141	10	0	57	21	3.56
	Left fusiform gyrus	26	20	-51	-39	-27	3.46
RI - RC							
	No significant voxels						

Table 2.7. Regions showing differential effects for correct and incorrect reversal trials.
All results are reported at $p < 0.001$, uncorrected, with cluster extent ≥ 10 voxels.
* Whole-brain corrected for multiple comparisons ($p < 0.05$) at the cluster level (minimum cluster size = 205 voxels).
k = cluster size. Coordinates reported in MNI space.

For completeness, we also examined differences between correct and incorrect responses while accounting for condition. We computed the contrast [NC - NI - RC + RI], which showed differences between normal contingency and reversal trials for correct compared to incorrect. Increased neural activity was observed in regions including subgenual ACC and bilateral posterior insula; subcortically, greater responses were seen in left hippocampus and bilateral caudate ($p < 0.001$, uncorrected; Figure S2.1, Table S2.1). The reverse contrast, [RC - RI - NC + NI], showed more robust effects, with enhanced responses in regions including premotor cortex and bilateral insula ($p < 0.05$, WBC; Figure S2.2, Table S2.2). Finally, we examined the contrast [NC - NI + RC - RI]; this contrast examined differential effects for correct and incorrect trials by condition while

controlling for incorrect responses on reversal trials, since those responses required the same motor action as the correct normal contingency response. Stronger BOLD response was observed in bilateral premotor areas, PCC, and ventral striatum extending into medial PFC ($p < 0.05$, WBC; Figure S2.3, Table S2.3).

Finally, to interrogate our fourth hypothesis, we examined linear changes in response – particularly in infrequent (i.e., reversal) trials – over time with respect to performance. For correct reversal trials, we saw decreases in response over time in a variety of regions, including medial preSMA, left and right vlPFC, right lateral PFC, and right inferior parietal lobule ($p < 0.05$, WBC; Figure 2.8, Table 2.8). No regions showed increase response over time for correct reversal trials. All other results showing linear changes in neural response as a function of response accuracy are described in Supplementary Materials (incorrect reversal trials: Figure S2.4 and Table S2.4 correct normal trials: Figure S2.5 and Table S2.5; incorrect normal contingency trials: Figure S2.6 and Table S2.6).

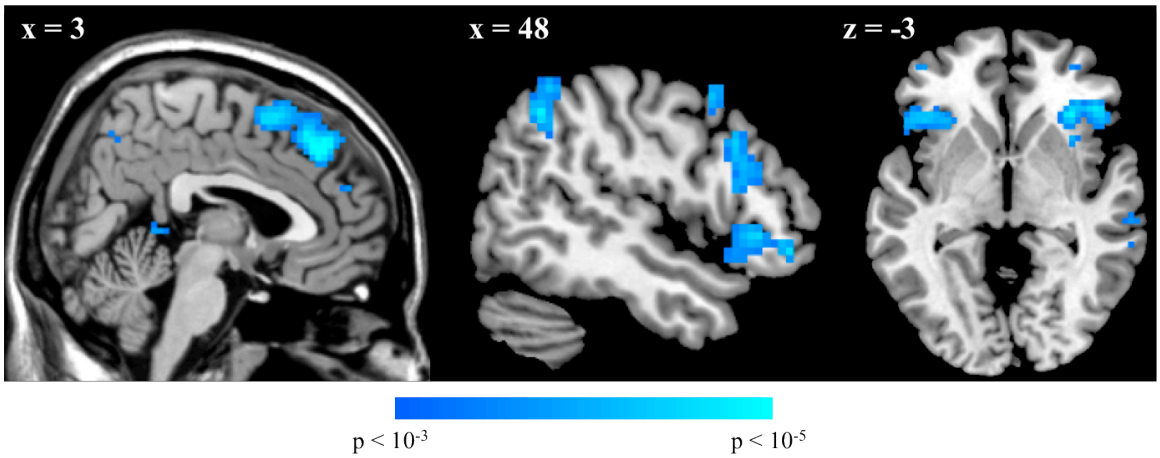

Figure 2.8. Voxels showing negative linear effects of time in correct reversal trials.

Region	k	BA	x	y	z	Peak Z score
Premotor cortex	351	6/8	3	36	45	4.69*
Right lateral prefrontal cortex	53	10	24	48	21	4.58*
Right inferior parietal lobule, angular gyrus	180	39/40	45	-54	45	4.33*
Right ventrolateral prefrontal cortex, anterior insula	162	11/47	45	30	-6	4.23*
Right dorsolateral prefrontal cortex	101	45/46	42	21	27	4.17*
Right middle temporal gyrus	34	21	69	-27	-6	4.07
Posterior cingulate cortex	17	29	6	-42	6	3.98
Right middle frontal gyrus	72	6	42	12	51	3.94*
Left ventrolateral prefrontal cortex, anterior insula	116	47	-48	21	-6	3.93*
Left angular gyrus, inferior parietal lobule	107	40	-51	-57	39	3.91*
Precuneus	12	7	-9	-63	20	3.82
Left middle temporal gyrus	25	21	-45	51	0	3.62
Left precentral gyrus	10	3	-33	9	33	3.55
Left dorsolateral prefrontal cortex	18	46	-48	21	33	3.53

Table 2.8. Regions showing negative linear effects of time in correct reversal trials.
All results are reported at $p < 0.001$, uncorrected, with cluster extent ≥ 10 voxels.
* Whole-brain corrected for multiple comparisons ($p < 0.05$) at the cluster level (minimum cluster size = 42 voxels).
k = cluster size. Coordinates reported in MNI space.

Discussion

In the present study, we investigated the relationship between response automaticity and cognitive control ability in a motivationally salient response inhibition task using fMRI. As participants developed experience with the task over time, their responses to both frequent and infrequent trials became more highly learned, as reflected by linear increases in performance over experimental sessions. These behavioral effects were reflected in concomitant linear changes in neural response in regions that have been implicated in response automaticity, including caudate (e.g., [162,163]) and cerebellum (e.g., [164]) for normal trials, and preSMA[158,165,166] for reversal trials. Neural responses

were further modulated by performance, where an effect of automaticity was observed in regions including right vlPFC – an area thought to be necessary for cognitive control[12] – only in trials where response inhibition was implemented successfully. These findings replicate and extend previous work identifying neural regions involved in cognitive control and response automaticity, and provide additional support for the theory that automaticity in cognitive control is associated with neural efficiency.

Neural main effects of task condition (Model 1) suggest that our task engaged brain regions that have been implicated by previous research on response inhibition and cognitive control. Compared to normal trials, reversal trials produced increases in activity in a wide variety of regions, including anterior insula, which may be involved in representing the physiological state associated with obtaining a motivationally salient outcome[167,168], bilateral vlPFC, which is linked to inhibitory control (e.g., [127,129,135]), and preSMA, which may facilitate the switch from controlled to automatic responding[157]. Additional regions identified include the bilateral inferior parietal lobule, which is thought to be involved in sensorimotor integration[169], and midbrain, which may reflect dopaminergic signaling from STN/VTA for response inhibition[145,146]. Separating these trials by performance (Model 2) provides additional insight into the neural processes underlying response inhibition. Compared to incorrect trials, correct reversal trials elicited responses in the supplementary motor cortex, potentially reflecting signals related to updated stimulus-response value[98] and also left vlPFC, which has been implicated in the maintenance of goals and sets[141]. While response inhibition has most consistently been linked to right vlPFC, the left vlPFC has also been identified in such tasks. Functional imaging studies with go/no-go and stop signal tasks (e.g., [117,120,170]), as well as task switching paradigms (e.g., [171,172]), have described bilateral activations of vlPFC. Possible laterality effects have not yet been fully characterized, but one suggestion is that the activation of either or both hemispheres is largely task-dependent[13].

Learned automaticity in neural response to reversal trials was evidenced by a decrease in BOLD response over time in premotor cortex and right vlPFC extending into insula; no regions showed a linear increase in signal over sessions. This effect was unique to reversal trials, since there were no common activations for temporal response patterns between normal and reversal trials. Moreover, as experience with cognitive control increased over time, correct responses were associated with reductions in neural response in several regions that have been linked to cognitive control, including medial preSMA[122,137-139,157], right vlPFC (e.g., [21,98,114-122,126-129]), right lateral PFC[98,114], and right inferior parietal cortex[15,130]. These data are in line with the work of Chiu and others (2012), who demonstrated that the magnitude of motor evoked potentials decreases as performance improves in the 'no-go' trials of a typical go/no-go paradigm[155], and extend their work to fMRI, which offers more precise localization of effects. Reductions in neural response in association with training and improvement in individual performance may be indicative of increased efficiency, especially in cognitive tasks (e.g., [164,173-176]). Together, such data imply that the cognitive control performance enhancements associated with increased automaticity may be mediated by increased neural efficiency.

Nonetheless, these neural data only provide correlative evidence for automaticity. Learning in this study was measured by improvements in response accuracy over time. We had expected that automaticity would also be manifest in RT, where correct responses would be associated with shorter response latencies as performance improved. While we did observe significant effects of condition, with normal trials having longer response latencies than reversal trials, and accuracy, where correct trials requiring longer response latencies than incorrect trials, we did not see an interaction between conditions or an effect of time. One possible reason for this finding is that the cognitive effort required for the two conditions was apparently similar enough that the largest difference in average RT was on the order of 23 ms. Moreover, across the runs, average reaction

time was relatively unchanged, and changes were only evident in slight reductions in standard deviation, particularly between the first and second half of the experiment. Even as improvements in accuracy indicated learning over time, the task remained difficult – the highest average performance (in run 4) for normal contingency was 71.4% and 35.7% for reversal trials – and required vigilance for the duration of the experiment.

Several additional issues should be considered in the interpretation of these findings. First, with respect to the role of vlPFC in response inhibition, recent data have suggested that right vlPFC activation in go/no-go tasks may reflect a more general attentional salience detection mechanism[148,177]. Neither our experiment nor any of the others cited here can fully rule out this interpretation, since response inhibition tasks typically make use of "oddball" style designs, where the stimuli requiring control are far less frequent than the other stimuli, enhancing their novelty or salience. However, it is worth noting that lesions to frontal areas, including the vlPFC, critically affect performance on the Wisconsin Card Sorting Test, a neuropsychological battery that, like many other task switching paradigms, measures behavioral flexibility in response to changing reinforcement schedules[178,179].

A second potential concern for analysis of data from experiments like this one where the frequency of event types is unbalanced (i.e., normal contingency versus reversal) is relative statistical power for parameter estimation. This issue is of particular importance for the interpretation of Model 2 results, since correct and incorrect reversal events were modeled separately in this GLM; wide variation in performance across individuals – for all 96 reversal trials, there was an order or magnitude difference in response accuracy (minimum percent correct = 5.21%; maximum percent correct = 52.1%) across participants – resulted in conditions where parameter estimates for some participants were much better than for others.

Another source of individual variability was task in strategy[180] – for example, whether to strive for speed or accuracy; such differences manifest in both brain and behavior and can impact interpretation. While we cannot know whether individuals were more motivated by speed or accuracy strategies, we can assume that strategic bias was minimized by the experimental design, which provided both speed and accuracy incentives. We limited the response period to 600 ms, since a short response period has also been shown to increase the likelihood of observing response inhibition[181] and is less likely than a long window to induce bias toward accuracy, since time for the evolution of cognitive processes is limited. We balanced any potential speed bias by providing motivationally salient feedback on each trial, a technique that has been shown to impact go/no-go learning both behaviorally and neurally in STN/VTA and vlPFC[182]. Indeed, our behavioral data indicate that we were able to mitigate any potential strategic bias; standard deviations were of comparable magnitude across normal and reversal trials, indicating that the speed incentive did not affect learning differentially during reversal trials. Moreover, when participants entered responses outside the 600 ms window on reversal trials, these responses were generally accurate, suggesting strong motivation to enter a correct response on each trial; additionally, post-task self-report suggested that participants were motivated by the feedback, and individuals were especially frustrated when they made errors of commission on reversal trials.

A fourth caveat is in the psychological interpretation of results from incorrect reversal trials. The experimental response parameters limited the possible error types to errors of commission and omission. An error in a reversal trial could either be the same as a correct normal response for that particular fractal (error of commission) or a miss (error of omission). However, since there were only two possible responses – a right or a left button press – to any given stimulus, it cannot be concluded that an error of commission was strictly due to interference from automaticity in normal

contingency trials. In order to remove this confound, future studies should include more possible error types.

Figure S2.1. Voxels showing differences for normal contingency and reversal trials when controlling for performance.

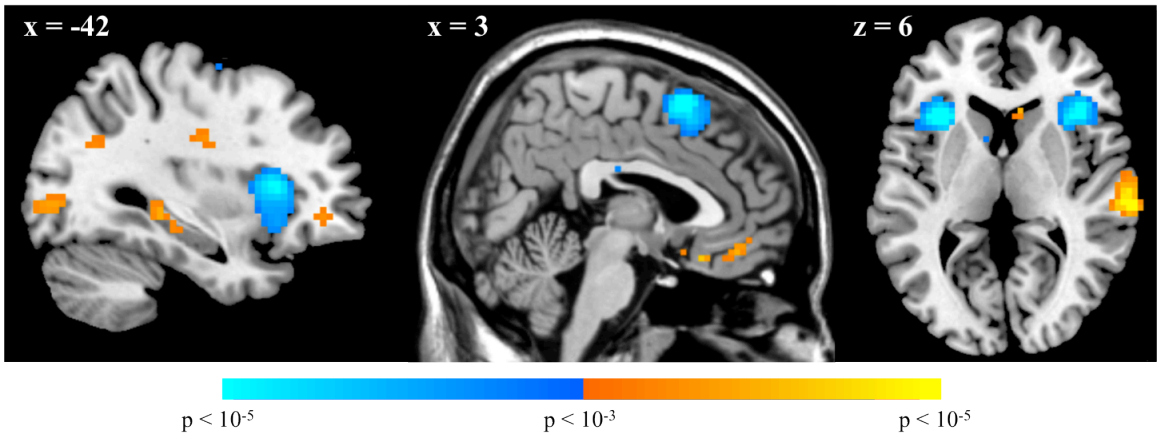

The warm color scale reflects regions more active for the contrast [NC - NI - RC + RI], while the cool color scale reflects regions more active for the opposite contrast, [RC - RI - NC + NI].

Table S2.1. Regions activated for the contrast [NC - NI - RC + RI].

Region	k	BA	x	y	z	Peak Z score
Right superior temporal gyrus	114	42	63	-24	6	4.50
Right paracentral lobule	44	5	12	-36	57	4.44
Right subgenual cingulate cortex	25	25	15	30	-6	4.42
Right caudate	20		21	3	30	4.24
Subgenual cingulate cortex	17	25	-3	24	-15	4.21
Left posterior insula	31	13	-27	-36	18	4.16
Left caudate	20		-21	15	24	4.02
Right postcentral gyrus	25	5	21	-42	63	3.94
Ventromedial prefrontal cortex	65	11	-3	45	-12	3.93
Right posterior insula	19	13	27	-27	24	3.93
Left hippocampus	15		-27	-27	-3	3.68
Right extrastriate cortex	19	18	24	-96	-3	3.45

All results are reported at $p < 0.001$, uncorrected, with cluster extent ≥ 10 voxels. k = cluster size. Coordinates reported in MNI space.

Figure S2.2. Voxels significantly activated for the contrast [RC - RI - NC + NI].

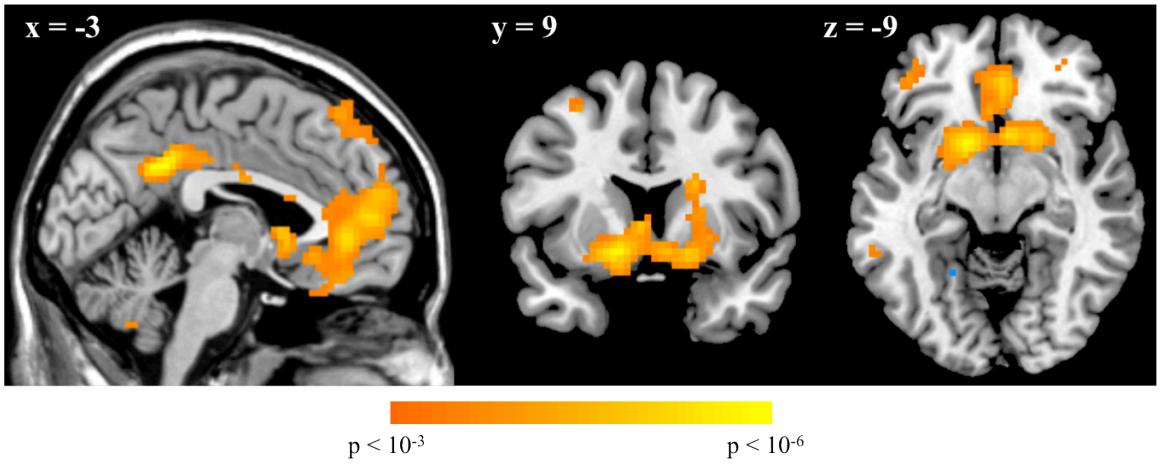

Table S2.2. Regions activated for the contrast [RC - RI - NC + NI].

Region	k	BA	x	y	z	Peak Z score
Left insula	276	13	-33	21	6	5.30*
Premotor cortex	266	6/8	6	15	63	5.07*
Right insula	313	13	36	24	-3	4.54*
Left ventrolateral prefrontal cortex	19	11	-42	42	-6	3.91
Left precentral gyrus	15	9	-57	12	42	3.88
Left superior parietal lobule	29	7	-30	-60	45	3.78
Right supramarginal gyrus	22	40	63	-57	39	3.57
Left dorsolateral prefrontal cortex	29	46	-48	21	24	3.49

All results are reported at $p < 0.001$, uncorrected, with cluster extent ≥ 10 voxels.
* Whole-brain corrected for multiple comparisons ($p < 0.05$) at the cluster level (minimum cluster size = 183 voxels).
k = cluster size. Coordinates reported in MNI space.

Figure S2.3. Voxels activated for the contrast [NC - NI + RC + RI].

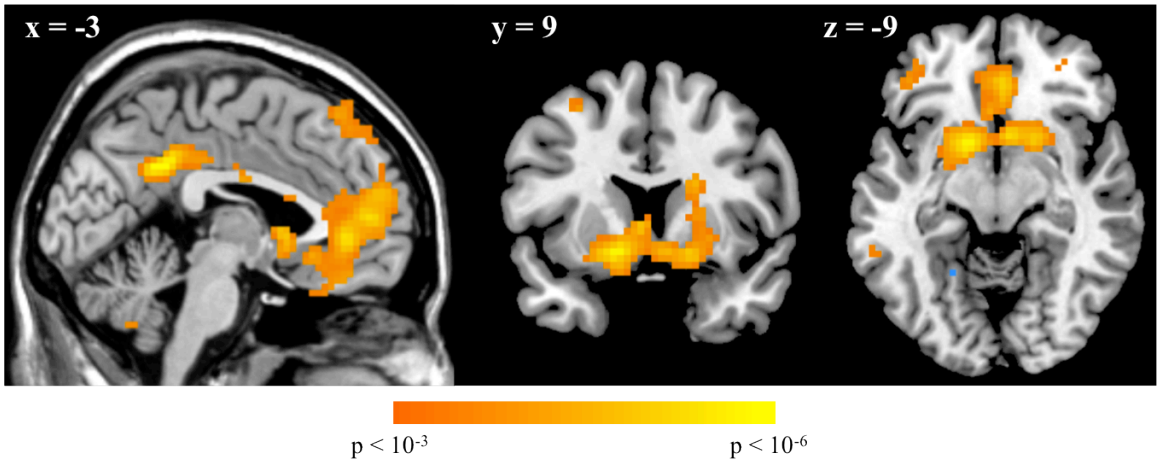

Table S2.3. Regions activated for the contrast [NC - NI + RC + RI].

Region	k	BA	x	y	z	Peak Z score
Left premotor cortex	394	6/8	-24	21	66	5.15*
Right premotor cortex	372	6/8	21	24	63	5.05*
Posterior cingulate cortex	310	31	-3	-48	33	5.07*
Ventral striatum, medial prefrontal cortex	1547	32/9/10	-15	9	-9	4.68*
Right visual cortex	126	18/17	24	-93	3	4.63
Right inferior parietal lobule	196	7/40	57	-63	45	4.49
Left inferior parietal lobule	83	7/39/40	-39	-72	45	4.28
Right inferior temporal gyrus	60	21	57	-9	-21	4.12
Left cuneus	45	17	-18	-93	0	4.09
Mediodorsal cingulate gyrus	94	24	-12	-12	33	3.96
Left inferior temporal gyrus	106	20/21	-60	-36	-18	3.92
Right cerebellum	10		42	-63	-42	3.90
Left inferior frontal gyrus	13	47	-45	36	6	3.76
Left ventrolateral prefrontal cortex	59	11	-39	45	-6	3.59
Left lateral prefrontal cortex	13	10	-33	54	9	3.41

All results are reported at $p < 0.001$, uncorrected, with cluster extent ≥ 10 voxels.
* Whole-brain corrected for multiple comparisons ($p < 0.05$) at the cluster level (minimum cluster size = 243 voxels).
k = cluster size. Coordinates reported in MNI space.

Figure S2.4. Voxels showing linear effects of time for incorrect reversal trials.

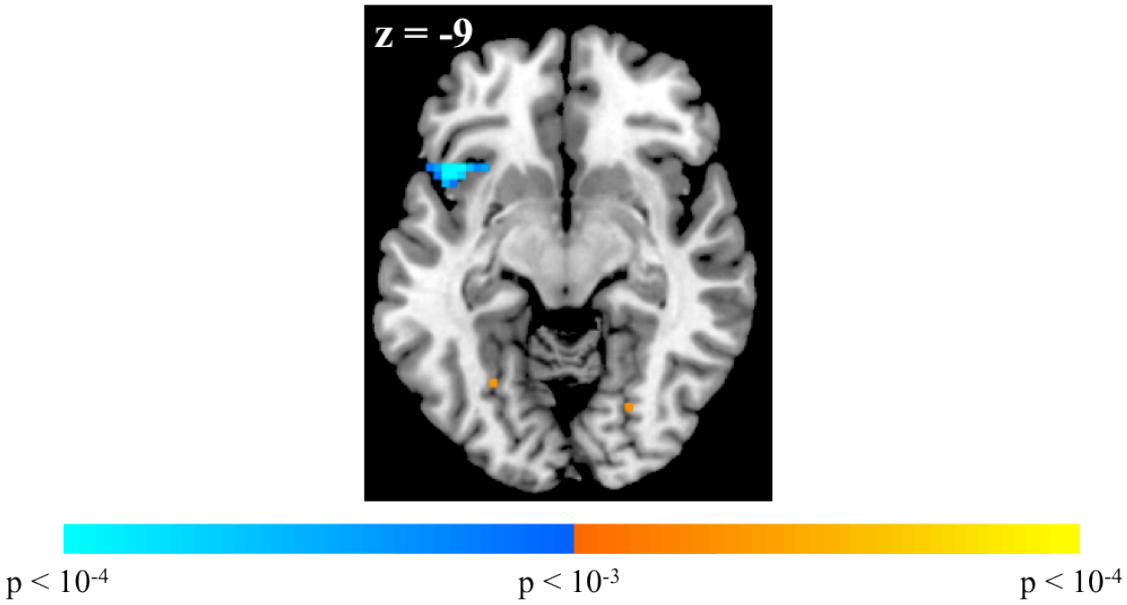

The warm color scale indicates positive linear effects, while the cool color scale reflects negative linear effects.

Table S2.4. Regions exhibiting linear change in response over time for incorrect reversal trials.

Contrast	Region	k	BA	x	y	z	Peak Z score
Linear increase over runs							
	Right cerebellum	23		36	-42	-36	4.33
	Right paracentral lobule	11	31	15	-24	54	4.17
	Right extrastriate cortex	41	18	12	-102	15	3.84
	Right cingulate gyrus	12	24	21	9	33	3.47
Linear decrease over runs							
	Left anterior insula	36	47	-42	18	-9	4.26
	Right fusiform gyrus	11	37	51	-51	-21	3.68
	Right superior temporal gyrus	11	22	51	-39	12	3.59
	Right supramarginal gyrus	11	40	45	-51	36	3.42

All results are reported at $p < 0.001$, uncorrected, with cluster extent ≥ 10 voxels.
k = cluster size. Coordinates reported in MNI space.

Figure S2.5. Voxels showing a linear increase in activation for correct normal contingency trials over time.

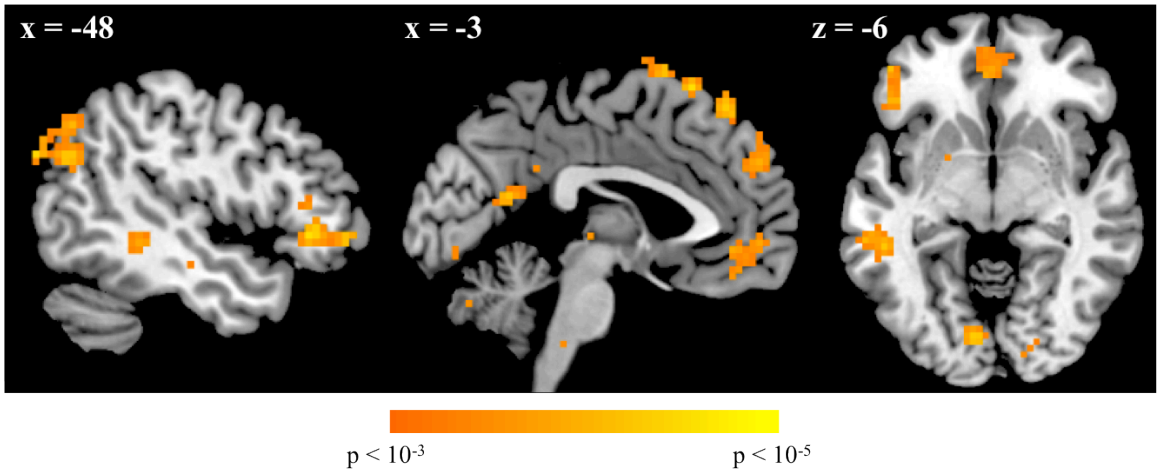

Table S2.5. Regions exhibiting linear increase in response over time for correct normal contingency trials.

Region	k	BA	x	y	z	Peak Z score
Premotor cortex	471	6/9/10	-12	30	63	4.61*
Left angular gyrus, inferior parietal lobule	138	39	-42	-81	36	4.57*
Right cerebellum	217		39	-51	-45	4.51*
Frontal lobe (white matter)	107		24	21	27	4.45*
Left superior temporal gyrus	35	39	-39	-48	21	4.29
Right middle temporal gyrus	26	20/21	57	-6	-27	4.21
Right superior frontal gyrus	35	8	24	42	51	4.2
Left cerebellum	103		-24	-75	-36	4.05*
Left ventrolateral prefrontal cortex	52	47/11	-48	30	-3	4.02*
Left middle temporal gyrus	56	21	-60	-36	-3	3.91*
Right superior frontal gyrus	90	9/10	21	51	36	3.87*
Left lingual gyrus	32	18	-9	-81	-6	3.85
Posterior cingulate cortex	94	31	0	-57	18	3.83*
Frontal lobe (white matter)	10		-15	12	24	3.81
Right supplementary motor area	15	6	24	-21	54	3.73
Left supplementary motor area	11	6	-3	12	72	3.73
Left supramarginal gyrus	33	40	-63	-48	42	3.69
Left putamen	11		-21	3	12	3.65
Right angular gyrus	16	39	54	-72	36	3.63
Left hippocampus, parahippocampal gyrus	20		-21	-12	-15	3.61
Left precuneus	10	7	-18	-57	39	3.6
Right putamen	14		21	9	9	3.59
Ventromedial prefrontal cortex	82	10/11	3	42	-15	3.58*
Left superior frontal gyrus	12	8	-33	24	48	3.42
Left extrastriate cortex	17	18	-12	99	9	3.41
Left cerebellum	20		-39	-54	-30	3.37

All results are reported at $p < 0.001$, uncorrected, with cluster extent ≥ 10 voxels.
* Whole-brain corrected for multiple comparisons ($p < 0.05$) at the cluster level (minimum cluster size = 45 voxels).
k = cluster size. Coordinates reported in MNI space.

Figure S2.6. Voxels showing a linear increase in activation for incorrect normal contingency trials over time.

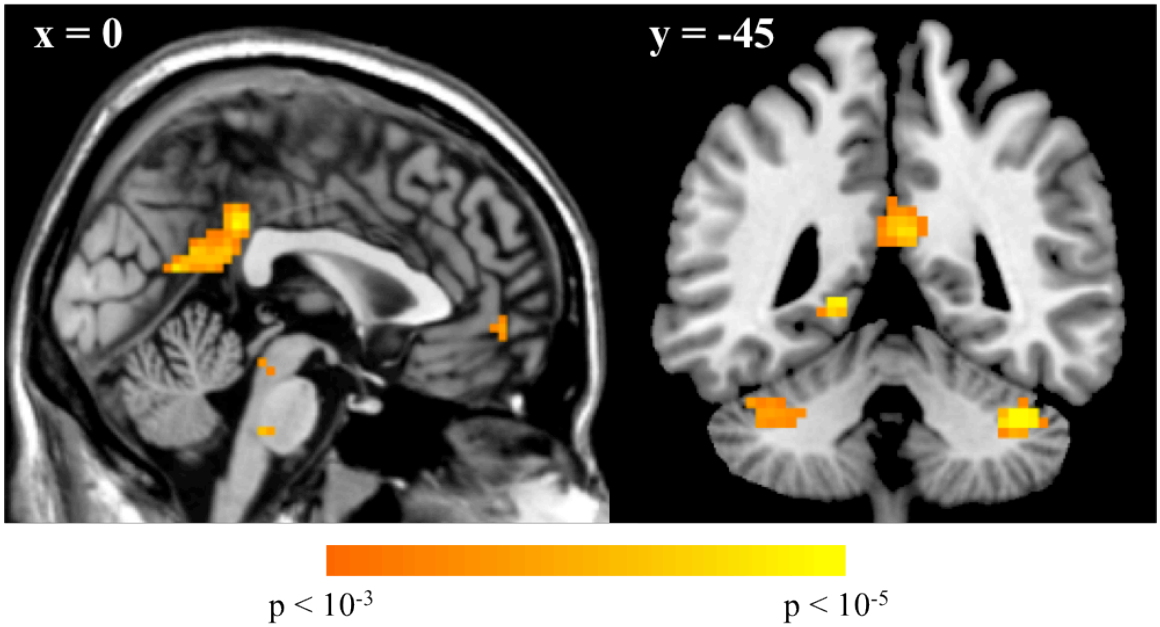

Table S2.6. Regions exhibiting linear increase in response over time for incorrect normal contingency trials.

Region	k	BA	x	y	z	Peak Z score
Right cerebellum	39		39	-45	-36	4.78
Left lingual gyrus	11	30	-15	-42	0	4.72
Left cerebellum	42		-45	-51	-33	4.54
Posterior cingulate cortex	137	23/31	0	39	33	4.41*
Left cerebellum	25		-27	-72	-39	3.93
Left middle temporal gyrus	18	21	-42	0	-30	3.86
Left precuneus	33	19	-42	-78	36	3.77
Pons	10		3	-27	-39	3.75
Right supplementary motor area	18	6	21	-24	54	3.62
Posterior cingulate cortex	11	30	-18	-54	9	3.52
Left cerebellum	19		-18	-63	-33	3.47

All results are reported at $p < 0.001$, uncorrected, with cluster extent ≥ 10 voxels.
* Whole-brain corrected for multiple comparisons ($p < 0.05$) at the cluster level (minimum cluster size = 45 voxels).
k = cluster size. Coordinates reported in MNI space.

Chapter 3

INTRA-PREFRONTOCORTICAL CONNECTIVITY IN TEMPORAL DISCOUNTING*

There is widespread interest in identifying computational and neurobiological mechanisms that influence the ability to choose long-term benefits over more proximal and readily available rewards in domains such as dietary and economic choice. We present the results of a human fMRI study that examines how neural activity relates to observed individual differences in the discounting of future rewards during a monetary ITC task. We found that portions of left dlPFC, in BA 9 and 46, were more active in trials where subjects chose delayed rewards, after controlling for the subjective value of those rewards. We also found that the connectivity from dlPFC-BA46 to a region of vmPFC widely associated with the computational of stimulus values, increased at the time of choice, and especially during trials in which subjects chose delayed rewards. Finally, we found that estimates of effective connectivity between these two regions played a critical role in predicting out-of-sample between-subject differences in discount rates. Together with previous findings in dietary choice, these results suggest that a common set of computational and neurobiological mechanisms facilitate virtuous choice in both settings.

Introduction

Impaired self-control is thought to play a critical role in sub-optimal decision-making, and in conditions like addiction and obesity[28,97]. As a result, there is a widespread, on-going effort to characterize the computational and neurobiological mechanisms underlying self-control. Two types of paradigms have been widely used in behavioral neuroscience to examine these mechanisms. First are tasks involving intertemporal decisions between rewards, often money, in which subjects choose between sooner-smaller amounts and later-larger ones[70,74,76,77,79-81,97,183,184]. Second, are tasks

* Work done in collaboration with Todd Hare and Antonio Rangel.

involving dietary choices, in which subjects make choices between foods that vary in their tastiness and healthiness[88,89,185].

In previous work investigating dietary self-control, we found important commonalities and differences between successful and unsuccessful dieters[88]. Behaviorally, the two groups differed on the relative weight that they placed on the health and taste attributes of foods in making their decisions (with successful dieters weighting both health and taste, and unsuccessful dieters weighting only taste). Neurally, the vmPFC encoded the value of foods at the time of choice equally for both groups. The critical difference had to do with the role of left dlPFC. In successful dieters, dlPFC came on-line and exhibited increased effective connectivity with vmPFC during choices that required self-control (e.g., refusing to eat tasty, but unhealthy, candy). In contrast, unsuccessful dieters did not exhibit this pattern of connectivity. Furthermore, in a subsequent study we found that non-dieting participants behaved like successful dieters if they were given an exogenous reminder to pay attention to health information, and that the reminder activated the same dlPFC-vmPFC networks that successful dieters activated on their own[89].

These findings led us to propose the following model of the computational and neurobiological processes at work in self-control[88,89,186]. In the model, the vmPFC computes the value of options at the time of decision, by first assessing their various attributes, and then integrating them into a net value for the option as a whole. Importantly, "basic" attributes like tastiness might always be represented in the final value. However, more abstract attributes like healthiness are only represented, or are represented more strongly, if the dlPFC comes online and modulates activity in vmPFC, directing its value computations to incorporate them. This modulation is critical for optimal decision-making, because if some of the attributes are not represented or weighted properly,

the vmPFC will assign values to options that are not consistent with the long-term, goal-relevant (e.g., proper nutrition) rewards they generate.

An important open question is whether this pattern of interregional neural activity is also involved in other decision domains, such as those involving intertemporal monetary tradeoffs. This question is important because comparing the mechanisms at work in different decision contexts is a critical step in identifying common mechanisms that facilitate self-control. Theoretically, these circuits should also influence the degree of discounting for delayed rewards in the case of ITC, as long as dlPFC modulation of vmPFC can lead to an increased (or decreased) weighting for delayed rewards.

Here we address this open question by testing the following three hypotheses. First, we hypothesized that the same sub-regions of left dlPFC that are more active during self-control in dietary choice would also be more active in ITC when the subjects choose the larger-delayed payment over the money available today, after controlling for their value difference. Note that it is crucial to control for the value difference, because if the subjective value of the delayed reward is large enough, the decision to wait becomes trivial. Second, we hypothesized that effective connectivity from left dlPFC to vmPFC would be stronger during trials in which subjects choose larger-delayed rewards (again controlling for subjective value), which is consistent with the idea that dlPFC can modulate the value signals in vmPFC so that they place more weight on the value of delayed payouts. Third, we hypothesized that the levels of activation in dlPFC, as well as its effective connectivity to vmPFC, would help to explain differences in discount rates across subjects.

These hypotheses are based not only on previous work in dietary choice, but also on findings from the previous literature on goal-directed choice. First, areas of vmPFC, and the ventral striatum (vStr), have consistently been shown to correlate with stimulus values at the time of choice across a

wide variety of decision contexts[187-196], including decisions involving intertemporal tradeoffs[74,76,88,89,197]. Second, previous studies have associated responses in left dlPFC with choosing to wait for delayed monetary rewards using transcranial magnetic stimulation (TMS) and fMRI[79,82]. In particular, Figner et al. (2010) showed that temporarily reducing activity in left dlPFC using TMS results in subjects making more impatient choices, thus, establishing a causal role for this region in temporal discounting[82]. Third, recent studies have found that resting-state connectivity in networks including left dlPFC was correlated with discount rates[198,199].

Despite the attractiveness of the theory, and the body of consistent evidence, critical questions remain open. In particular, none of the previous studies have examined the effective connectivity between dlPFC and vmPFC during ITCs, nor can they establish that the dlPFC influences discount rates through a mechanism that involves the modulation of the stimulus values computed in vmPFC, or that the effective connectivity runs from dlPFC to vmPFC, and not the other way around. Here we are able to address these questions by estimating dynamic causal models[200], and using their estimates to explain and predict differences in discount rates across individuals.

Materials and methods

Participants. Twenty-seven (18 males; age: mean = 24.1 years, range = 19-40) were included in the study. Two additional subjects were excluded because of excessive head motion during the scanning session (≥ 2 mm in translation or rotation). All participants had normal or corrected-to-normal vision, no history of neurological, psychiatric, or metabolic illness, and were not taking any medications that interfere with the BOLD signal at the time of scanning. The Institutional Review Board at California Institute of Technology approved the methods and procedures used in this study.

ITC task. On every trial, subjects chose between getting $25 at the end of the experiment, and getting an equal or larger amount at a later date. The later offers ranged from $25 to $54, with a delay from 7 to 200 days. Subjects made 216 decisions. The unique combinations of amount and delay used are shown in Table S3.1. All subjects saw the same set of options, although in different random orders. Each option was shown twice. Note that presenting all subjects with the same options was necessary to subsequently test how neural activity relates to discount rates. Although beneficial for the hypotheses tested in previous studies[74,77,201], tailoring the choice sets around the indifference points of each subject would create a confound when examining how individual differences in neural activity relate to discount rates, since less patient subjects would be shown delayed rewards with higher monetary values.

As described in Figure 3.1, each trial began with an offer presented onscreen. Participants were required to press within 3 s to indicate whether or not they accepted the delayed reward offered. Only the varying delayed option was presented onscreen. A button press response resulted in the termination of the offer screen, and the appearance of a feedback screen for 250 ms displaying 'Yes', if the delayed offer was accepted, or 'No', if it was rejected. The phrase 'No decision received' was displayed if the subject failed to respond within 3 s (mean = 2% of trials, median = 0%). Trials were separated by a fixation cross of random duration (uniform: 2-6 s). The assignment of left/right button presses to accept/reject responses was counterbalanced across subjects. At the end of the experiment a single trial was randomly chosen and implemented: subjects received the chosen option in addition to $50 (available immediately) for participating in the study.

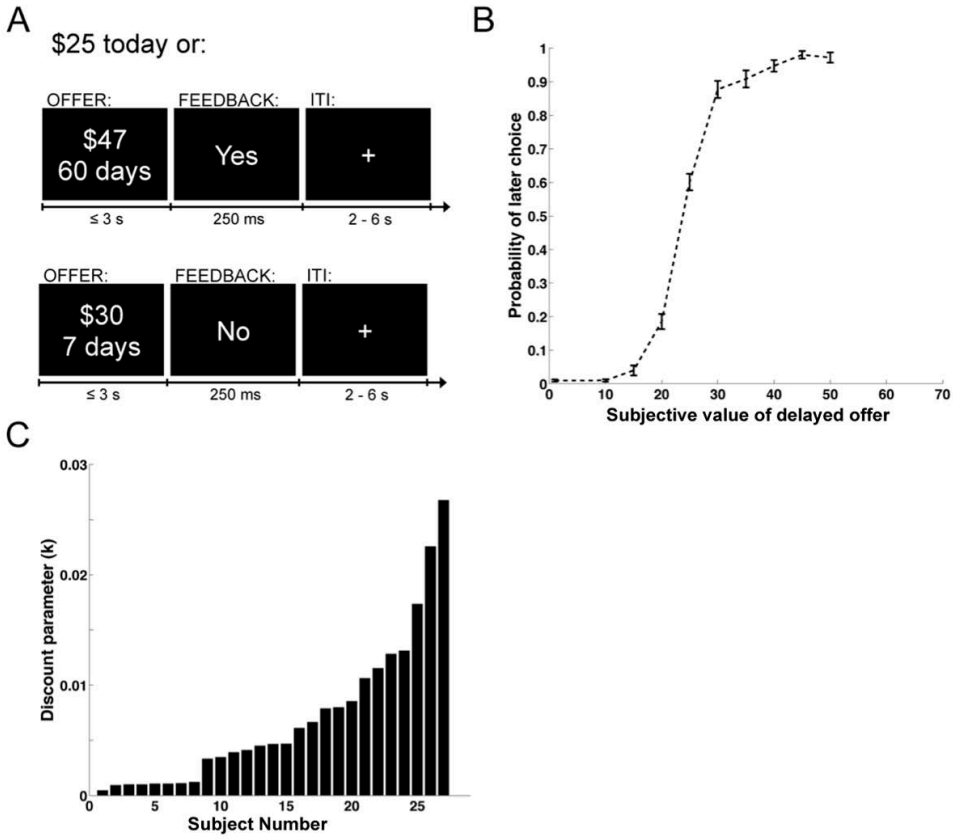

Figure 3.1. Task design and behavioral data. A) Example display screens and timing parameters. B) Choice curve displaying the probability of choosing the larger, delayed reward. The y-axis shows the probability of selecting the future reward and the x-axis displays the stimulus value of the future reward. Error bars represent the standard error of the mean. C) Bar graph showing the distribution of discounting parameters.

All payments were made using prepaid debit cards given to the subjects at the end of the experiment. This allowed us to make the delayed payments available on the appropriate date, without requiring subjects to return to the lab.

Behavioral data analysis. We estimated an individual discount factor (denoted by *k*) for each subject using maximum likelihood. In particular, we assumed that subjects assigned value to the

delayed options using a hyperbolic discounting function, in which the value of $\$A$ with a delay of D days is given by

$$dSV = A/(1+kD),$$

where dSV denotes the discounted stimulus value. We also assumed that the probability of accepting the delayed option is given by the soft-max function

$$P(\text{Yes}) = (1+exp(b*(25 - dSV)))^{-1},$$

where b is a non-negative parameter that modulates the slope of the psychometric choice function. Note that in this formula the value of the constant reference option is $25.

Imaging data acquisition. fMRI data were collected in a Siemens (Erlangen, Germany) 3.0 Tesla Trio MRI scanner. Using an eight-channel, phased array head coil, we collected gradient echo, T2*-weighted EPI images with BOLD contrast. In order to optimize BOLD sensitivity, we used a tilted acquisition in an orientation 30^o oblique to the AC-PC line[159]. The imaging parameters were as follows: TR = 2500 ms; TE = 30 ms; flip angle = 80^o; FOV = 192 mm; in-plane resolution = 3-mm x 3-mm; and 40 3-mm slices (0.3-mm gap) with ascending acquisition. While in the scanner, subjects completed two sessions of the ITC task (with 323 volumes acquired per session). They also completed an additional task involving the degustation of liquid rewards that is not relevant to this study (task order was counterbalanced across participants). High-resolution, whole-brain, T1-weighted structural images (TR = 1500 ms; TE = 3.05 ms; flip angle = 10^o; voxel resolution = 1 mm^3; single-shot, ascending acquisition) were also collected for each participant. These images were coregistered with the their respective EPI images to assist with the anatomical localization of the functional activations.

fMRI data preprocessing. Imaging data were preprocessed using SPM8 (Wellcome Department of Imaging Neuroscience, Institute of Neurology, London, UK). Data were corrected for motion with realignment to the mean image, spatially normalized to the Montreal Neurological Institute EPI template, resampled to 3 mm^3 voxels, and spatially smoothed using a Gaussian kernel (full-width-at-half-maximum = 8 mm). Data were also temporally filtered using a filter width of 128 s.

GLMs. We estimated two different mixed effect models of the BOLD responses, with AR(1). The models were designed to localize in our sample the areas of vmPFC and vStr that, as discussed in the introduction, have been repeatedly shown to correlate with stimulus values at the time of choice. The models are identical except for the specification of the value modulators.

The first model, GLM-1, had the following regressors of interest: 1) an indicator function beginning at the onset of each decision screen with duration equal to the reaction time for that trial, 2) the indicator function modulated by the subject specific value of each delayed offer (*dSV*), and 3) the indicator function modulated by the variable *Accept* (which equals 1 if the subject chooses the delayed outcome, and zero otherwise). The third regressor was orthogonalized with respect to the second one in order to assign any shared variance between them to the *dSV* regressor. The model also included session dummies, linear time trends, and head movements as regressors of no interest.

The second model, GLM-2, was identical except for the specification of the parametric regressor. In particular, for the reasons described in the results section, we defined a relative discounted subjective value (*rdSV*) variable, which is equal to *dSV* (and equivalent to *dSV*-25) for subjects that choose the delayed variable more than 50% of the time (15 subjects), and is equal to –dSV (equivalent to 25-*dSV*) for those that choose the immediate option more frequently (12 subjects).

Both GLMs were estimated in three steps. First we estimated the model at the individual level. Second, we calculated the following first-level single-subject contrasts: regressor 2 *vs*. baseline, and regressor 3 *vs*. baseline. Third, we calculated second-level group contrasts using one-sample t-tests on the single-subject contrasts.

We controlled for multiple comparisons at the cluster level using an individual voxel threshold of $p < 0.005$ to achieve a whole brain corrected (WBC) p-values less than 0.05 (cluster sizes are listed in each supplemental table). We also used small volume corrections (SVCs) in areas of *a priori* interest to the study of the self-control mechanisms that are at the core of the hypotheses tested here. We carried out an SVC in the vmPFC using an anatomical mask based on the AAL atlas[202] that included the rectal gyrus, medial orbitofrontal, and anterior cingulate cortex below $z = 5$ (1619 3-mm^3 voxels). A region in left dorsolateral PFC, in BA 46, has been shown to play a role in various types of self-control tasks[82,88,89]. Because anatomical masks of dlPFC lacked the required specificity to isolate this region, we carried out SVC using a mask composed of a 10-mm radius sphere centered around the target coordinates (xyz = [-36 30 27]) used by Figner and others (2010) to demonstrate a causal role of dlPFC on discounting behavior[82]. Finally, previous studies of dietary self-control have also implicated a different region of left dlPFC, in BA 9, and so we carried out SVC for activations in this area using a similar masking procedure (10 mm radius sphere centered on peak coordinate: xyz = [-48 15 24]; taken from Hare et al.[88]).

Dynamic causal modeling. We tested the hypothesis that the effective connectivity from left dlPFC-BA46 to vmPFC plays a critical role in self-control using dynamic causal modeling (DCM)[200]. The analysis proceeded in several steps.

First, for each subject we extracted average activation time courses from vmPFC and left dlPFC-BA46. In particular, for every subject we defined an ROI with a 5-mm radius, and a center given by

each subject's most significant voxel within the group ROIs. The group ROI in vmPFC was defined based on the conjunction between voxels showing an effect for the *rdSV* and *Accept* regressors from GLM-2 at an uncorrected threshold of $p < 0.005$. The group ROI in dlPFC-BA 46 was defined as all voxels showing an effect for the *Accept* regressor from GLM-2 at an uncorrected threshold of $p < 0.005$.

Second, we optimized the basic architecture of the DCM, in terms of where experimental inputs entered. To do so, we estimated 64 different DCMs that could be organized into four different families (Figure 3.5A), based on how the variables *rdSV* and *Accept* affect activity in dlPFC and vmPFC. Each family contained 16 models that varied in terms of the combinations of connectivity between vmPFC and dlPFC-BA46 as a function of three events: fixation, all choice periods, and choice periods in which the delayed option is selected.

Third, we compared each model family using Bayesian model selection[203] to determine the most likely pattern of task related inputs into dlPFC and vmPFC.

Fourth, having optimized the model inputs, we calculated the parameter estimates and posterior probabilities of the full model (i.e., the one containing coupling parameters from dlPFC-BA46 to vmPFC and vice versa for all choice types and inter-trial fixation, as shown in Figure 3.5). Parameter estimates were computed using Bayesian parameter averaging over subjects[204]. For completeness, we also tested the effective connectivity parameters from dlPFC-BA46 to vmPFC using two-tailed, one-sample t-tests against zero across individuals.

Prediction exercise. We tested the hypothesis that the effective connectivity from left dlPFC-BA46 to vmPFC predicts between-subjects differences in the discount rate using the following out-of-sample prediction exercise. For every subject, we estimated an elastic net regression (alpha

parameter = 0.3) on the other *N*-1 subjects with the log of the individual discount rates (*k*) as the dependent variable, and the complete set of estimated DCM parameters (exclusive of the hemodynamic parameters) as the independent variables. We then used the fitted coefficients from the elastic net model to predict if the discount parameter for the excluded individual was above or below the mean value for the *N*-1 subjects. The procedure was repeated for every subject. Finally, we computed the balanced accuracy of the prediction using the confusion matrix, in which the rows represent the true labels and the columns represent the predicted labels, generated by our classification results[205]. Briefly, this method controls for any imbalance in the data classes that may bias the classifier accuracy. The balanced accuracy is computed as

$$\frac{1}{2}\left(\frac{\mathrm{TP}}{\mathrm{TP}+\mathrm{FN}}+\frac{\mathrm{TN}}{\mathrm{TN}+\mathrm{FP}}\right),$$

where TP, FN, TN, and FP represent the number of true positives, false negatives, true negatives, and false positives respectively.

In order to further test the specificity of our findings, we carried out different versions of this prediction exercise, in which subsets of the DCM parameters were excluded (see the Results section for details), or other candidate regions replaced dlPFC-BA46 or vmPFC in the DCM. In all cases, we used the same fully connected DCM model with a fixed input to dlPFC-BA46 (or its replacement, when appropriate) on accepted trials and an input parametrically varying with the subjective value of the delayed reward to vmPFC (or its replacement).

Specificity test: dlPFC-BA9 to vmPFC. This test was designed to test the specificity of BA46 on the results. To do this, we repeated the DCM and prediction exercises described above using the left dlPFC-BA9 shown in Figure 3.2.

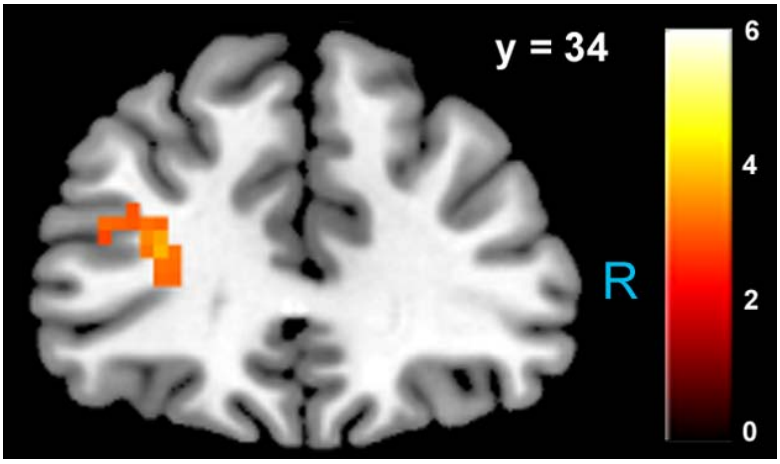

Figure 3.2. Increased activity in left dlPFC when choosing to accept larger, delayed rewards after controlling for subjective value ($p < 0.05$, SVC). The region of BA 46 shown here lies directly beneath the TMS stimulation site from Figner et al. (2010) that showed causal effects on temporal discounting behavior[82].

Specificity test: dlPFC-BA46 to vStr. Activity in vStr has often been shown to correlate with stimulus values at the time of choice, and in fact was significantly correlated with *dSV* in GLM-1. Therefore, we repeated the DCM and prediction exercise described above using the vStr ROI shown in Figure 3.3, instead of the vmPFC. The details of the analysis are identical to those described above, except that the experimental input variable *dSV* was used instead of *rdSV*. This change was based on the fact that, as described below, vStr responses at the time of choice reflected *dSV*, but not *rdSV* at the group level.

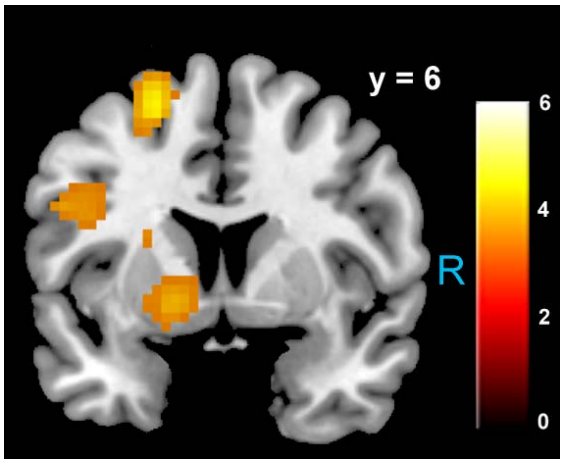

Figure 3.3. Ventral striatum region positively correlated with *dSV* in GLM-1 ($p < 0.05$, WBC).

Results

Choice behavior. We began the analysis by estimating individual discount rates (denoted by *k*) using maximum likelihood, and under the well-validated assumption that subjects exhibit hyperbolic discounting[58,90,206]. These estimates also allowed us to compute the discounted stimulus value (*dSV*) that each subject assigned to each option. As shown in Figure 3.1B, which depicts the group's psychometric choice curve, the estimated values provided a good description of the choice data. Figure 3.1C provides an ordered histogram of the estimated discount parameters (with larger values denoting more frequent choices for immediate reward), and shows that there were sizable differences across individuals in the estimated discount parameters. This is important because one of the goals of the study is to relate individual differences in brain activity to differences in discounting behavior.

Reaction times. Subjects responded well under the time limit of 3 seconds for both immediate (mean = 1.22 s, SD = 0.24 s, $t_{26} = -39.2$, $p < 0.001$) and delayed choices (mean = 1.20 s, SD = 0.25 s, $t_{26} = -37.2$, $p < 0.001$). An ANOVA on reaction times as a function of choice (accept delayed offer *vs.* take money now) and group (those who chose to wait for delayed rewards on the majority

of trials – wait group, WG – versus those who most often took the money available today – now group, NG) showed no main effects of choice or group (p=0.76 and p=0.49, respectively). However, there was an interaction between the tendency to wait and choice ($F_{(1,48)} = 4.79$, $p < 0.05$). This interaction was driven by the fact that WG subjects showed faster reaction times when choosing the delayed reward (mean = 1133 ± 70 ms) than when choosing the immediate reward (mean = 1277 ± 63 ms; $t_{14} = -3.99$, $p < 0.001$), whereas NG subjects had slower reaction times when choosing the delayed reward (mean = 1278 ± 62 ms) compared to immediate rewards (mean = 1143 ± 60 ms; $t_{11} = 2.58$, $p < 0.05$).

GLM analyses localizing the dlPFC and vmPFC ROIs. A central goal of this study was to investigate the role of effective connectivity between the area of vmPFC that has been widely associated with the computation of stimulus values at the time of choice, and an area of left dlPFC, in BA 46, that has been shown to exert a causal influence on discounting behavior in monetary ITCs and implicated in self-control processes in various domains. See the introduction and discussion for references. In order to carry out the connectivity analyses, we first needed to localize these two brain regions in our sample.

To do this, we first estimated a GLM of the BOLD responses that contained *dSV* and *Accept* (defined as 1 if the subject chose to accept the delayed option, and 0 otherwise) as parametric modulators at the time of decision (GLM-1). Based on previous studies, we expected that activity in vmPFC and vStr would correlate with the *dSV* regressor, as these areas have been shown to encode subjective values at the time of choice[207,208]. Note that in our task, the immediate option was invariant ($25), whereas the delayed option changed every trial. Therefore, all trial-wise variation affected by the value of the delayed option is driven by *dSV*, even if the brain computes relative value signals (e.g., *dSV*-25 or 25-*dSV*).

The contrast for the *Accept* regressor showed that, after controlling for *dSV*, regions of left dlPFC in BA 46 and BA 9 were more active when subjects chose the larger, delayed option ($p < 0.05$, SVC; Figure 3.2; Table S3.2). No regions were more active when declining the larger delayed reward in favor of the $25 today. Note that this increased activity when accepting delayed options is present *after* controlling for *dSV*, indicating that it does not reflect a mere tendency of the subjects to choose larger rewards more frequently (indeed 12 out of 27 subjects in our sample choose the objectively smaller reward today most often).

To our surprise, the contrast for *dSV* showed that voxels in a large cluster including vStr, but not in vmPFC, were positively correlated with *dSV* ($p < 0.05$, WBC; Figure 3.3; see Table S3.3 for a full list of activations). No regions showed negative correlations with dSV at whole brain or small volume corrected thresholds.

Given that previous studies have found evidence consistent with the encoding of relative value signals in vmPFC at the time of choice[188,209,210], we carried out an additional, post-hoc model (GLM-2). We hypothesized that there might be individual differences in the computation of the relative subjective value. In fact, a class of popular models in behavioral economics predicts that subjects will use as their reference item (i.e., the one that is subtracted when computing relative value) the option that they choose most frequently[211]. Based on this, we defined a relative discounted subjective value regressor (*rdSV*) that is given by *dSV* (equivalent to *dSV*-25) for those that chose the delayed option more than 50% of the time, and by *-dSV* (equivalent to 25-*dSV*) for those that selected the immediate option most frequently.

We estimated a new GLM (GLM-2) with *rdSV* and *Accept* as parametric modulators at the time of decision. Consistent with the post-hoc hypothesis that value computations were made relative to the most frequent choice, we found that BOLD responses in vmPFC ($p < 0.05$, SVC; Figure 3.4; Table

S3.4) and the anterior superior temporal gyri ($p < 0.05$, WBC) were positively correlated with the modified value regressor. In addition, several regions including the anterior insula (AI), dorsomedial prefrontal cortex (dmPFC), inferior parietal cortex, middle frontal gyri, and posterior cingulate showed negative correlations with *rdSV* ($p < 0.05$, WBC; Figure 3.4B; Table S3.5). Both the vmPFC region that positively correlated with *rdSV* and the portions of the AI and dmPFC that negatively correlated with *rdSV* show considerable overlap with results from recent meta-analyses[207,208] on the encoding of subjective value (Figure 3.4C and Figure 3.4D).

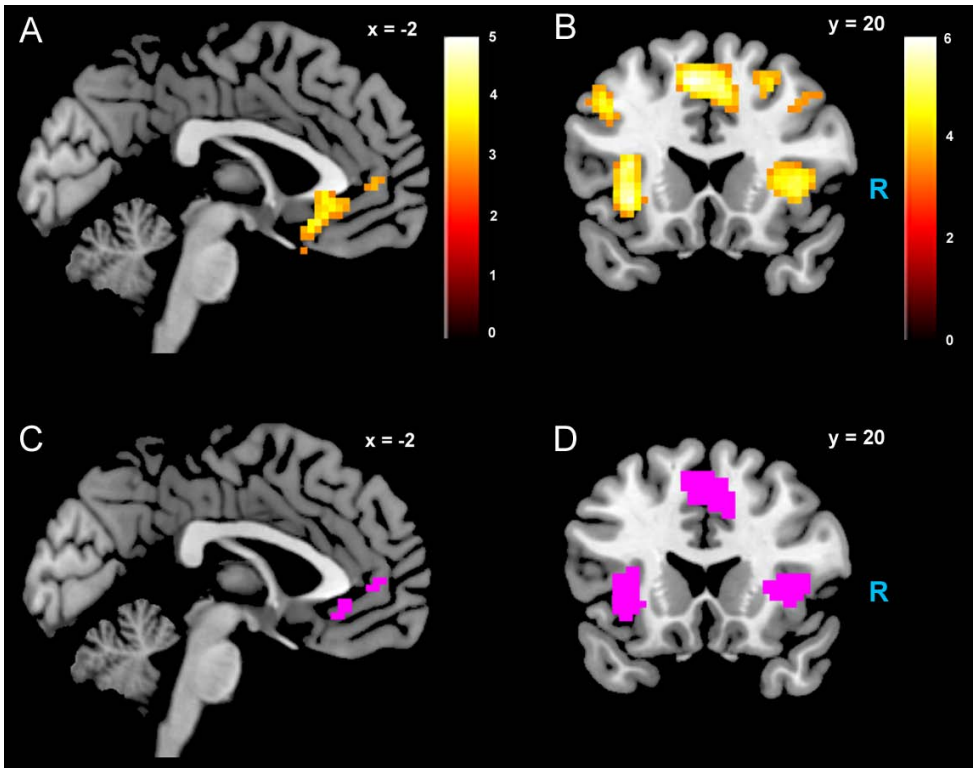

Figure 3.4. Areas correlated with the *rdSV* regressor from GLM-2. A) A region of vmPFC showing increased activity as a function of *rdSV* ($p < 0.05$, SVC). B) Regions of the dmPFC and AI where activity decreased as a function of *rdSV* ($p < 0.05$, WBC). C) Voxels in vmPFC where the activation for *rdSV* in the current study overlaps with significant voxels in meta-analyses of positive correlations with subjective value by Bartra et al.[207] and Clithero and Rangel[208]. All voxels shown in violet are significant in all three studies. D) Voxels in dmPFC and AI where responses to *rdSV* overlap with the results of meta-analyses for regions that negatively correlated 33 with subjective value at the time of choice in Bartra et al.[207] All voxels shown in violet are significant in both studies.

This overlap with previous results for both positive and negative correlations with subjective value suggests that there is significant variation between subjects in how discounted subjective values are computed, and that this computation may be related to choice frequencies (e.g., most often wait or rarely wait) consistent with our post-hoc hypothesis. Naturally, we cannot infer any causal relationships between choice frequency, and the directionality of relative discounted subjective value computations from these results; it may be that a third as yet unknown variable drives choice preference, value computation, or both. However, this analysis provides us with a sample-specific ROI of vmPFC in which to test our main hypothesis about dlPFC modulation and the prediction of individual differences.

Consistent with GLM-1, GLM-2 showed that regions of left dlPFC in BA 46 and 9 were more active when subjects chose the larger, delayed option ($p < 0.05$, SVC; Table S3.6). Just as in GLM-1, no regions were more active when declining the larger delayed reward in favor of the $25 today. Note that both GLM-1 and GLM-2 control for the value of delayed rewards in a similar manner. Since in the individual subject GLMs only the sign of *dSV* changes, the variance explained is the same in both models, and only the sign on the regression coefficients changes.

Tests of effective connectivity. Next, we used the ROIs in dlPFC-BA46 and vmPFC to test our first hypothesis; namely, that effective connectivity from left dlPFC-BA4 to vmPFC plays a critical role in delaying gratification. This test was carried out on time courses extracted from the vmPFC and dlPFC-BA46 ROIs identified in GLM-2. We focused on the ROI in BA 46, instead of the one in BA 9, because a previous TMS study found a causal role for this region in choosing to wait for larger delayed rewards in monetary ITCs[82]. Furthermore, our previous effective connectivity analyses of dietary self-control choices suggested that BA 9 might modulate vmPFC via

intermediate effects on BA 46[88]. As explained in the Methods section, the test was performed in several steps.

First, we estimated four different DCM families that were grouped based on how the experimental variables *rdSV* and *Accept* entered into the model as driving inputs (Figure 3.5A). Each family contained 16 models that varied on how the vmPFC and dlPFC-BA46 affect each other as a function of three task events: fixation, choice periods, and choice periods when the delayed option is selected.

Second, we used Bayesian model selection to identify the most likely family of models. The most likely model family (exceedance probability = 0.87), shown in Figure 3.5A, had two driving inputs: an input to vmPFC given by the *rdSV* of the delayed option on every trial, and an input to dlPFC-BA46 given by *Accept*.

Third, we examined the effective connectivity parameters between dlPFC-BA46 and vmPFC using Bayesian parameter averaging on the fully connected model (Figure 3.5B) with the most likely experimental inputs across subjects. We found increased signaling from dlPFC-BA46 to vmPFC at the time of choice, and further increases when subjects selected the later option (posterior probability > 0.90 and 0.95, respectively; Figure 3.5C). In contrast, the signaling in the other direction was not significantly different from zero. For completeness, we also compared the estimated DCM coefficients using one-sample t-tests, which lead to the same conclusion: effective connectivity parameters from dlPFC-BA46 to vmPFC increased during all choices and further increased when subjects selected the later option ($t_{26} = 2.65$ and $t_{26} = 3.80$ respectively; $p < 0.01$), but signaling in the opposite direction did not increase significantly during any task events, suggesting that there is increased connectivity from dlPFC-BA46 to vmPFC during decisions to wait for larger delayed rewards, but not in the other direction.

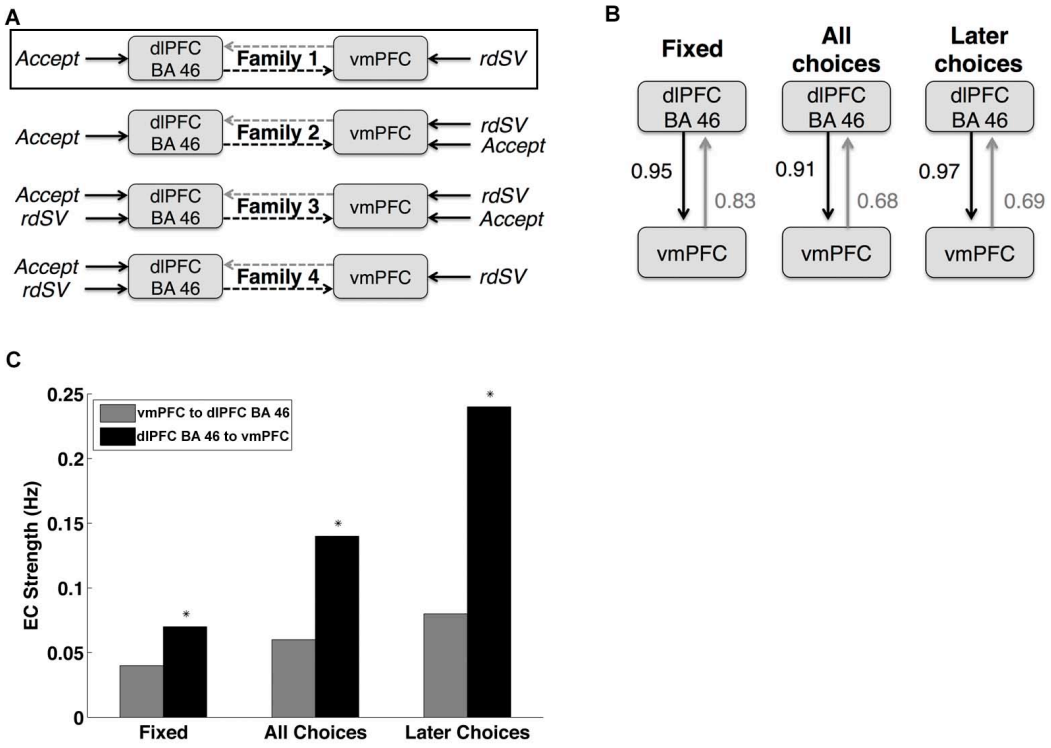

Figure 3.5. Dynamic causal modeling results. A) Schematic representations of the four DCM families compared in order to optimize the task related driving input to dlPFC-BA46 and vmPFC. Bayesian Model comparison showed that Family 1, outlined in black, was the most likely description of the data generating process. B) Diagram of the fully connected model from the most likely family showing the posterior probabilities of coupling or coupling modulation greater than zero between vmPFC to dlPFC-BA46. 'Fixed' refers to the baseline coupling during all time points. 'All Choices' refers to coupling modulation at the time of decision for all choices regardless of whether the immediate or delayed option was selected. 'Later Choices' refers to coupling modulation during only those decisions when the larger, delayed option was chosen. C) Bar chart showing the effective connectivity (EC) strengths in Hertz (Hz) between dlPFC-BA46 and vmPFC at different task periods. The colors and labels correspond to the diagram in panel B. Asterisks indicate DCM parameters that are significantly different from zero when tested using both Bayesian parameter averaging (posterior probability > 0.90) and one sample t-tests ($p < 0.01$).

Between-subjects prediction. Next, we used the results of the DCM to test our second hypothesis, namely, that it is possible to use inter-individual differences in the strength of effective connectivity between dlPFC-BA46 and vmPFC, as well as differences in local responses in those regions, to predict differences in discount rates.

For each subject we estimated an elastic net regression model using only the data from the *N*-1 other subjects, with discount rates as the dependent variable, and the estimated DCM parameters as the predictors. The estimated parameters of the model were then used to predict whether the discount rate of the excluded subject was above or below the mean of the group. The procedure was repeated to obtain a prediction for each subject. We found that the mean balanced accuracy (MBA) across all subjects was 71% correct (95% posterior probability interval = 54-85%). In addition, there was a significant correlation between discount rates predicted by the model and the discount rates estimated from the behavioral choices (Spearman's rho = 0.42, $p < 0.02$).

Next, we compared the accuracy of several versions of this prediction exercise, to test the specific role of the various components of the DCM in predicting the individual discount rates. Note that all parameters were estimated in the fully connected version of the model (shown in Figure 3.5) and were simply omitted from the elastic net regressions during these tests. The first test excluded the local driving input response parameters in vmPFC (Spearman's rho = 0.14, p = 0.48; MBA = 65%; 95% post. prob. int. = 47-80%). The second test excluded the local driving input response parameters for dlPFC-BA46 (Spearman's rho = -0.03, p = 0.90; MBA = 60%; 95% post. prob. int.= 44-76%). The third test excluded the effective connectivity parameters from dlPFC-BA46 to vmPFC (Spearman's rho = -0.12, p=0.54; MBA = 58%; 95% post. prob. int. = 41-74%). The fourth test excluded the effective connectivity parameters in the other direction (Spearman's rho = 0.02, p = 0.91; MBA = 54%; 95% post. prob. int. = 37-70%).

The logic of these tests is as follows: the prediction accuracy of a regression model that excludes a key parameter should drop. In contrast, excluding a parameter that does not play a role in ITC should not affect the model's ability to predict the discount rates. We found that omitting effective connectivity parameters between dlPFC-BA46 and vmPFC in either direction, or parameters

measuring local task induced responses within dlPFC-BA46 or vmPFC, reduced the accuracy to chance levels. Together, these findings show that the local responses in both areas, as well as both directions of effective connectivity between dlPFC and vmPFC, are critical for explaining the individual differences in discounting. Table S3.7 lists the relative size and direction of the effects of each DCM parameter on discount rates.

The vStr has also been repeatedly implicated in value-based choice and learning, and we found that this area correlated with *dSV* in GLM-1. Therefore, we repeated the prediction exercise to investigate the role of effective connectivity between left dlPFC-BA46 and vStr. The procedures and results paralleled those for vmPFC. First, we estimated a DCM paralleling that shown in Fig. 5, except that we replaced vmPFC with the vStr and used *dSV* rather than *rdSV* as a driving input, because that is the variable reflected by vStr (Table S3.8). The group ROI in vStr was defined by all voxels showing a significant effect for *dSV* in GLM-1 at $p < 0.001$ uncorrected. Second, we found that the elastic net model significantly predicted individual differences in discount rates (MBA = 75%; 95% post. prob. int. = 60-88%). Third, the discount rates predicted by the model were significantly correlated with those estimated from the behavior (Spearman's rho = 0.48, $p < 0.02$). Fourth, removing DCM parameters from the elastic net regressions also showed that both local (MBA without = 64%; 95% post. prob. int. = 47%-80%) and effective connectivity (MBA without = 48%; 95% post. prob. int. = 31%-65%) parameters were required for significant predictions. Together, these findings show that the local responses in vStr, as well as the connectivity between dlPFC and vStr, can also explain a significant portion of the variability in individual discounting rates.

Finally, we tested the specificity of these results with regard to the left dlPFC-BA46 region. We replaced left dlPFC-BA46 in DCMs using both the vmPFC and vStr with either the more posterior

left dlPFC-BA9 ROI that was also found to increase its activity when subjects chose the delayed rewards, or an ROI created by mirroring the 10-mm sphere centered on the estimated coordinates from Figner and colleagues[82] on the right hemisphere. This resulted in a total of four new DCMs and elastic net regression models. None of these combinations yielded significantly better than chance predictions (best MBA = 55%) or significant correlations with the true discount rates. The results replacing left dlPFC-BA 46 with the analogous region in the right hemisphere are consistent with previous TMS results showing that only stimulation of the left hemisphere impacted choices for the delayed monetary rewards[82].

Discussion

The results in this paper suggest that a similar set of computational and neurobiological mechanisms are at work in tasks involving dietary self-control and in monetary ITC. In particular, we found that two distinct areas of left dlPFC, in BA 9 and 46, became more active in trials in which subjects choose the delayed option, which on average requires more self-control. We also found that the connectivity from left dlPFC-BA46 to a region of vmPFC widely associated with the computational of stimulus values[207,208] increased at the time of choice, and especially during trials in which subjects chose to wait for the delayed reward. In addition, we were able to explain between-subject differences in discount rates using the estimated parameters from a DCM including the activity within dlPFC-BA46 and vmPFC or vStr, and the coupling between them, but only if the effective connectivity parameters between the two areas were included.

These results parallel previous findings in the domain of dietary choice, in which individuals chose among foods that differed in their tastiness and healthiness[88,89], although an explicit between-subject prediction exercise was not performed in those previous studies. This suggests that the mechanisms mediating self-control described in the introduction are at work in both tasks, and thus helps to advance our understanding of common computational and neurobiological components of various

forms of self-control. In this model, vmPFC computes the value of options by identifying its various attributes, assigning value to them, and then integrating them into a net value for the option. A critical component of the model is that basic attributes (like immediate monetary payoffs, or the tastiness of foods) are preferentially incorporated into the values computed in vmPFC, but that more abstract attributes (like delayed monetary payoffs, or the healthiness of foods) are generally given less weight unless left dlPFC comes online and modulates activity in vmPFC, so that it weights all attributes according to the current goals (e.g., eat healthy or maximize monetary payoff). Note that the types of attributes that need to be represented and evaluated in both types of tasks are different, but that poor self-control could be attributed to the same source in both cases: reduced weighting of abstract attributes in vmPFC in the absence of dlPFC modulation.

One limitation of the study must be emphasized. Our experiment is not able to differentiate between heterogeneity in the discount rates attributable to patience or self-control abilities (potentially mediated by differences in dlPFC functioning or connectivity), and heterogeneity due to differences in individual circumstances (e.g., immediate budgetary constraints) that are not directly associated with patience or self-control. Differences in individual circumstances, therefore, do not enter our prediction model and may be one reason why the model is less than perfectly accurate. In other words, our analysis cannot indicate if less patient subjects failed to wait for delayed rewards because they are unable to do so, or because their best option was to take the immediate monetary payout.

These results provide novel interpretations of results in the sizable literature on ITC paradigms. Consider three important examples. First, there is an on-going debate on whether or not there are multiple and competing value signals at work in self-control. In particular, previous findings[79,80] have been interpreted as suggesting that vmPFC-vStr and dlPFC compute parallel but distinct value

signals, with a vmPFC-vStr valuation system placing more value on immediate, concrete outcomes, and areas such as dlPFC computing the value of long-term, abstract goals. In this view, the quality of decisions depends on competition between the two valuation systems. In contrast, others have proposed that one value system integrates information about all stimulus attributes, both immediate and long-term, to form an overall value for the stimulus[74,212]. In this view, the quality of decision-making depends solely on the weighting of different stimulus attributes in value computation. The results here, and in previous work[88,89], suggest an obvious way of reconciling both views. In this class of tasks, choices seem to be driven by the stimulus value signals encoded in a vmPFC-based valuation system, but the activation of dlPFC is critical for the deployment of self-control because it appears to promote increased weighting of foresighted stimulus attributes in the vmPFC value signals, as evidenced by increased effective connectivity to vmPFC during larger delayed choices.

Second, our results provide a mechanistic explanation of the influential study of Figner and colleagues (2010), which found that applying inhibitory TMS over left – but not right – dlPFC-BA46 resulted in a decrease in subjects' willingness to wait for delayed rewards[82]. Consistent with the implication of a causal role for left dlPFC in self-control from these previous results, we find that this region is more active when subjects chose larger future rewards over payments on the same day, after controlling for the subjective value of the future payments. Furthermore, our data and analyses indicate that the left BA 46 region of dlPFC contributes to delaying gratification by influencing the valuation process in vmPFC at the time of choice, rather than intervening after valuation has occurred, as was suggested by Figner et al. (2010). This suggestion by Figner and colleagues was based on their finding that choices over delayed options, but not the attractiveness ratings of those delayed rewards were affected by TMS to left dlPFC[82]. However, our data on effective connectivity from dlPFC to vmPFC at the time of choice are more consistent with a mechanism in which dlPFC activity directly impacts valuation processes at the time of choice. We

note, however, that these results are not contrary to Figner and colleagues' assertion that the role of dlPFC is specific to decisions as opposed to outcome free ratings.

Third, recent EEG and fMRI studies have found that individual measurements of activity and connectivity within networks, including of left dlPFC taken at rest, exhibited a sizable correlation with discount rates taken in separate behavioral tasks[198,199]. Similarly, a study of alcoholics found that responses in left dlPFC also correlated individual discount rates[213]. Our results provide a novel mechanistic explanation for these findings. Furthermore, our prediction exercises show that measures of effective connectivity between dlPFC and vmPFC are a critical aspect of being able to predict individual discount rates.

We investigated the specificity of the dlPFC-vmPFC interactions in self-control by repeating a similar exercise replacing vmPFC with vStr or left dlPFC-BA46 with left dlPFC-BA9 or right dlPFC-BA46. The specificity test using left dlPFC-BA9 was motivated by the fact that this area was more active when subjects delayed gratification (in this task, as well as in the dietary choice experiments). However, it did not result in significant correlations with or above average predictions of between-subject discount rates. This is consistent with our previous findings in dietary self-control where dlPFC-BA9 did not directly interact with vmPFC, but rather affected a more anterior region in BA 46, near the region we find in the current monetary ITC task.

The test between dlPFC-BA46 and vStr was motivated by the fact that vStr is also an area of great interest in the field because it has been shown to be correlated with the subjective values, including those of delayed options, in this and many other studies[207,214]. In particular, the vStr is a logical target of modulation given its well known role in both reward anticipation and outcome evaluation[215-217], effort motivation[218], and successful emotional regulation[219]. In this case, we found that the pattern of results was very similar to the one for the dlPFC-BA46 to vmPFC results. There

are two natural interpretations of this finding. One is that both vmPFC and vStr are computing value signals that are modulated by left dlPFC. Another interpretation is that the modulation of vStr changes motivation, anticipation, or salience signals processed in vStr rather than value computations. Unfortunately, these two hypotheses cannot be tested against one another in the present dataset. However, previous work showing that stimulus values are more likely to be reflected in vmPFC than in vStr provides some evidence in favor of the second interpretation[75,220].

The ITC task utilized here, as well as the dietary choice task that we have used in our previous related work[88], examines the deployment of self-control in the context of goal-directed choice. Other types of self-regulation might be better characterized by competition between habitual and goal-directed systems[221-223], or by the type of response inhibition associated with action control in paradigms such as the go/no-go, Flanker, or Stroop tasks[224,225]. Future work should systematically investigate the commonalities and differences between these various sources of self-regulation. Another avenue for further investigation is our finding that subjects appear to compute the discounted subjective value of delayed rewards relative to their most common choice, perhaps viewing this as a default. While not true in every case, the majority of subjects who most often chose the immediate reward appeared to positively encode a relative value signal in vmPFC equal to the difference between the immediate reward and the larger delayed reward (i.e., \$25 - *dSV*). They also showed negative correlations with this relative value signal in a network of regions that includes dmPFC, AI, and parietal regions consistently shown to negatively correlate with SV[207]. This network has been implicated in computations related to conflict, error processing, decision difficulty, and evidence accumulation[226-231]. On the other hand, subjects who most often waited for the delayed reward frequently encoded the opposite relative value signal of *dSV* - \$25 in both sets of regions. This suggests that it is important to control for reference point variation across subjects when examining the neural correlates of subjective values at the group level.

While our findings may at first seem contradictory to previous reports where all subjects showed positive correlations with a value signal proportional to *later reward - immediate reward*, this can potentially be explained by important methodological differences. Many previous studies of ITC have customized the offer sets for each participant to maintain an acceptance rate close to 50% for all subjects[74,77,201,212]. In contrast, we purposefully utilized the same offer set for all subjects to examine individual differences in neural responses. By keeping the response rate near 50% for all subjects, these previous studies may have also generated a more homogeneous encoding of relative value in their participants, thus avoiding the heterogeneity present in our dataset. These previous datasets also highlight that, with regard to relative value computations, our findings are likely driven by choice or action probabilities rather than as a function of discount rates or self-control ability; this is because these previous datasets show that when subjects with high discount rates are presented with choices around their indifference points, they also have positive correlations with delayed reward values in vmPFC. Such changes in the directionality of relative value computations as a function of choice or action probability represent an important target for future research.

In summary, our data provide evidence that the dlPFC supports the delay of gratification by modulating activity in a vmPFC region that reflects the stimulus value of available rewards. Our between-subjects prediction results indicate that both local activity levels and connection strengths between these brain regions mediate delay of gratification tendencies in this task. These findings also suggest that examining effective connectivity parameters in pathological populations with self-control deficits may provide useful insights into the biological basis of their dysfunction.

Table S3.1. Amounts by delay.

Delay	Amount
7	25 26 28 30 32 35
10	25 26 27 29 30 32
12	25 26 28 31 33 35
14	25 26 28 32 35 39
21	26 27 29 30 32 38
25	27 29 31 33 35 46
28	26 28 32 35 39 46
30	26 27 29 30 32 38
40	27 33 35 40 47 54
45	26 29 31 35 40 46
50	27 30 35 40 46 54
60	29 33 35 40 47 54
90	26 30 33 40 46 54
95	31 33 35 40 47 54
100	26 31 38 39 46 54
150	31 33 35 40 47 54
180	27 31 35 39 46 54
200	26 28 35 39 47 54

Delays are listed in days and amounts are shown in USD.

Table S3.2. Regions more active when accepting delayed rewards controlling for discounted stimulus value in GLM-1.

Region	BA	Side	Cluster Size	x	y	z	Z
Cerebellum		R	74	27	-39	-24	4.56
Occipital cortex	30/18	L	1166	-9	-66	12	4.23*
Inferior frontal/precentral gyrus	9	L	109	-51	3	24	4.17
–Small volume corrected peak			23	-48	6	24	3.97 *s3*
Precentral/inferior frontal gyrus	6/9	R	118	36	-18	36	4.01
Precuneus	7	R	23	24	-60	36	3.92
Anterior cingulate/orbitofrontal	32/24/10	L	82	-6	30	0	3.85
–Small volume corrected size/peak			62	-3	30	0	3.59 *s1*
Caudate/putamen		L	80	-21	24	0	3.85
Thalamus		R	39	6	-6	3	3.61
Cerebellum		L	38	-54	-54	-30	3.56
Occipital cortex	18	R	86	21	-87	12	3.54
Middle/inferior frontal gyrus	46	L	38	-30	33	15	3.42
–Small volume corrected peak			15	-33	33	18	3.12 *s2*
Thalamus		R	61	21	-27	0	3.38
Middle frontal gyrus	6	R	55	30	6	54	3.36
Cerebellum		L	91	-36	-57	-27	3.36
Superior frontal gyrus	6	R	33	0	-9	72	3.28
Precentral gyrus	6	L	80	-30	-12	60	3.15
Occipital cortex	19	R	61	36	-78	-12	3.11
Medial frontal gyrus	6	L	23	-9	-6	54	3.08
Superior parietal cortex/precuneus	7	L	79	-18	-75	60	3.08
Middle frontal gyrus	10/9	R	26	36	48	30	3.03
Middle temporal gyrus	37	R	29	48	-51	0	3.02
Superior frontal gyrus	6	L	22	-24	6	75	2.98

Height threshold $t = 2.78$ ($p < 0.005$) and extent of at least 20 voxels for table inclusion
Gray highlighting and * signify that the activation survives whole brain correction ($p < 0.05$) for multiple comparisons at the cluster level.
s1 signifies that the activation survives small volume correction within an anatomical mask of vmPFC.
s2 signifies that the activation survives small volume correction within a 10 mm sphere centered on the estimated MNI coordinates from Figner et al. (2010; xyz = [-36 30 27]).
s3 signifies that the activation survives small volume correction within a 10 mm sphere centered on the MNI coordinates from Hare et al. (2009; xyz = [-48 15 24]).

Table S3.3. Regions reflecting discounted stimulus value at the time of choice in GLM-1.

Region	BA	Side	Cluster Size	x	y	z	Z score
Middle frontal gyrus	6	L	1277	-21	9	60	4.56*
Middle/inferior frontal gyrus	46	L		-36	36	15	4.06
Ventral striatum		L		-15	6	-3	3.55
Parietal lobe white matter		R	247	30	-33	27	4.18*
Caudate		R		24	-18	24	3.97
Inferior temporal lobe	19/37	L	61	-48	-57	-6	3.58
Occipital cortex	19	L		-48	-63	-12	3.47
Ventral striatum		R	151	9	6	-3	3.26
Thalamus		L		-3	-18	12	3.21
Thalamus		L		-12	-6	9	3.1
Middle frontal gyrus	10/46	R	34	42	45	21	3.13

Height threshold $t = 2.78$ ($p < 0.005$) and extent of at least 20 voxels for table inclusion.
Gray highlighting and * signify that the activation survives whole brain correction ($p < 0.05$) for multiple comparisons at the cluster level.
Labels in bold text are for the peak voxel within each cluster. Labels in plain text identify local maxima more than 8 mm apart in different anatomical regions of larger clusters.

Table S3.4. Regions positively correlated with relative discounted stimulus value at the time of choice in GLM-2.

Region	BA	Side	Cluster Size	x	y	z	Z score
Superior temporal gyrus	21/22	R	944	66	-6	-3	4.11*
Cingulate gyrus	24	R	152	3	-12	42	4.01
Superior temporal gyrus	21	L	641	-39	-9	-9	3.88*
Anterior cingulate/orbitofrontal cortex	32/24/10	L	118	-9	30	-6	3.73
–Small volume corrected size/peak			81	-9	30	-6	3.73 [s1]
Cingulate gyrus	24/31	L	165	-12	48	21	3.7
Precuneus	3/5	R	96	18	-42	45	3.5
Precuneus/cingulate gyrus	5/7	L	40	-9	-42	51	3.36
Middle temporal gyrus	39	L	32	-51	-72	21	3.08

Height threshold $t = 2.78$ ($p < 0.005$) and extent of at least 20 voxels for table inclusion.
Gray highlighting and * signify that the activation survives whole brain correction ($p < 0.05$) for multiple comparisons at the cluster level.
[s1] Signifies that the activation survives small volume correction within an anatomical mask of vmPFC.

Table 3.5. Regions negatively correlated with relative discounted stimulus value at the time of choice in GLM-2.

Region	BA	Side	Size	x	y	z	Z score
Inferior parietal lobe	40	R	624	42	-57	54	4.96*
Anterior insula/inferior frontal gyrus	13/45	R	153	36	30	3	4.85*
Dorsomedial prefrontal cortex/SMA	6/32	L	425	-6	21	48	4.84*
Superior frontal/anterior cingulate gyrus		R		12	27	39	4.84
Supplementary motor area (SMA)		R		6	18	45	4.84
Anterior insula	13	L	105	-33	21	-3	4.61*
Inferior frontal gyrus	45/47	L		-33	21	12	4.61
Middle frontal gyrus	9	L	188	-39	12	39	4.55*
Middle frontal gyrus		L		-45	21	12	4.55
Middle frontal gyrus		L		-51	33	36	4.55
Lingual gyrus/posterior cingulate	30	R	66	21	-51	6	4.45*
Precuneus	7	L	189	-12	-66	36	4.35*
Inferior parietal lobe	40/7	L	239	-33	-60	45	4.27*
Middle frontal gyrus	9/46	R	101	51	30	39	4.21*
Middle frontal gyrus		R		48	36	27	4.21
Middle frontal gyrus		R		45	18	42	4.21
Thalamus		L	29	-15	-27	12	4.12
Thalamus		L		-27	-33	12	4.12
Lateral orbitofrontal cortex	11	R	24	30	48	-9	4.06
Thalamus		R	37	9	-12	9	3.97
Pons/midbrain		R	26	0	-15	-33	3.6

Height threshold $t = 3.44$ ($p < 0.001$) and extent of at least 20 voxels for table inclusion. (A larger individual voxel threshold was used here to separate large clusters.)
Gray highlighting and * signify that the activation survives whole brain correction ($p < 0.05$) for multiple comparisons at the cluster level.

Table S3.6. Regions more active when accepting delayed rewards controlling for discounted stimulus value in GLM-2.

Region	BA	Side	Cluster size	x	y	z	Z score
Cerebellum		R	65	27	-39	-24	4.55
Inferior frontal/ precentral gyrus	9/6	L	127	-48	3	24	4.27
–*Small volume corrected peak*			24	-48	6	24	4.06 [s3]
Precentral/inferior frontal gyrus	6/9	R	205	36	-18	36	4.19*
Occipital cortex	30/18	L	1071	-9	-66	12	4.18*
Anterior cingulate/orbitofrontal cortex	32/24/10	L	102	-6	30	0	3.99
–*Small volume corrected peak*			78	-3	30	0	3.69 [s1]
Caudate/putamen		L	77	-21	24	0	3.74
Precuneus	7	R	20	24	-60	36	3.7
Thalamus		R	47	6	-6	3	3.66
Cerebellum		L	35	-54	-54	-30	3.51
Occipital cortex	18	R	80	24	-87	9	3.45
Thalamus		R	64	21	-27	0	3.38
Middle/inferior frontal gyrus	46	L	40	-30	33	15	3.37
–*Small volume corrected peak*			18	-33	33	18	3.10 [s2]
Cerebellum		L	84	-36	-57	-27	3.36
Superior frontal gyrus	6	R	35	0	-9	72	3.29
Superior parietal cortex/precuneus	7	L	114	-18	-75	60	3.29
Middle frontal gyrus	10/9	R	41	36	48	30	3.21
Precentral gyrus	6	L	134	-33	-12	60	3.15
Medial frontal gyrus	6	L	20	-9	-6	57	3.13
Middle temporal gyrus	37	R	37	48	-51	0	3.09
Occipital cortex	19	R	51	36	-78	-12	3.03

Height threshold $t = 2.78$ ($p < 0.005$) and extent of at least 20 voxels for table inclusion.
Gray highlighting and * signify that the activation survives whole brain correction ($p < 0.05$) for multiple comparisons at the cluster level.
[s1] signifies that the activation survives small volume correction within an anatomical mask of vmPFC.
[s2] signifies that the activation survives small volume correction within a 10-mm sphere centered on the estimated MNI coordinates from Figner et al. (2010; xyz = [-36 30 27]).
[s3] signifies that the activation survives small volume correction within a 10-mm sphere centered on the MNI coordinates from Hare et al. (2009; xyz = [-48 15 24]).

Table S3.7. Regression coefficients predicting log(*k*) as a function of DCM parameters.

Task period	DCM parameter	vmPFC model	vStr model
Fixed			
	v → d	9.6	-0.2
	d → v	-22.5	-2.8
All choices			
	v → d	-75.3	-128.5
	v self	-6.7	19.4
	d → v	59.9	73.9
	d self	-13.3	-15.3
Later choices			
	v → d	43.6	87.7
	v self	2.4	-47.5
	d → v	-14.4	-64.3
	d self	-10.8	22.4
Driving inputs			
	Value → v	7.8	7.5
	Accept → d	21.4	24.7

This table reports the regression coefficients from two elastic net regressions using the DCM parameters specified above to predict discount rates (log(*k*)). Comparing the coefficients across parameters shows the relative size and direction of the effects of each DCM parameter on discount rates. See the main text of the results section for quantification of the influence of each parameter on the model's ability to predict discount rates.
Note that smaller k values indicate lower discount rates and, therefore, parameters with negative regression coefficients increase the likelihood of choosing delayed reward options in our temporal discounting paradigm.
These regressions are identical to those used in the prediction exercises described in the main text except that they were run with all 27 subjects at once. The regressions were estimated using the DCM parameters for both functional MRI runs separately, and the values listed in this table represent the average of coefficients across runs for conciseness and clarity.

The labels 'Fixed,' 'All choices,' 'Later choices,' and 'Driving inputs' correspond the portions of the DCMs described in the main text and shown in Figure 5.
The label 'v → d' refers to signaling from vmPFC (column 3) or vStr (colum4) to dlPFC-BA46. The label 'd → v' refers to signaling from dlPFC-BA46 to vmPFC (column 3) or vStr (colum4). The label 'v or d self' refers to the parameters for the inhibitory self-connections to each region at the specified time points. The label 'Value → v' refers to an input equal to *rdSV* from GLM-2 into vmPFC or *dSV* into vStr. The label 'Accept → d' refers to an input equal the *Accept* regressor specifying later choices in both GLM-1 and GLM-2.

Table S3.8. Group-averaged DCM parameters for the model including ventral striatum and dlPFC-BA46.

EC direction	Fixed	All Choices	Later Choices
vStr → dlPFC	0.21 ($P_c = 1$)	+0.06 ($P_m = 0.88$)	+0.05 ($P_m = 0.85$)
dlPFC → vStr	0.18 ($P_c = 1$)	+0.07 ($P_m = 0.90$)	+0.06 ($P_m = 0.90$)

P_c = probability that the absolute value of the coupling parameter is greater than zero (rounded to two decimals).
P_m = probability that the coupling parameter is modulated by task condition (rounded to two decimals).
Task input parameters for discounted subjective value as in GLM-1 to vStr and later choices to dlPFC-BA46 were (0.04, P = 1; 0.02, P = 1), respectively.

Chapter 4

INDIVIDUAL DIFFERENCES IN TEMPORAL DISCOUNTING AND THE NEURAL REPRESENTATION OF IMAGINED REWARDS*

Human and non-human animals generally discount the value of delayed rewards, but there are large individual differences in the steepness of this discount function. Although widely studied across the social and biological sciences, many questions about the psychological and neurobiological processes that underlie these differences in temporal discounting behavior remain unresolved. One potential factor affecting temporal discounting behavior is the ability to imagine experiencing a reward. Here, we present the results of an fMRI investigation of the relationship between individual differences in the temporal discounting and neural response in a task where the receipt of primary liquid rewards was imagined. We found that, compared to consumption, imagining rewards elicited neural response in regions that have been implicated in the processing of both real and imagined rewards. Participants who showed relatively greater activity in two of these regions, lateral OFC and vmPFC, when imagining the current consumption of juice rewards had shallower discount rates when choosing between immediate and delayed monetary rewards. Critically, there was no aspect of temporal delay or choice in the juice reward task, suggesting that the process of imagining rewards may be a more basic ability that is utilized during intertemporal decision making.

Introduction

The ability to delay gratification is an important factor in success at the personal and species-wide levels[102,232]. We frequently encounter choices with potential outcomes that can occur immediately or in the distant future, and often, waiting pays off in terms of health, wealth, and well-being. Despite the logical appeal of forgoing a smaller reward now to obtain a larger reward later, individuals do

* Work done in collaboration with Todd Hare and Antonio Rangel.

not always make the optimal decision and instead, show a tendency to discount the value of delayed rewards[90,183].

Behavioral studies of temporal discounting have shown that there is considerable variation across individuals on their ability to postpone gratification in order to obtain larger delayed rewards (e.g.,[59,90]). One hypothesis suggests that this variation may be due in part to individual differences in the ability to represent the value of future rewards. The human ability to imagine future episodes vividly[101] may contribute to ITC by allowing individuals to experience an event's (undiscounted) reward value at the time of decision, facilitating self-control behavior[54,77,106].

Recent neuroimaging work has addressed the role of episodic prospection in delay of gratification using ITC tasks. Peters and Büchel (2010) demonstrated that participants made more patient, future-minded choices when presented offers paired with self-generated episodic events in a delay discounting task, where high-imagery participants discount rate was on average 16% lower than that of low-imagery participants. This "episodic tag effect" was represented in regions including the vmPFC and was correlated with neural signals associated with subjective value in the anterior cingulate cortex[77]. Similarly, Benoit and colleagues (2011) manipulated the framing of the circumstances under which a future reward would be received; they found that, compared to estimating what a particular offer might be able to purchase, imagining spending that amount resulted in significantly attenuated temporal discounting. Moreover, participants reported higher emotional and experiential intensity for imagined spending trials. Associated neuroimaging data revealed that the mPFC was widely activated during imagining, and that a locus in rostral mPFC reflected the modulation of the imagination effect by reward magnitude[106]. Together, these data demonstrate that the use of episodic imagery at the time of choice activates prefrontal reward networks and enhances future-oriented decision making. These studies do not, however,

demonstrate whether it is the episodic nature of the imagery during decision making or rather a more fundamental property of reward representation that drives the effect of imagery on ITC.

In the present study, we examined the relationship between the ability to imagine the receipt of a primary rewards in a non-choice context and intertemporal decision making. Participants completed an fMRI experiment where they either imagined the receipt of a liquid reward (fruit juice) or actually consumed the liquid. Separately, these individuals also completed an ITC task, which allowed us to estimate each individual's discount rate, a parameter that reflects the degree to which an individual is able to delay gratification. We sought to determine the extent to which individual discount rate was associated with the strength of the neural representation of imagined reward, predicting that neural response in regions involved in representing reward imagery would be associated with the ability to delay gratification.

Methods

Participants. A total of 37 individuals participated in the study. Six people were excluded because their experimental data were corrupted or their choice patterns did not allow us to accurately estimate discount parameters. A single subject was excluded from the experiment because of excessive head movement (≥ 2 mm in translation or rotation). Thirty healthy individuals were included (22 males; mean age, 24.2 years; age range, 19-40 years). All participants had normal or corrected-to-normal vision, no history of neurological, psychiatric, or metabolic illness, and were not taking any medications that interfere with the BOLD signal at the time of scanning. The Institutional Review Board at the California Institute of Technology (Pasadena, CA) approved the methods and procedures used in this study.

ITC task. The ITC task is described in detail elsewhere (see Chapter 3). Briefly, on each trial, participants were instructed to choose between earning a smaller amount of money today and a

larger amount at some time in the future. The smaller, sooner offer was always $25 while the larger later offer ranged from $25 to $54; the delays ranged from 7 to 200 days in the future.

We estimated an individual discount factor (denoted by k) for each subject using maximum likelihood procedures. Specifically, we assumed that participants assigned value to the delayed options using a hyperbolic discounting function, in which the value of \$$A$ with a delay of D days is given by

$$dSV = A/(1+kD),$$

where dSV denotes the discounted stimulus value. We also assumed that the probability of accepting the delayed option is given by the soft-max function

$$P(\text{Yes}) = (1+exp(b*(25 - dSV)))^{-1},$$

where b is a non-negative parameter that modulates the slope of the psychometric choice function. Note that in this formula the value of the constant reference option is $25.

Imagine task. Upon arriving for the experiment, participants completed a survey that assessed their preference for three fruit juices (apple, grape, or fruit punch) and their current level of thirst. The most preferred juice was used during the subsequent neuroimaging experiment. The experiment involved the imagined (Imagine) or real consumption (Consume) of water and the preferred juice inside the scanner. Water and juice were randomly assigned to either a blue triangle or an orange square. These shapes served as cues that identified the type of liquid that would be delivered in each trial. After receiving detailed instructions, participants were allowed several practice trials to become familiar with receiving liquid rewards in the scanner.

At the onset of each trial, a stimulus, that consisted of the colored shape cue surrounded by either a gray rectangle (Consume) or a gray thought bubble (Imagine), appeared onscreen for 4 s (Figure 4.1B).

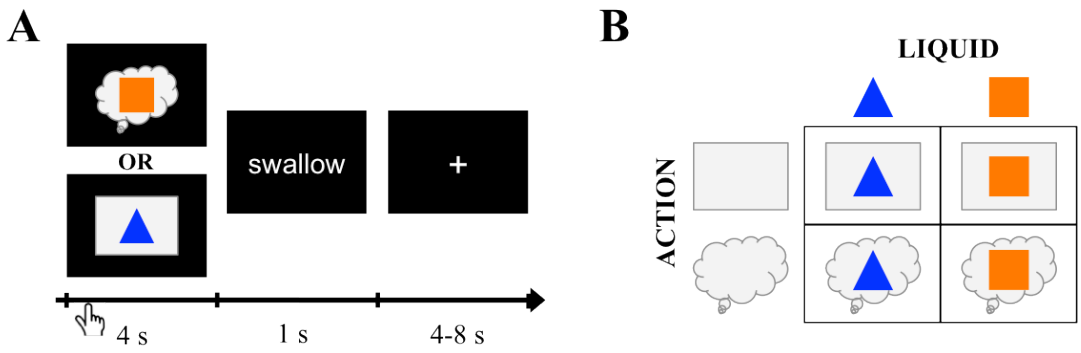

Figure 4.1. Task diagram. A) Individual trial sequence. B) Reward type (juice or water) was signaled by orange square or blue triangle cues. A light gray square or thought bubble surrounding the cue indicated either real or imagined consumption of the liquid rewards.

Participants were instructed to press a button as soon as they had recognized the meaning of the cue (i.e., whether it signaled a juice or water trial); the assignment of each liquid to either the left or right button was randomized across subjects. This procedure ensured that participants were attending to both the onset of the stimulus and the type of cue. In Consume trials, the delivery of 0.75 mL liquid was initiated at trial onset and reached the mouth after a delay of ~200 ms. Participants were instructed to "fully taste the liquid" for the duration of the cue. In Imagine trials, no liquid was delivered. Nonetheless, participants were instructed to behave as they did in the Consume trials. Thus, they were to *imagine* tasting the liquid, and concordantly "taste" and "swish around" the imaginary liquid. Again, participants were instructed to taste the liquid for the entire period that the cue was onscreen. In both trial types, participants were instructed to swallow either the real or imaginary liquid when the word 'swallow' appeared onscreen. (Instructions are detailed in Appendix B.) Each trial was followed by a fixation period (mean = 6 s; range = 4-8 s; Figure

4.1A). There were 120 trials in total (30 per condition) divided into eight experimental blocks, and each block of either Imagine or Consume was comprised of 15 trials with a mix of both juice and water trials. Both block order and stimulus presentation order within blocks were randomized across participants.

Following the fMRI session, participants completed a questionnaire to assess their perceived level of success in the task (see Appendix C). Using a 10-point, anchored scale (1 = "not successful at all," 5 = "somewhat successful," 10 = "extremely successful"), each individual reported how successful he or she felt at imagining tasting the liquid overall and separately for water and juice. Additionally, participants were asked to report how similar the experiences of imagining and consuming were both overall and separately for each liquid, where (1 = "not similar at all," 5 = "somewhat similar," 10 = "extremely similar"). The similarity ratings were not obtained for one subject.

Imaging data acquisition. Functional imaging data were collected using a Siemens (Erlangen, Germany) 3.0 Tesla Trio MRI scanner. Using an eight-channel, phased array head coil, we collected gradient echo, T2*-weighted EPI images with BOLD contrast. In order to optimize BOLD sensitivity, we used a tilted acquisition in an orientation 30^{o} oblique to the AC-PC line[159]. The imaging parameters were as follows: TR = 2500 ms; TE = 30 ms; flip angle = 80^{o}; FOV = 192 mm; in-plane resolution = 3 mm x 3 mm; and 40 3 mm slices (0.3 mm gap) with ascending, interleaved acquisition. The first four volumes of each run were discarded to allow for sufficient time for the magnetic field to achieve steady-state magnetization. Task order was counterbalanced across participants over two sessions (285 volumes per session). High-resolution, whole-brain, T1-weighted structural images (TR = 1500 ms; TE = 3.05 ms; flip angle = 10^{o}; voxel resolution = 1 mm^3; single-shot, ascending acquisition) were also collected for each of the participants. These

images were co-registered with the their respective EPI images to assist with the anatomical localization of the functional activations.

fMRI data preprocessing. Imaging data were preprocessed using SPM8 (Wellcome Department of Imaging Neuroscience, Institute of Neurology, London, UK). Data were corrected for motion with realignment to the mean image, spatially normalized to the Montreal Neurological Institute EPI template and resampled to 3 mm^3 voxels, and spatially smoothed using a Gaussian kernel (full-width-at-half-maximum = 8 mm). Data were also temporally filtered using a filter width of 128 s. All images were visualized using MRIcron software (http://www.sph.sc.edu/comd/rorden/mricron/).

GLM. First, we estimated a GLM with AR(1) for each individual. We specified five regressors, one for each of the possible trial conditions (i.e., R1: Consume Water, R2: Consume Juice, R3: Imagine Water, R4: Imagine Juice) and one for all Swallow (R5) trials. All events were modeled with their full stimulus duration (4.22 s for R1-4 and 1 s for R5). Motion parameters and session constants were also included as regressors of no interest.
At the first level, we computed contrasts for regressors R1-4, the main effect of [Imagine - Consume], and contrasts for imagining versus consuming juice controlling for responses to water [(Imagine Juice - Imagine Water) - (Consume Juice - Consume Water)]. These contrasts were entered into a 2x2 ANOVA, one-sample t-tests, or between-subject correlations with discount rate at the second level. We corrected for multiple comparisons across the whole brain using Gaussian Random Field Theory at the cluster level ($p < 0.05$) with an individual voxel threshold of $p < 0.001$. For completeness, we also report all clusters with an extent greater than 10 voxels at $p < 0.001$ in Table 4.1 and Table 4.2.

Between-subject correlations with the discount parameter *k* and contrasts estimates from ROIs (defined by separate and independent studies) were computed in MATLAB (Version 8.0.0.783, The MathWorks, Inc., Natick, Massachusetts).

Results

Behavioral Results. Post-task ratings suggested that participants were able to perform the imagination and liquid reward task as instructed. Participants indicated that they felt at least somewhat successful in imagining the receipt of liquid rewards during the Imagine trials (mean success rating = 5.67, SD = 1.97; rating of 5 = "somewhat successful") and that the experience of imagining was similar to actually receiving the liquids (mean similarity rating = 5.97, SD = 1.59; rating of 5 = "somewhat similar"). Lastly, the pleasantness ratings for juice and water receipt demonstrated that, at the group level, participants found the juice to be significantly more pleasant than water (juice: mean = 5.83, SD = 0.83; water: mean = 4.83, SD = 1.53; $t_{29} = 2.86$, $p = 0.008$).

Discount rates (*k)* for future rewards were computed based on the choices made during a separate ITC task using a standard hyperbolic model as described in Chapter 3. This parameter represents the degree to which an individual discounts or reduces the value of rewards obtained at a later date, and thus smaller values of *k* indicate a greater willingness to delay gratification. The discount parameters in the current sample ranged from 0.0005 to 0.0267 (mean = 0.0079, SD = 0.0069).

fMRI Results. We computed a 2x2 ANOVA to identify regions showing main effects or interactions of the factors action (Consume, Imagine) and liquid (Juice, Water). While there were main effects of action (depicted in Figure 4.2; $p < 0.05$, whole-brain corrected), there were no significant effects for liquid or any interactions after correction for multiple comparisons. Areas in the prefrontal, parietal, occipital, and fusiform cortices were more active during Imagine compared

to Consume trials (Table 4.1), while bilateral regions of the insula showed more activity for Consume versus Imagine trials (Table 4.2).

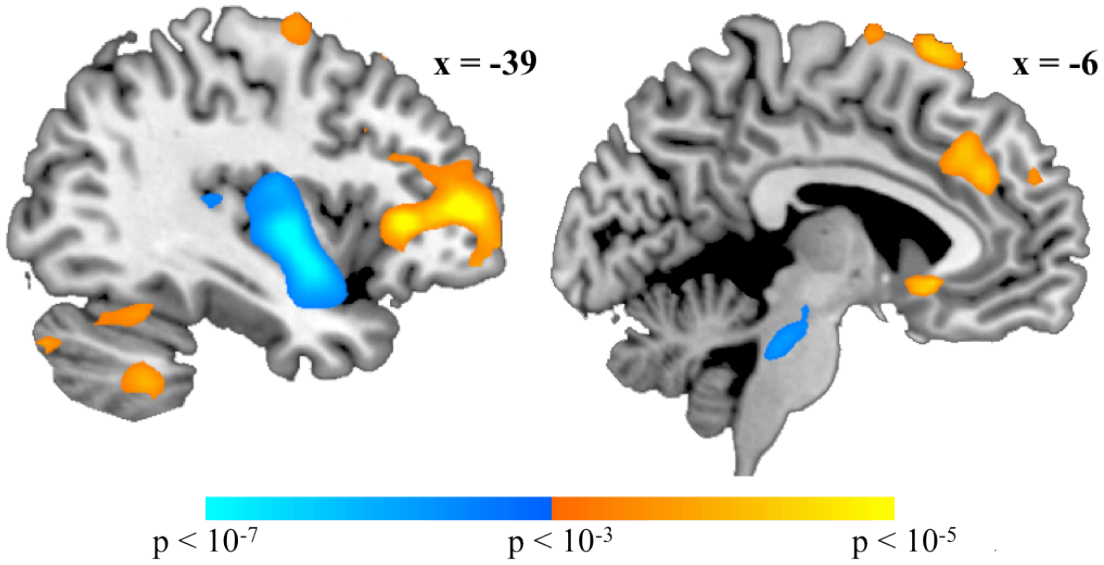

Figure 4.2. Voxels showing a significant difference between real and imagined consumption of liquid rewards. The warm color scale depicts voxels that are more active during the Imagine condition compared to Consume, while the cool color scale shows voxels that are more active during Consume compared to Imagine.

Region	k	BA	x	y	z	Peak Z score
Left ventrolateral prefrontal cortex	618	10/46/47	-39	38	9	4.68*
Right inferior parietal lobule	136	39/40	51	-75	42	4.67*
Left middle occipital gyrus	104	19	-48	-69	-12	4.64
Supplementary motor cortex	147	6	-3	18	72	4.31
Extrastriate cortex	171	18/19	6	-99	36	4.27
Right fusiform gyrus	472	19/37	51	-69	-15	4.14*
Right precentral gyrus	25	6	54	-3	60	4.11
Subgenual cingulate cortex	51	25	-6	21	-6	3.99
Dorsomedial prefrontal cortex	290	9/32	-3	30	36	3.93*
Right cerebellum	22		18	-39	-60	3.78
Left middle temporal gyrus	10	21	-69	-33	-15	3.75
Right ventrolateral prefrontal cortex	30	47	48	30	3	3.74
Right middle frontal gyrus	11	10	42	54	-3	3.74
Left cerebellum	149		-39	-51	-45	3.67
Left inferior parietal lobule	24	39	-51	-78	33	3.62
Left precentral gyrus	30	6	-42	-3	66	3.61
Right cerebellum	27		36	-84	-33	3.54
Right precentral gyrus	17	6	33	12	72	3.53
Right middle temporal gyrus	30	21	57	-45	-3	3.51
Precuneus	12	7	3	-57	72	3.42
Left superior frontal gyrus	15	8	-33	24	54	3.41
Paracentral lobule	15	3	-3	-27	81	3.38
Left precentral gyrus	17	6	-36	9	66	3.36
Right caudate	10		9	21	9	3.33
Left middle temporal gyrus	11	37	-57	-51	-12	3.30

Table 4.1. Regions more active for Imagine compared to Consume.
All results are reported at $p < 0.001$, uncorrected, with cluster extent ≥ 10 voxels.
* Whole-brain corrected for multiple comparisons ($p < 0.05$) at the cluster level (minimum cluster size = 88 voxels). k = cluster size. Coordinates reported in MNI space.

Region	k	BA	x	y	z	Peak Z score
Right insula	306	13	39	-3	3	5.77*
Left insula	462	13	-42	-6	3	5.43*
Pons	166		9	-27	-24	4.51
Posterior cingulate gyrus	17	31	-18	-27	45	4.24
Right precentral gyrus	18	6	24	-6	51	3.78
Right supramarginal gyrus	20	40	42	-32	42	3.61
Left postcentral gyrus	28	4	-63	-21	27	3.42
Right postcentral gyrus	21	2/3	57	-21	27	3.42

Table 4.2. Regions for active for Consume compared to Imagine.
All results are reported at $p < 0.001$, uncorrected, with cluster extent ≥ 10 voxels.
* Whole-brain corrected for multiple comparisons ($p < 0.05$) at the cluster level (minimum cluster size = 88 voxels). k = cluster size. Coordinates reported in MNI space.

Discount rates and neural responses to imagined reward. To test our main hypothesis that the ability to simulate reward receipt through imagination is associated with the degree to which future rewards are discounted, we conducted two between-subjects correlations for imagining versus consuming juice, controlling for water, and the estimated discount parameter k. We computed this correlation in ROIs defined on the basis of previous, independent reports on the neural activity associated with the hedonic value of liquid rewards and the imagination of reward receipt. The first region was defined as a sphere (radius = 10 mm) centered on the peak coordinates (MNI xyz = [0 33 -21]) in a vmPFC region that was modulated by imagining reward receipt in a previous study[233]. This analysis was designed to test whether individuals who where more willing to wait for future monetary payments (i.e., had lower discount parameters) showed increased neural activity for imagined rewards in a region previously implicated in imagining rewards; there was a negative correlation between k and BOLD response in this region (Pearson's $r = -0.36$; one-tailed $p = 0.026$; Figure 4.3A). The second region was defined as a 10-mm radius sphere centered on the peak response (MNI xyz coordinates = [38 42 -10]) in right lateral orbitofrontal cortex (lOFC) for

receiving preferred liquid rewards[234]. This analysis was designed to test whether subjects with lower discount parameters had increased neural activity for imagined rewards in a region sensitive to the actual receipt of liquid reward. In support of this hypothesis, we found a negative correlation (Pearson's r = -0.40; one-tailed p = 0.01) between discount parameters and the difference between imagined and real juice rewards [(Imagine Juice - Imagine Water) - (Consume Juice - Consume Water)] (Figure 4.3B).

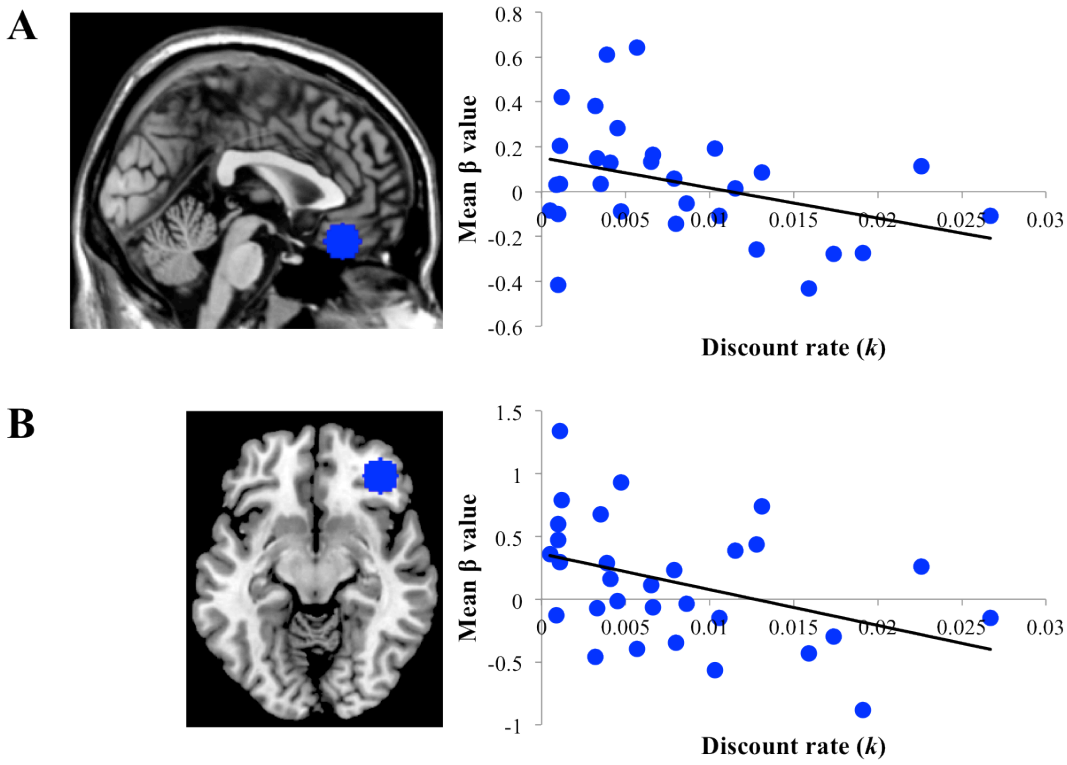

Figure 4.3. Imagination and discounting. Scatter plots depicting the relationship between the contrast coefficients for [(Imagine Juice - Imagine Water) - (Consume Juice - Consume Water]) averaged across the (A) vmPFC and (B) right lOFC regions of interest.

It should be noted that although the k parameters were not normally distributed, the Pearson correlation method does not assume normality and, therefore, we did not apply any transformations to the k parameters. Nonetheless, calculating the correlations with k using the non-parametric, rank-

dependent Spearman method yields results that are consistent with the Pearson correlation for these data (vmPFC: Spearman's rho = -0.32, one-tailed p = 0.040; lOFC: Spearman's rho = -0.39, one-tailed p = 0.016).

For completeness, we also conducted a whole-brain, between-subjects correlation analysis with the discount parameters and the contrast of imagining versus consuming juice after subtracting out the water control from both conditions. There was one significant cluster spreading across the thalamus and midbrain (peak Z = 4.48, MNI xyz coordinates = [-3 -18 -3]) showing a negative correlation with *k* that survived whole brain correction at $p < 0.05$. There were no regions that showed significant positive correlations with *k* after correction for multiple comparisons.

Discussion

We investigated the brain-behavior associations underlying the ability to imagine the receipt of a primary reward and temporal discounting behavior. Consistent with the hypothesis that individuals who generate greater neural responses for imagined rewards would show greater propensity to delay gratification, we found that temporal discounting was negatively correlated with brain activity in regions previously associated with the processing of both real and imagined rewards[24,233-236]. These data suggest that the strength of the neural representation of imagined rewards may drive individual differences in real-world economic decision-making.

Neural response to consumption and imagination of rewarding liquids. Compared to Imagine trials, Consume trials exhibited greater neural response in bilateral insula. While the responses elicited by our task do not extend to the primary gustatory areas of anterior insula/frontal operculum[237] (AI/FO), they are centered in regions of the insula thought to be involved in interoception, or awareness of the physiological state[167,168]. One possible explanation for the lack of primary gustatory cortex activation for Consume compared to Imagine is the relative infrequency of

neurons responsive to taste or tactile stimulation of the mouth in AI/FO (6% and 4% of neurons, respectively, compared to 24% sensitive to mouth and jaw movements)[238]. Note that participants were instructed to keep their head and jaw as still as possible while performing the same "swishing" movements inside the mouth in both the Consume and Imagine conditions. The similarity of mouth movements, therefore, may have obscured any differences between conditions in primary gustatory cortex.

In contrast, compared to consumption, imagining the receipt of an appetitive liquid activated a distributed network of both cortical and subcortical regions, with particularly significant activations in left vlPFC, right inferior parietal lobule, right fusiform gyrus, and dorsomedial PFC. These data are consistent with the findings of a recent meta-analysis of neuroimaging studies of sensorimotor imagery, which reported regions involved in both modality-general and gustatory-specific imagery[239]. Moreover, our findings, which suggest that the coordination of a variety of higher-order areas facilitates imagery processes, are aligned with McNorgan's theory (2012) positing that imagery generation depends mainly on the recruitment of "upstream […] unimodal convergence zones," rather than primary sensory cortices[239].

Relationship between temporal discounting and imagined reward. Study participants exhibited a wide range of temporal discounting behavior, and these differences in willingness to wait were correlated with significant variation in BOLD responses in lateral OFC and vmPFC regions previously associated with processing both real and imagined rewards. A negative correlation between the willingness to delay gratification (as indexed by discount rate) and neural responses to imagined rewards was identified in right lOFC, a region that has been shown to respond to the actual receipt of liquid rewards[234], and during the anticipation of primary rewards[240], suggesting that this region may play a role in evaluating both expected and received primary rewards. A similar

relationship between neural response and discount rate was seen in a vmPFC region previously implicated in the representation of imagined rewards[233,241], such that increased willingness to delay gratification was associated with an enhanced response for imagining compared to consuming a rewarding liquid. Bray and colleagues (2010) have previously shown that vmPFC is activated when imagining rewards, but not when imagining visual motion or motor actions[233], and neural activity in vmPFC has been linked repeatedly to the processing of primary and secondary reward values at the time of decision making in addition to reflecting reward outcome or receipt (e.g., [75,136,193,194,242-244]). Moreover, prior expectations have been found to influence vmPFC responses to the receipt of appetitive liquids[245]. Plassmann and colleagues showed that cognitive expectations developed from information about the price of wines could modulate responses in vmPFC to wine consumption and that these vmPFC responses scaled with subjective pleasantness ratings. Together, these previous results are consistent with the idea that vmPFC is involved in computing the pleasantness or utility of outcomes and can be influenced by both the presence and expectation of rewards. In light of our current data, these findings suggest that a greater ability to imagine and simulate rewarding experiences in vmPFC – regardless of when these rewards occur – can reduce the discounting of future outcomes.

Our data complement and extend previous findings on the role of imagery and time perception in ITC. Two neuroimaging studies[77,106] have shown that enhancing the concreteness and vividness (i.e., aiding imagination) of a future outcome at the time of choice enhanced hippocampal-prefrontal interactions and reduced discount rates. We demonstrate an association between imagining the experience (i.e., consuming right now) of primary rewards in the absence of choice and monetary discounting behavior in a separate ITC task. Note that unlike these previous studies, which enhanced the vividness of future monetary outcomes to reduce discounting, our data link individual differences in reward imagination across modality (juice versus money) and time (now versus

future) to discount rates. These findings suggest that a fundamental ability to imagine the utility of both present and future outcomes may enhance the ability to delay gratification and promote optimal choice behavior. Another recent study[246] has shown that BOLD responses in the ventral striatum and vmPFC during the evaluation of temporal durations (e.g., 28 days), also in the absence of choice, are correlated with temporal discounting rates. Thus, individual differences in the neural representation of imagined reward consumption and the perception of delays are predictive of individual differences in delay of gratification behaviors. Interestingly, both reward imagination and delay perception predict ITC behavior when measured in the absence of actual choices, making them potentially useful diagnostic measures when choice behavior cannot be collected for ethical or practical reasons. The cognitive and neurobiological processes of both reward imagination and delay perception present intriguing targets for future research on temporal discounting behaviors and potential avenues for therapeutic interventions aimed at improving the ability to delay immediate gratification in favor better long-term outcomes.

Chapter 5

CONCLUSIONS

Defining goals and implementing the appropriate behaviors necessary to achieve them are central functions of human cognition. The PFC is crucial for such goal-directed decision making, and its comparatively large size[247] and richly elaborated connections to other brain regions are thought to be critical to the relative success of both human and non-human primates[10]. Functional and structural neuroimaging in behaving humans has provided compelling support for this theory, showing that regions of the PFC are important for a wide variety of learning and decision making paradigms, especially when cognitive control is required[4,10]. Nonetheless, the diverse range of prefrontocortical functions and the many methods used to study them have left many aspects of the neurobiology of cognitive control uncharacterized, particularly with respect to individual differences in cognitive control ability. The work described in this thesis provides additional functional evidence for the role of the PFC in cognitive control, describing how learned automaticity impacts prefrontocortical flexibility in implementing cognitive control (Chapter 2) and also elaborating the nature of neural processes and connections involved in delaying gratification in ITC (Chapters 3 and 4).

One critical role of the PFC is to organize behaviors using hierarchical rules[85,248,249], providing a framework for the optimization of behavior through goal prioritization. Crucially, this system is robust to environmental changes, and cognitive control can be implemented quickly and flexibly in response to changes in reward contingency. Response inhibition is central to cognitive control, facilitating the execution of context-appropriate, goal-directed behaviors through the suppression of inappropriate responses. In Chapter 2, we showed that the right vlPFC – a region that has consistently been implicated in response inhibition – plays an important role in suppressing these

competing responses, even as they become more automatic with increasing exposure over time. Specifically, as automaticity emerges in response to frequent events, cognitive control ability for relatively rare events develops with exposure to infrequent events, and this enhanced performance is associated with a neural efficiency signal (i.e., a decrease in BOLD signal with learning over time) in right vlPFC. These data suggest that individual differences in cognitive control ability – especially with respect to the capacity to adapt behavior to a rapidly changing environment – may be modulated by the extent to which learning of cognitive control is encoded efficiently in right vlPFC. Future work will be necessary to validate this theory further.

The PFC is also able to negotiate decisions that involve the assessment of outcomes that are less immediate and more abstract (e.g., choosing a healthy food item to support a long-term weight loss goal). Cognitive control is critical for these decisions, particularly in light of the extensive evidence demonstrating that humans[67,68] and other species[60,62,65,66] exhibit a strong tendency towards temporal discounting. The reciprocal connections between subcortical regions and PFC[7-9] are thought to facilitate cognitive control in situations such as intertemporal choice[10,77,82], allowing for top-down modulation of emotion and reward circuitry by PFC. Using dynamic causal modeling – a technique that allows for the estimation of *directional* effective connectivity between regions[200] – we were able to describe the functional nature of the circuit between left dlPFC and vmPFC during ITC. We found that the strength of the unidirectional, modulatory connection from left dlPFC to vmPFC, is enhanced at the time of choice only in trials when the delayed option is chosen. The strength of this connection was also predictive of individual behavior, again demonstrating a link between brain and behavior. Moreover, these data support a neurocomputational model of cognitive regulation of the self that is consistent with both intertemporal[74,79,80,212] and dietary choice[88,89]; this parsimonious model offers a step toward consolidation of a diverse literature and may also be instructive in furthering understanding of lapses in self-control in both healthy and clinical populations.

Additionally, we examined the relationship between discounting behavior and the neural representation of reward, finding a positive correlation between the strength of neural response in regions associated with both real and imagined rewards (lateral OFC and vmPFC, respectively) and the ability to delay gratification in a separate ITC task. Again, these findings underscore the utility of an individual differences-based approach in studying the neuroscience of cognitive control, particularly since inter-individual variability in this domain of executive function is not only ubiquitous in healthy decision making[250] but also marks dysfunction in many forms of psychopathology, including substance abuse disorders[94-97]. An individual differences-based approach enhances both experimental and inferential power[250,251], allowing for a shift from traditional methods that emphasize group statistics to techniques that capitalize on individual variability. Future studies should take advantage of the intense variability evident in each individual's brain structure and function, as well as its link to environmental states[252], since these factors may offer particular insight into how individual cognitive control ability varies depending on context and experience. Fully elaborating the relationships between these factors will be instrumental in developing a mechanistic model of cognitive control and identifying potential targets for therapeutic intervention in many psychological disorders.

BIBLIOGRAPHY

1. Cajal, S. R. *Recollections of My Life*. (MIT Press, 1989).
2. Poldrack, R. A. The future of fMRI in cognitive neuroscience. *NeuroImage* **62**, 1216-1220 (2012).
3. Ogawa, S., Lee, T. M., Nayak, A. S. & Glynn, P. Oxygenation-sensitive contrast in magnetic resonance image of rodent brain at high magnetic fields. *Magn Reson Med* **14**, 68-78 (1990).
4. Miller, E. K. The prefrontal cortex and cognitive control. *Nat Rev Neurosci* **1**, 59-65 (2000).
5. Aron, A. R. The neural basis of inhibition in cognitive control. *Neuroscientist* **13**, 214-228, (2007).
6. Pandya, D. N. & Barnes, C. L. in *The frontal lobes revistied*, Architecture and connections of the frontal lobe (ed E. Perecman), 41-72. (IRBN Press, 1987).
7. Goldman-Rakic, P. S. in *Handbook of physiology: The nervous system* Vol. V, Higher functions of the brain (ed F. Plum), 373-417. (American Physiological Society, 1987).
8. Fuster, J. M. *The prefrontal cortex*. (Raven Press, 1989).
9. Barbas, H. & Pandya, D. N. in *Frontal lobe function and dysfunction*, Patterns of connections of the prefrontal cortex in the rhesus monkey associated with cortical architecture (eds H.S. Levin, H.M. Eisenberg, & A.L. Benton), 35-58. (Oxford University Press, 1991).
10. Miller, E. K. & Cohen, J. D. An integrative theory of prefrontal cortex function. *Annu Rev Neurosci* **24**, 167-202 (2001).
11. Ridderinkhof, K. R., van den Wildenberg, W. P., Segalowitz, S. J. & Carter, C. S. Neurocognitive mechanisms of cognitive control: the role of prefrontal cortex in action selection, response inhibition, performance monitoring, and reward-based learning. *Brain Cogn* **56**, 129-140 (2004).
12. Aron, A. R., Fletcher, P. C., Bullmore, E. T., Sahakian, B. J. & Robbins, T. W. Stop-signal inhibition disrupted by damage to right inferior frontal gyrus in humans. *Nat Neurosci* **6**, 115-116 (2003).
13. Aron, A. R., Robbins, T. W. & Poldrack, R. A. Inhibition and the right inferior frontal cortex. *Trends Cogn Sci* **8**, 170-177 (2004).
14. Mostofsky, S. H. & Simmonds, D. J. Response inhibition and response selection: two sides of the same coin. *J Cogn Neurosci* **20**, 751-761 (2008).
15. Simmonds, D. J., Pekar, J. J. & Mostofsky, S. H. Meta-analysis of Go/No-go tasks demonstrating that fMRI activation associated with response inhibition is task-dependent. *Neuropsychologia* **46**, 224-232 (2008).
16. Bunge, S., Burrows, B. & Wagner, A. Prefrontal and hippocampal contributions to visual associative recognition: interactions between cognitive control and episodic retrieval. *Brain Cogn* **56**, 141-152 (2004).
17. Passingham, R. E., Toni, I. & Rushworth, M. F. Specialisation within the prefrontal cortex: the ventral prefrontal cortex and associative learning. *Exp Brain Res* **133**, 103-113 (2000).

18. Rowe, J. B., Toni, I., Josephs, O., Frackowiak, R. S. & Passingham, R. E. The prefrontal cortex: response selection or maintenance within working memory? *Science* **288**, 1656-1660 (2000).
19. Rowe, J. B. & Passingham, R. E. Working memory for location and time: activity in prefrontal area 46 relates to selection rather than maintenance in memory. *NeuroImage* **14**, 77-86 (2001).
20. Bunge, S. A., Hazeltine, E., Scanlon, M. D., Rosen, A. C. & Gabrieli, J. Dissociable contributions of prefrontal and parietal cortices to response selection. *NeuroImage* **17**, 1562-1571 (2002).
21. Garavan, H., Ross, T. J. & Stein, E. A. Right hemispheric dominance of inhibitory control: an event-related functional MRI study. *Proc Natl Acad Sci USA* **96**, 8301-8306 (1999).
22. Rubia, K. *et al.* Mapping motor inhibition: conjunctive brain activations across different versions of go/no-go and stop tasks. *NeuroImage* **13**, 250-261 (2001).
23. Zheng, D., Oka, T., Bokura, H. & Yamaguchi, S. The key locus of common response inhibition network for no-go and stop signals. *J Cogn Neurosci* **20**, 1434-1442 (2008).
24. Grabenhorst, F. & Rolls, E. T. Value, pleasure and choice in the ventral prefrontal cortex. *Trends Cogn Sci* **15**, 56-67 (2011).
25. Rolls, E. T. The orbitofrontal cortex and reward. *Cereb Cortex* **10**, 284-294 (2000).
26. Rolls, E. T. & Grabenhorst, F. The orbitofrontal cortex and beyond: from affect to decision-making. *Prog Neurobiol* **86**, 216-244 (2008).
27. Bechara, A., Tranel, D. & Damasio, H. Characterization of the decision-making deficit of patients with ventromedial prefrontal cortex lesions. *Brain* **123 (Pt 11)**, 2189-2202 (2000).
28. Chambers, R. A., Bickel, W. K. & Potenza, M. N. A scale-free systems theory of motivation and addiction. *Neurosci Biobehav Rev* **31**, 1017-1045 (2007).
29. Donders, F. C. On the speed of mental processes. *Acta psychologica* **30**, 412-431 (1969).
30. Logan, G. D. & Cowan, W. B. On the ability to inhibit thought and action: A theory of an act of control. *Psychol Rev* **91**, 295 (1984).
31. Verbruggen, F. & Logan, G. D. Models of response inhibition in the stop-signal and stop-change paradigms. *Neurosci Biobehav Rev* **33**, 647-661 (2009).
32. Kim, S. & Lee, D. Prefrontal cortex and impulsive decision making. *Biol Psychiatry* **69**, 1140-1146 (2011).
33. Sebastian, A. *et al.* Disentangling common and specific neural subprocesses of response inhibition. *NeuroImage* **64**, 601-615 (2013).
34. Albin, R. L., Young, A. B. & Penney, J. B. The functional anatomy of basal ganglia disorders. *Trends Neurosci* **12**, 366-375 (1989).
35. DeLong, M. R. Primate models of movement disorders of basal ganglia origin. *Trends Neurosci* **13**, 281-285 (1990).
36. Nambu, A., Tokuno, H. & Takada, M. Functional significance of the cortico–subthalamo–pallidal 'hyperdirect'pathway. *Neurosci Res* **43**, 111-117 (2002).
37. Frank, M. J. Dynamic dopamine modulation in the basal ganglia: a neurocomputational account of cognitive deficits in medicated and nonmedicated Parkinsonism. *J Cogn Neurosci* **17**, 51-72 (2005).

38. Mink, J. W. The basal ganglia: focused selection and inhibition of competing motor programs. *Prog Neurobiol* **50**, 381-425 (1996).
39. Gerfen, C. R. Molecular effects of dopamine on striatal-projection pathways. *Trends Neurosci* **23**, S64-S70 (2000).
40. Frank, M. J. & Fossella, J. A. Neurogenetics and pharmacology of learning, motivation, and cognition. *Neuropsychopharmacology* **36**, 133-152 (2010).
41. Hikida, T., Kimura, K., Wada, N., Funabiki, K. & Nakanishi, S. Distinct roles of synaptic transmission in direct and indirect striatal pathways to reward and aversive behavior. *Neuron* **66**, 896-907 (2010).
42. Kravitz, A. V. *et al.* Regulation of parkinsonian motor behaviours by optogenetic control of basal ganglia circuitry. *Nature* **466**, 622-626 (2010).
43. Maia, T. V. & Frank, M. J. From reinforcement learning models to psychiatric and neurological disorders. *Nat Neurosci* **14**, 154-162 (2011).
44. Ainslie, G. Specious reward: a behavioral theory of impulsiveness and impulse control. *Psychol Bull* **82**, 463-496 (1975).
45. Green, L., Fisher, E., Perlow, S. & Sherman, L. Preference reversal and self control: Choice as a function of reward amount and delay. *Behav Anal Lett* **12** (1981).
46. Hoch, S. J. & Loewenstein, G. F. Time-inconsistent preferences and consumer self-control. *J Consum Res*, 492-507 (1991).
47. Kirby, K. N. & Herrnstein, R. J. Preference reversals due to myopic discounting of delayed reward. *Psych Sci* **6**, 83-89 (1995).
48. Mischel, W. Processes in delay of gratification. *Adv Exp Soc Psychol* **7**, 249-292 (1974).
49. Mischel, W., Shoda, Y. & Rodriguez, M. I. Delay of gratification in children. *Science* **244**, 933-938 (1989).
50. Rachlin, H. Self-control: Beyond commitment. *Behav Brain Sci* **18**, 109-121 (1995).
51. Rachlin, H. & Green, L. Commitment, choice and self-control. *J Exp Anal Behav* **17**, 15-22 (1972).
52. Schelling, T. C. Egonomics, or the art of self-management. *Am Econ Rev* **68**, 290-294 (1978).
53. Thaler, R. H. & Shefrin, H. M. An economic theory of self-control. *J Polit Econ*, 392-406 (1981).
54. Berns, G. S., Laibson, D. I. & Loewenstein, G. Intertemporal choice--toward an integrative framework. *Trends Cogn Sci* **11**, 482-488 (2007).
55. Ersner-Hershfield, H., Garton, M. T., Ballard, K., Samanez-Larkin, G. R. & Knutson, B. Don't stop thinking about tomorrow: Individual differences in future self-continuity account for saving. *Judgm Decis Mak* **4**, 280-286 (2009).
56. Hardisty, D. J. & Weber, E. U. Discounting future green: money versus the environment. *J Exp Psychol Gen* **138**, 329 (2009).
57. Keough, K. A., Zimbardo, P. G. & Boyd, J. N. Who's smoking, drinking, and using drugs? Time perspective as a predictor of substance use. *Basic Appl Soc Psych* **21**, 149-164 (1999).
58. Frederick, S., Loewenstein, G. & O'Donoghue, T. Time Discounting and Time Preference: A Critical Review. *J Econ Lit* **40**, 351-401 (2002).

59. Kirby, K. N. & Maraković, N. N. Modeling myopic decisions: Evidence for hyperbolic delay-discounting within subjects and amounts. *Organ Behav Hum Dec* **64**, 21-30 (1995).
60. Green, L., Myerson, J., Holt, D. D., Slevin, J. R. & Estle, S. J. Discounting of delayed food rewards in pigeons and rats: is there a magnitude effect? *J Exp Anal Behav* **81**, 39-50 (2004).
61. Green, L., Myerson, J., Shah, A. K., Estle, S. J. & Holt, D. D. Do adjusting-amount and adjusting-delay procedures produce equivalent estimates of subjective value in pigeons? *J Exp Anal Behav* **87**, 337-347 (2007).
62. Mazur, J. E. Tradeoffs among delay, rate, and amount of reinforcement. *Behav Proceesses* **49**, 1-10 (2000).
63. Richards, J. B., Mitchell, S. H., Wit, H. & Seiden, L. S. Determination of discount functions in rats with an adjusting-amount procedure. *J Exp Anal Behav* **67**, 353-366 (1997).
64. Hayden, B. Y. & Platt, M. L. Temporal discounting predicts risk sensitivity in rhesus macaques. *Curr Biol* **17**, 49-53 (2007).
65. Hwang, J., Kim, S. & Lee, D. Temporal discounting and inter-temporal choice in rhesus monkeys. *Front Behav Neurosci* **3** (2009).
66. Kim, S., Hwang, J. & Lee, D. Prefrontal coding of temporally discounted values during intertemporal choice. *Neuron* **59**, 161-172 (2008).
67. Johnson, M. W. & Bickel, W. K. Within-subject comparison of real and hypothetical money rewards in delay discounting. *J Exp Anal Behav* **77**, 129-146 (2002).
68. Madden, G. J., Begotka, A. M., Raiff, B. R. & Kastern, L. L. Delay discounting of real and hypothetical rewards. *Exp Clin Psychopharmacol* **11**, 139-145 (2003).
69. Takahashi, T., Oono, H. & Radford, M. H. Psychophysics of time perception and intertemporal choice models. *Physica A: Statistical Mechanics and its Applications* **387**, 2066-2074 (2008).
70. Carter, R. M., Meyer, J. R. & Huettel, S. A. Functional neuroimaging of intertemporal choice models: A review. *Journal of Neuroscience, Psychology, and Economics* **3**, 27-45 (2010).
71. Samuelson, P. A. A note on measurement of utility. *Rev Econ Stud* **4**, 155-161 (1937).
72. Ainslie, G. Picoeconomics: The Strategic Interaction of Successive Motivational States Within the Person (Studies in Rationality and Social Change). *Cambridge, England and New York* (1992).
73. Myerson, J. & Green, L. Discounting of delayed rewards: Models of individual choice. *J Exp Anal Behav* **64**, 263-276 (1995).
74. Kable, J. W. & Glimcher, P. W. The neural correlates of subjective value during intertemporal choice. *Nat Neurosci* **10**, 1625-1633 (2007).
75. Hare, T. A., O'Doherty, J. P., Camerer, C. F., Schultz, W. & Rangel, A. Dissociating the role of the orbitofrontal cortex and the striatum in the computation of goal values and prediction errors. *J Neurosci* **28**, 5623-5630 (2008).
76. Ballard, K. & Knutson, B. Dissociable neural representations of future reward magnitude and delay during temporal discounting. *NeuroImage* **45**, 143-150 (2009).

77. Peters, J. & Büchel, C. Episodic future thinking reduces reward delay discounting through an enhancement of prefrontal-mediotemporal interactions. *Neuron* **66**, 138-148 (2010).
78. Tanaka, S. C. *et al.* Prediction of immediate and future rewards differentially recruits cortico-basal ganglia loops. *Nat Neurosci* **7**, 887-893 (2004).
79. McClure, S. M., Laibson, D. I., Loewenstein, G. & Cohen, J. D. Separate neural systems value immediate and delayed monetary rewards. *Science* **306**, 503-507 (2004).
80. McClure, S. M., Ericson, K. M., Laibson, D. I., Loewenstein, G. & Cohen, J. D. Time discounting for primary rewards. *J Neurosci* **27**, 5796-5804 (2007).
81. Gregorios-Pippas, L., Tobler, P. N. & Schultz, W. Short-term temporal discounting of reward value in human ventral striatum. *J Neurophysiol* **101**, 1507-1523 (2009).
82. Figner, B. *et al.* Lateral prefrontal cortex and self-control in intertemporal choice. *Nat Neurosci* **13**, 538-539 (2010).
83. Roesch, M. R. & Olson, C. R. Neuronal activity dependent on anticipated and elapsed delay in macaque prefrontal cortex, frontal and supplementary eye fields, and premotor cortex. *J Neurophysiol* **94**, 1469-1497 (2005).
84. Tsujimoto, S. & Sawaguchi, T. Neuronal activity representing temporal prediction of reward in the primate prefrontal cortex. *J Neurophysiol* **93**, 3687-3692 (2005).
85. Botvinick, M. M. Hierarchical models of behavior and prefrontal function. *Trends Cogn Sci* **12**, 201-208 (2008).
86. Fuster, J. M. Prefrontal cortex and the bridging of temporal gaps in the perception-action cycle. *Ann N Y Acad Sci* **608**, 318-329; discussion 330-316 (1990).
87. Fuster, J. M. Upper processing stages of the perception-action cycle. *Trends Cogn Sci* **8**, 143-145 (2004).
88. Hare, T. A., Camerer, C. F. & Rangel, A. Self-control in decision-making involves modulation of the vmPFC valuation system. *Science* **324**, 646-648 (2009).
89. Hare, T. A., Malmaud, J. & Rangel, A. Focusing Attention on the Health Aspects of Foods Changes Value Signals in vmPFC and Improves Dietary Choice. *J Neurosci* **31**, 11077-11087 (2011).
90. Green, L. & Myerson, J. A discounting framework for choice with delayed and probabilistic rewards. *Psychol Bull* **130**, 769-792 (2004).
91. Evenden, J. Impulsivity: a discussion of clinical and experimental findings. *J Psychopharmacol* **13**, 180-192 (1999).
92. Monterosso, J. & Ainslie, G. Beyond discounting: possible experimental models of impulse control. *Psychopharmacology* **146**, 339-347 (1999).
93. Richards, J. B., Zhang, L., Mitchell, S. H. & Wit, H. Delay or probability discounting in a model of impulsive behavior: effect of alcohol. *J Exp Anal Behav* **71**, 121-143 (1999).
94. Bickel, W. K. *et al.* Behavioral and neuroeconomics of drug addiction: competing neural systems and temporal discounting processes. *Drug Alcohol Depend* **90**, S85-S91 (2007).
95. Dalley, J. W., Everitt, B. J. & Robbins, T. W. Impulsivity, compulsivity, and top-down cognitive control. *Neuron* **69**, 680-694 (2011).
96. MacKillop, J. *et al.* Delayed reward discounting and addictive behavior: a meta-analysis. *Psychopharmacology* **216**, 305-321 (2011).

97. Peters, J. & Büchel, C. The neural mechanisms of inter-temporal decision-making: understanding variability. *Trends Cogn Sci* **15**, 227-239 (2011).
98. Mitchell, D. G. V. *et al.* Adapting to Dynamic Stimulus-Response Values: Differential Contributions of Inferior Frontal, Dorsomedial, and Dorsolateral Regions of Prefrontal Cortex to Decision Making. *J Neurosci* **29**, 10827 (2009).
99. Pronin, E. & Ross, L. Temporal differences in trait self-ascription: when the self is seen as an other. *J Pers Soc Psychol* **90**, 197 (2006).
100. Wakslak, C. J., Nussbaum, S., Liberman, N. & Trope, Y. Representations of the self in the near and distant future. *J Pers Soc Psychol* **95**, 757-773 (2008).
101. Suddendorf, T. & Corballis, M. C. The evolution of foresight: What is mental time travel, and is it unique to humans? *Behav Brain Sci* **30**, 299-313 (2007).
102. Boyer, P. Evolutionary economics of mental time travel? *Trends Cogn Sci* **12**, 219-224 (2008).
103. Bartels, D. M. & Rips, L. J. Psychological connectedness and intertemporal choice. *J Exp Psychol Gen* **139**, 49-69 (2010).
104. Hershfield, H. E. Future self-continuity: how conceptions of the future self transform intertemporal choice. *Ann N Y Acad Sci* **1235**, 30-43 (2011).
105. van Gelder, J. L., Hershfield, H. E. & Nordgren, L. F. Vividness of the future self predicts delinquency. *Psychol Sci* **24**, 974-980 (2013).
106. Benoit, R. G., Gilbert, S. J. & Burgess, P. W. A neural mechanism mediating the impact of episodic prospection on farsighted decisions. *J Neurosci* **31**, 6771-6779 (2011).
107. D'Argembeau, A., Xue, G., Lu, Z.-L., van der Linden, M. & Bechara, A. Neural correlates of envisioning emotional events in the near and far future. *NeuroImage* **40**, 398-407 (2008).
108. Munakata, Y. *et al.* A unified framework for inhibitory control. *Trends Cogn Sci* **15**, 453-459 (2011).
109. Steinhauser, M., Hubner, R. & Druey, M. Adaptive control of response preparedness in task switching. *Neuropsychologia* **47**, 1826-1835 (2009).
110. Logan, G. D., Cowan, W. B. & Davis, K. A. On the ability to inhibit simple and choice reaction time responses: a model and a method. *J Exp Psychol Hum Percept Perform* **10**, 276-291 (1984).
111. Verbruggen, F. & Logan, G. D. Response inhibition in the stop-signal paradigm. *Trends Cogn Sci* **12**, 418-424 (2008).
112. Verbruggen, F. & Logan, G. D. After-effects of goal shifting and response inhibition: A comparison of the stop-change and dual-task paradigms. *Q J Exp Psychol* **61**, 1151-1159 (2008).
113. Swick, D., Ashley, V. & Turken, U. Are the neural correlates of stopping and not going identical? Quantitative meta-analysis of two response inhibition tasks. *NeuroImage* **56**, 1655-1665 (2011).
114. Chikazoe, J. *et al.* Functional dissociation in right inferior frontal cortex during performance of go/no-go task. *Cereb Cortex* **19**, 146-152 (2009).
115. Durston, S. *et al.* Parametric manipulation of conflict and response competition using rapid mixed-trial event-related fMRI. *NeuroImage* **20**, 2135-2141 (2003).

116. Hester, R. L. *et al.* Predicting Success: Patterns of Cortical Activation and Deactivation Prior to Response Inhibition. *J Cogn Neurosci* **16**, 776-785 (2004).
117. Konishi, S. *et al.* Common inhibitory mechanism in human inferior prefrontal cortex revealed by event-related functional MRI. *Brain* **122 (Pt 5)**, 981-991 (1999).
118. Leung, H.-C. & Cai, W. Common and differential ventrolateral prefrontal activity during inhibition of hand and eye movements. *J Neurosci* **27**, 9893-9900 (2007).
119. Li, C.-S. R., Huang, C., Constable, R. T. & Sinha, R. Imaging response inhibition in a stop-signal task: neural correlates independent of signal monitoring and post-response processing. *J Neurosci* **26**, 186-192 (2006).
120. Menon, V., Adleman, N. E., White, C. D., Glover, G. H. & Reiss, A. L. Error-related brain activation during a Go/NoGo response inhibition task. *Hum Brain Mapp* **12**, 131-143 (2001).
121. Rubia, K., Smith, A. B., Brammer, M. J. & Taylor, E. Right inferior prefrontal cortex mediates response inhibition while mesial prefrontal cortex is responsible for error detection. *NeuroImage* **20**, 351-358 (2003).
122. van Gaal, S., Ridderinkhof, K. R., Scholte, H. S. & Lamme, V. A. F. Unconscious activation of the prefrontal no-go network. *J Neurosci* **30**, 4143-4150 (2010).
123. Allport, A., Styles, E. A. & Hsieh, S. in *Attention and performance 15: Conscious and nonconscious information processing* (eds C. Umilta & M. Moscovitch) 421-452 (MIT Press, 1994).
124. Rogers, R. D. & Monsell, S. Costs of a predicatble switch between simple congitive tasks. *J Exp Psychol Gen* **124**, 207-231 (1995).
125. Kenner, N. M. *et al.* Inhibitory motor control in response stopping and response switching. *J Neurosci* **30**, 8512-8518 (2010).
126. Rogers, R. D., Andrews, T. C., Grasby, P. M., Brooks, D. J. & Robbins, T. W. Contrasting Cortical and Subcortical Activations Produced by Attentional-Set Shifting and Reversal Learning in Humans. *J Cogn Neurosci* **12**, 142-162, (2000).
127. Sohn, M. H., Ursu, S., Anderson, J. R., Stenger, V. A. & Carter, C. S. The role of prefrontal cortex and posterior parietal cortex in task switching. *Proc Natl Acad Sci U S A* **97**, 13448-13453 (2000).
128. Cools, R., Clark, L., Owen, A. M. & Robbins, T. W. Defining the neural mechanisms of probabilistic reversal learning using event-related functional magnetic resonance imaging. *J Neurosci* **22**, 4563-4567 (2002).
129. Greening, S. G., Finger, E. C. & Mitchell, D. G. V. Parsing decision making processes in prefrontal cortex: response inhibition, overcoming learned avoidance, and reversal learning. *NeuroImage* **54**, 1432-1441 (2011).
130. Chikazoe, J. *et al.* Preparation to inhibit a response complements response inhibition during performance of a stop-signal task. *J Neurosci* **29**, 15870-15877 (2009).
131. Durston, S., Thomas, K. M., Worden, M. S., Yang, Y. & Casey, B. J. The effect of preceding context on inhibition: an event-related fMRI study. *NeuroImage* **16**, 449-453 (2002).

132. Li, C. S. *et al.* Error-specific medial cortical and subcortical activity during the stop signal task: a functional magnetic resonance imaging study. *Neuroscience* **155**, 1142-1151 (2008).
133. Liddle, P. F., Kiehl, K. A. & Smith, A. M. Event-related fMRI study of response inhibition. *Hum Brain Mapp* **12**, 100-109 (2001).
134. Liston, C., Matalon, S., Hare, T. A., Davidson, M. C. & Casey, B. J. Anterior cingulate and posterior parietal cortices are sensitive to dissociable forms of conflict in a task-switching paradigm. *Neuron* **50**, 643-653 (2006).
135. Ghahremani, D. G., Monterosso, J., Jentsch, J. D., Bilder, R. M. & Poldrack, R. A. Neural components underlying behavioral flexibility in human reversal learning. *Cereb Cortex* **20**, 1843-1852 (2010).
136. O'Doherty, J., Kringelbach, M. L., Rolls, E. T., Hornak, J. & Andrews, C. Abstract reward and punishment representations in the human orbitofrontal cortex. *Nat Neurosci* **4**, 95-102 (2001).
137. Duann, J. R., Ide, J. S., Luo, X. & Li, C. S. Functional connectivity delineates distinct roles of the inferior frontal cortex and presupplementary motor area in stop signal inhibition. *J Neurosci* **29**, 10171-10179 (2009).
138. Zandbelt, B. B. & Vink, M. On the role of the striatum in response inhibition. *PloS one* **5**, e13848 (2010).
139. Crone, E. A., Wendelken, C., Donohue, S. E. & Bunge, S. A. Neural evidence for dissociable components of task-switching. *Cereb Cortex* **16**, 475-486 (2006).
140. Gläscher, J., Hampton, A. N. & O'Doherty, J. P. Determining a role for ventromedial prefrontal cortex in encoding action-based value signals during reward-related decision making. *Cereb Cortex* **19**, 483-495 (2009).
141. Garavan, H., Ross, T. J., Murphy, K., Roche, R. A. & Stein, E. A. Dissociable executive functions in the dynamic control of behavior: inhibition, error detection, and correction. *NeuroImage* **17**, 1820-1829 (2002).
142. Kelly, A. M. C. *et al.* Prefrontal-subcortical dissociations underlying inhibitory control revealed by event-related fMRI. *Eur J Neurosci* **19**, 3105-3112 (2004).
143. Hampton, A. N. & O'Doherty, J. P. Decoding the neural substrates of reward-related decision making with functional MRI. *Proc Natl Acad Sci U S A* **104**, 1377-1382 (2007).
144. Padmala, S. & Pessoa, L. Interactions between cognition and motivation during response inhibition. *Neuropsychologia* **48**, 558-565 (2010).
145. Aron, A. R. & Poldrack, R. A. Cortical and subcortical contributions to Stop signal response inhibition: role of the subthalamic nucleus. *J Neurosci* **26**, 2424-2433 (2006).
146. Li, C. S., Yan, P., Sinha, R. & Lee, T. W. Subcortical processes of motor response inhibition during a stop signal task. *NeuroImage* **41**, 1352-1363 (2008).
147. Corbetta, M. & Shulman, G. L. Control of goal-directed and stimulus-driven attention in the brain. *Nat Rev Neurosci* **3**, 215-229 (2002).
148. Hampshire, A., Chamberlain, S. R., Monti, M. M., Duncan, J. S. & Owen, A. M. The role of the right inferior frontal gyrus: inhibition and attentional control. *NeuroImage* **50**, 1313-1319 (2010).

149. Hampshire, A., Thompson, R., Duncan, J. S. & Owen, A. M. Selective tuning of the right inferior frontal gyrus during target detection. *Cogn Affect Behav Neurosci* **9**, 103-112 (2009).
150. Wang, L. *et al.* Effective connectivity of the fronto-parietal network during attentional control. *J Cogn Neurosci* **22**, 543-553 (2010).
151. Lovstad, M. *et al.* Contribution of subregions of human frontal cortex to novelty processing. *J Cogn Neurosci* **24**, 378-395 (2012).
152. Rushworth, M. F. S., Walton, M. E., Kennerley, S. W. & Bannerman, D. M. Action sets and decisions in the medial frontal cortex. *Trends Cogn Sci* **8**, 410-417 (2004).
153. Wittmann, B. C., Daw, N. D., Seymour, B. & Dolan, R. J. Striatal activity underlies novelty-based choice in humans. *Neuron* **58**, 967-973 (2008).
154. Zink, C. F., Pagnoni, G., Martin-Skurski, M. E., Chappelow, J. C. & Berns, G. S. Human striatal responses to monetary reward depend on saliency. *Neuron* **42**, 509-517 (2004).
155. Chiu, Y. C., Aron, A. R. & Verbruggen, F. Response suppression by automatic retrieval of stimulus-stop association: evidence from transcranial magnetic stimulation. *J Cogn Neurosci* **24**, 1908-1918 (2012).
156. Lenartowicz, A., Verbruggen, F., Logan, G. D. & Poldrack, R. A. Inhibition-related activation in the right inferior frontal gyrus in the absence of inhibitory cues. *J Cogn Neurosci* **23**, 3388-3399 (2011).
157. Hikosaka, O. & Isoda, M. Switching from automatic to controlled behavior: cortico-basal ganglia mechanisms. *Trends Cogn Sci* **14**, 154-161 (2010).
158. Waldschmidt, J. G. & Ashby, F. G. Cortical and striatal contributions to automaticity in information-integration categorization. *NeuroImage* **56**, 1791-1802 (2011).
159. Deichmann, R., Gottfried, J. A., Hutton, C. & Turner, R. Optimized EPI for fMRI studies of the orbitofrontal cortex. *NeuroImage* **19**, 430-441 (2003).
160. Maldjian, J. A., Laurienti, P. J., Kraft, R. A. & Burdette, J. H. An automated method for neuroanatomic and cytoarchitectonic atlas-based interrogation of fMRI data sets. *NeuroImage* **19**, 1233-1239 (2003).
161. Lancaster, J. L. *et al.* Automated Talairach atlas labels for functional brain mapping. *Hum Brain Mapp* **10**, 120-131 (2000).
162. Poldrack, R. A., Prabhakaran, V., Seger, C. A. & Gabrieli, J. D. Striatal activation during acquisition of a cognitive skill. *Neuropsychology* **13**, 564-574 (1999).
163. Doyon, J. & Ungerleider, L. G. in *Neuropsychology of Memory*, Funtional anatomy of motor skill learning (eds L.R. Squire & D.L. Schacter), 225-238. (The Guilford Press, 2002).
164. Hardwick, R. M., Rottschy, C., Miall, R. C. & Eickhoff, S. B. A quantitative meta-analysis and review of motor learning in the human brain. *NeuroImage* **67**, 283-297 (2013).
165. Ashby, F. G., Turner, B. O. & Horvitz, J. C. Cortical and basal ganglia contributions to habit learning and automaticity. *Trends Cogn Sci* **14**, 208-215 (2010).
166. Poldrack, R. A. *et al.* The neural correlates of motor skill automaticity. *J Neurosci* **25**, 5356-5364 (2005).

167. Craig, A. D. How do you feel? Interoception: the sense of the physiological condition of the body. *Nat Rev Neurosci* **3**, 655-666 (2002).
168. Craig, A. D. B. How do you feel--now? The anterior insula and human awareness. *Nat Rev Neurosci* **10**, 59-70 (2009).
169. Andersen, R. A. in *The handbook of physiology, section I: The nervous system* Vol. V: Higher functions of the brain Part 2 (eds F. Plum, V.B. Mountcastle, & S.R. Geiger) 483-518. (American Physiological Society, 1987).
170. Bunge, S. A., Hazeltine, E., Scanlon, M. D., Rosen, A. C. & Gabrieli, J. D. Dissociable contributions of prefrontal and parietal cortices to response selection. *NeuroImage* **17**, 1562-1571 (2002).
171. Dove, A., Pollmann, S., Schubert, T., Wiggins, C. J. & von Cramon, D. Y. Prefrontal cortex activation in task switching: an event-related fMRI study. *Brain Res* **9**, 103-109 (2000).
172. Monchi, O., Petrides, M., Petre, V., Worsley, K. & Dagher, A. Wisconsin Card Sorting revisited: distinct neural circuits participating in different stages of the task identified by event-related functional magnetic resonance imaging. *J Neurosci* **21**, 7733-7741 (2001).
173. Bassett, D. S. *et al.* Cognitive fitness of cost-efficient brain functional networks. *Proc Natl Acad Sci U S A* **106**, 11747-11752 (2009).
174. Neubauer, A. C. & Fink, A. Intelligence and neural efficiency. *Neurosci Biobehav Rev* **33**, 1004-1023 (2009).
175. Rypma, B. *et al.* Neural correlates of cognitive efficiency. *NeuroImage* **33**, 969-979 (2006).
176. Rypma, B. & D'Esposito, M. The roles of prefrontal brain regions in components of working memory: effects of memory load and individual differences. *Proc Natl Acad Sci U S A* **96**, 6558-6563 (1999).
177. Walther, S., Friederich, H. C., Stippich, C., Weisbrod, M. & Kaiser, S. Response inhibition or salience detection in the right ventrolateral prefrontal cortex? *Neuroreport* **22**, 778-782 (2011).
178. Aron, A. R., Monsell, S., Sahakian, B. J. & Robbins, T. W. A componential analysis of task-switching deficits associated with lesions of left and right frontal cortex. *Brain* **127**, 1561-1573 (2004).
179. Demakis, G. J. A meta-analytic review of the sensitivity of the Wisconsin Card Sorting Test to frontal and lateralized frontal brain damage. *Neuropsychology* **17**, 255-264 (2003).
180. Wolfensteller, U. & von Cramon, D. Y. Bending the rules: strategic behavioral differences are reflected in the brain. *J Cogn Neurosci* **22**, 278-291 (2010).
181. Steinhauser, M. & Hubner, R. Response-based strengthening in task shifting: evidence from shift effects produced by errors. *J Exp Psychol Hum Percept Perform* **32**, 517-534 (2006).
182. Guitart-Masip, M. *et al.* Go and no-go learning in reward and punishment: interactions between affect and effect. *NeuroImage* **62**, 154-166 (2012).
183. Ainslie, G. *Breakdown of Will*. (Cambridge University Press, 2001).
184. Rachlin, H. *The science of self-control*. (Harvard University Press, 2000).

185. Volkow, N. D., Wang, G.-J. & Baler, R. D. Reward, dopamine and the control of food intake: implications for obesity. *Trends Cogn Sci* **15**, 37-46 (2011).
186. Rangel, A. & Hare, T. A. Neural computations associated with goal-directed choice. *Curr Opin Neurobiol* **20**, 262-270 (2010).
187. Basten, U., Biele, G., Heekeren, H. R. & Fiebach, C. J. How the brain integrates costs and benefits during decision making. *Proc Natl Acad Sci U S A* **107**, 21767-21772 (2010).
188. Boorman, E. D., Behrens, T. E., Woolrich, M. W. & Rushworth, M. F. How green is the grass on the other side? Frontopolar cortex and the evidence in favor of alternative courses of action. *Neuron* **62**, 733-743 (2009).
189. Clithero, J. A., Smith, D. V., Carter, R. M. & Huettel, S. A. Within- and cross-participant classifiers reveal different neural coding of information. *NeuroImage* **56**, 699-708 (2011).
190. Hare, T. A., Camerer, C. F., Knoepfle, D. T. & Rangel, A. Value computations in ventral medial prefrontal cortex during charitable decision making incorporate input from regions involved in social cognition. *J Neurosci* **30**, 583-590 (2010).
191. Kahnt, T., Heinzle, J., Park, S. Q. & Haynes, J.-D. Decoding different roles for vmPFC and dlPFC in multi-attribute decision making. *NeuroImage*, 1-7 (2010).
192. Lebreton, M., Jorge, S., Michel, V., Thirion, B. & Pessiglione, M. An Automatic Valuation System in the Human Brain: Evidence from Functional Neuroimaging. *Neuron* **64**, 431-439 (2009).
193. Park, S. Q., Kahnt, T., Rieskamp, J. & Heekeren, H. R. Neurobiology of Value Integration: When Value Impacts Valuation. *J Neurosci* **31**, 9307-9314 (2011).
194. Plassmann, H., O'Doherty, J. P. & Rangel, A. Appetitive and aversive goal values are encoded in the medial orbitofrontal cortex at the time of decision making. *J Neurosci* **30**, 10799-10808 (2010).
195. Shenhav, A. & Greene, J. D. Moral judgments recruit domain-general valuation mechanisms to integrate representations of probability and magnitude. *Neuron* **67**, 667-677 (2010).
196. Tom, S. M., Fox, C. R., Trepel, C. & Poldrack, R. A. The neural basis of loss aversion in decision-making under risk. *Science* **315**, 515-518 (2007).
197. Peters, J. & Buchel, C. Neural representations of subjective reward value. *Behav Brain Res* **213**, 135-141 (2010).
198. Gianotti, L. R. R., Figner, B., Ebstein, R. P. & Knoch, D. Why some people discount more than others: baseline activation in the dorsal PFC mediates the link between COMT genotype and impatient choice. *Front Neurosci* **6**, 54 (2012).
199. Li, N. *et al.* Resting-state functional connectivity predicts impulsivity in economic decision-making. *J Neurosci* **33**, 4886-4895 (2013).
200. Friston, K. J., Harrison, L. M. & Penny, W. D. Dynamic causal modelling. *NeuroImage* **19**, 1273-1302 (2003).
201. Peters, J. & Büchel, C. Overlapping and distinct neural systems code for subjective value during intertemporal and risky decision making. *J Neurosci* **29**, 15727-15734 (2009).

202. Tzourio-Mazoyer, N. *et al.* Automated anatomical labeling of activations in SPM using a macroscopic anatomical parcellation of the MNI MRI single-subject brain. *NeuroImage* **15**, 273-289 (2002).
203. Stephan, K. E., Penny, W. D., Daunizeau, J., Moran, R. J. & Friston, K. J. Bayesian model selection for group studies. *NeuroImage* **46**, 1004-1017 (2009).
204. Kasess, C. H. *et al.* Multi-subject analyses with dynamic causal modeling. *NeuroImage* **49**, 3065-3074 (2010).
205. Brodersen, K. H., Ong, C. S., Stephan, K. E. & Buhmann, J. M. in *Procceedings of the 20th International Conference on Pattern Recognition*, 3121-3124 (2010).
206. McKerchar, T. L. *et al.* A comparison of four models of delay discounting in humans. *Behav Processes* **81**, 256-259 (2009).
207. Bartra, O., McGuire, J. T. & Kable, J. W. The valuation system: a coordinate-based meta-analysis of BOLD fMRI experiments examining neural correlates of subjective value. *NeuroImage* **76**, 412-427 (2013).
208. Clithero, J. A. & Rangel, A. Informatic parcellation of the network involved in the computation of subjective value. *Soc Cogn Affect Neurosci* (2013).
209. Hunt, L. T. *et al.* Mechanisms underlying cortical activity during value-guided choice. *Nat Neurosci* **15**, 470-476 (2012).
210. Lim, S.-L., O'Doherty, J. P. & Rangel, A. The Decision Value Computations in the vmPFC and Striatum Use a Relative Value Code That is Guided by Visual Attention. *J Neurosci* **31**, 13214-13223 (2011).
211. Kőszegi, B. & Rabin, M. A Model of Reference-Dependent Preferences. *Q J Econ* **121**, 1133-1165 (2006).
212. Kable, J. W. & Glimcher, P. W. An "as soon as possible" effect in human intertemporal decision making: behavioral evidence and neural mechanisms. *J Neurophysiol* **103**, 2513-2531 (2010).
213. Boettiger, C. A. *et al.* Immediate reward bias in humans: fronto-parietal networks and a role for the catechol-O-methyltransferase 158(Val/Val) genotype. *J Neurosci* **27**, 14383-14391 (2007).
214. Levy, D. J. & Glimcher, P. W. The root of all value: a neural common currency for choice. *Curr Opin Neurobiol* **22**, 1027-1038 (2012).
215. Knutson, B., Adams, C. M., Fong, G. W. & Hommer, D. Anticipation of increasing monetary reward selectively recruits nucleus accumbens. *J Neurosci* **21**, RC159 (2001).
216. McClure, S. M., Berns, G. S. & Montague, P. R. Temporal prediction errors in a passive learning task activate human striatum. *Neuron* **38**, 339-346 (2003).
217. O'Doherty, J. P., Buchanan, T. W., Seymour, B. & Dolan, R. J. Predictive neural coding of reward preference involves dissociable responses in human ventral midbrain and ventral striatum. *Neuron* **49**, 157-166 (2006).
218. Schmidt, L., Lebreton, M., Cléry-Melin, M.-L., Daunizeau, J. & Pessiglione, M. Neural Mechanisms Underlying Motivation of Mental Versus Physical Effort. *PLoS Biol* **10**, e1001266 (2012).

219. Wager, T. D., Davidson, M. L., Hughes, B. L., Lindquist, M. A. & Ochsner, K. N. Prefrontal-subcortical pathways mediating successful emotion regulation. *Neuron* **59**, 1037-1050 (2008).
220. Litt, A., Plassmann, H., Shiv, B. & Rangel, A. Dissociating valuation and saliency signals during decision-making. *Cereb Cortex* **21**, 95-102 (2011).
221. Balleine, B. W. D., Nathaniel W.; O'Doherty, John. in *Neuroeconomics: Decision Making and the Brain*, Multiple systems for value learning (eds E. Fehr, P.W. Glimcher, C.F. Camerer, & R.A. Poldrack), 393-410. (Elsevier, 2008).
222. Dayan, P., Niv, Y., Seymour, B. & Daw, N. D. The misbehavior of value and the discipline of the will. *Neural Netw* **19**, 1153-1160 (2006).
223. Rangel, A., Camerer, C. F. & Montague, P. R. A framework for studying the neurobiology of value-based decision making. *Nat Rev Neurosci* **9**, 545-556 (2008).
224. Congdon, E. *et al.* Engagement of large-scale networks is related to individual differences in inhibitory control. *NeuroImage* **53**, 653-663 (2010).
225. Wager, T. D. *et al.* Common and unique components of response inhibition revealed by fMRI. *NeuroImage* **27**, 323-340 (2005).
226. Botvinick, M. M. Conflict monitoring and decision making: reconciling two perspectives on anterior cingulate function. *Cogn Affect Behav Neurosci* **7**, 356-366 (2007).
227. Carter, C. S. *et al.* Anterior cingulate cortex, error detection, and the online monitoring of performance. *Science* **280**, 747-749 (1998).
228. Hare, T. A., Schultz, W., Camerer, C. F., O'Doherty, J. P. & Rangel, A. Transformation of stimulus value signals into motor commands during simple choice. *Proc Natl Acad Sci U S A* **108**, 18120-18125 (2011).
229. Pochon, J.-B., Riis, J., Sanfey, A. G., Nystrom, L. E. & Cohen, J. D. Functional imaging of decision conflict. *J Neurosci* **28**, 3468-3473 (2008).
230. Venkatraman, V., Rosati, A. G., Taren, A. A. & Huettel, S. A. Resolving response, decision, and strategic control: evidence for a functional topography in dorsomedial prefrontal cortex. *J Neurosci* **29**, 13158-13164 (2009).
231. Wunderlich, K., Rangel, A. & O'Doherty, J. P. Neural computations underlying action-based decision making in the human brain. **106**, 17199-17204 (2009).
232. Mischel, W. *et al.* Willpower over the life span: decomposing self-regulation. *Soc Cogn Affect Neurosci* **6**, 252-256 (2011).
233. Bray, S., Shimojo, S. & O'Doherty, J. P. Human medial orbitofrontal cortex is recruited during experience of imagined and real rewards. *J Neurophysiol* **103**, 2506-2512 (2010).
234. O'Doherty, J., Rolls, E. T., Francis, S. T., Bowtell, R. & McGlone, F. Representation of pleasant and aversive taste in the human brain. *J Neurophysiol* **85**, 1315-1321 (2001).
235. Liu, X., Hairston, J., Schrier, M. & Fan, J. Common and distinct networks underlying reward valence and processing stages: a meta-analysis of functional neuroimaging studies. *Neurosci Biobehav Rev* **35**, 1219-1236 (2011).
236. Sescousse, G., Caldú, X., Segura, B. & Dreher, J.-C. Processing of primary and secondary rewards: A quantitative meta-analysis and review of human functional neuroimaging studies. *Neurosci Biobehav Rev* **37**, 681-696 (2013).

237. Pritchard, T. C., Hamilton, R. B., Morse, J. R. & Norgren, R. Projections of thalamic gustatory and lingual areas in the monkey, Macaca fascicularis. *J Comp Neurol* **244**, 213-228 (1986).
238. Scott, T. R. & Plata-Salamán, C. R. Taste in the monkey cortex. *Physiol Behav* **67**, 489-511 (1999).
239. McNorgan, C. A meta-analytic review of multisensory imagery identifies the neural correlates of modality-specific and modality-general imagery. *Front Hum Neurosci* **6**, 285 (2012).
240. O'Doherty, J. P., Deichmann, R., Critchley, H. D. & Dolan, R. J. Neural responses during anticipation of a primary taste reward. *Neuron* **33**, 815-826 (2002).
241. Miyapuram, K. P., Tobler, P. N., Gregorios-Pippas, L. & Schultz, W. BOLD responses in reward regions to hypothetical and imaginary monetary rewards. *NeuroImage* **59**, 1692-1699 (2012).
242. Chib, V. S., Rangel, A., Shimojo, S. & O'Doherty, J. P. Evidence for a common representation of decision values for dissimilar goods in human ventromedial prefrontal cortex. *J Neurosci* **29**, 12315-12320 (2009).
243. McNamee, D., Rangel, A. & O'Doherty, J. P. Category-dependent and category-independent goal-value codes in human ventromedial prefrontal cortex. *Nat Neurosci* **16**, 479-485 (2013).
244. Shenhav, A., Barrett, L. F. & Bar, M. Affective value and associative processing share a cortical substrate. *Cogn Affect Behav Neurosci* (2012).
245. Plassmann, H., O'Doherty, J. P., Shiv, B. & Rangel, A. Marketing actions can modulate neural representations of experienced pleasantness. *Proc Natl Acad Sci U S A* **105**, 1050-1054 (2008).
246. Cooper, N., Kable, J. W., Kim, B. K. & Zauberman, G. Brain Activity in Valuation Regions while Thinking about the Future Predicts Individual Discount Rates. *J Neurosci* **33**, 13150-13156 (2013).
247. Fuster, J. M. *Memory in the Cerebral Cortex: An Empirical Approach to Neural Networks in the Human and Nonhuman Primate*. (MIT Press, 1995).
248. Badre, D. Cognitive control, hierarchy, and the rostro-caudal organization of the frontal lobes. *Trends Cogn Sci* **12**, 193-200 (2008).
249. Bunge, S. A. How we use rules to select actions: a review of evidence from cognitive neuroscience. *Cogn Affect Behav Neurosci* **4**, 564-579 (2004).
250. Braver, T. S., Cole, M. W. & Yarkoni, T. Vive les differences! Individual variation in neural mechanisms of executive control. *Curr Opin Neurobiol* **20**, 242-250 (2010).
251. Yarkoni, T. & Braver, T. S. in *Handbook of Individual Differences in Cognition: Attention, Memory, and Executive Control*, Cognitive neuroscience approaches to individual differences in working memory amd executive control: conceptual and methodological issues (eds A. Gruszka, G. Matthews, & B. Szymura), 87-108 (Springer, 2010).
252. Kanai, R. & Rees, G. The structural basis of inter-individual differences in human behaviour and cognition. *Nat Rev Neurosci* **12**, 231-242 (2011).

Appendix A

RESPONSE INHIBITION TASK INSTRUCTIONS

In this experiment, you will be cued to respond to different fractals. Each fractal cue is associated with a button press response.

The experiment is comprised of four separate sections. You will be allowed to rest between each section.

Press any key to continue to the next slide.

On the next slide, you will see the four fractal cues and their associated responses.

Take as much time as is necessary to familiarize yourself with each cue and its associated response.

Press any key to continue to the next slide.

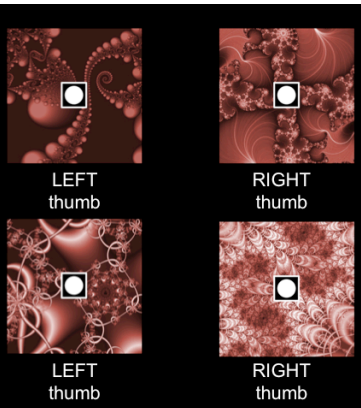

Press any key to continue to the next slide.

Most of the time, the fractal cues will have a circle in the center, as you saw on the previous slide.

Sometimes, however, the fractal will not have a circle in the center; instead, a triangle will appear, as shown below.

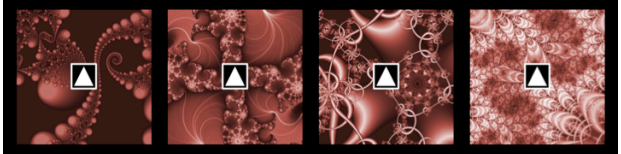

Press any key to continue to the next slide.

Whenever you see a cue with a triangle in the center, you should respond to the cue using the *opposite* hand.

For example, if you normally respond to the cue (i.e., when it has the circle in the center) with your left thumb, you should now respond using your right thumb. Similarly, if you normally respond to the cue using your right thumb, you should now respond using your left thumb.

Press any key to continue to the next slide.

Each fractal cue will appear onscreen for only 600 ms. You should make your response during this time. Responses made after the fractal cue has disappeared from the screen will be recorded as "incorrect."

Therefore, you should respond as quickly and accurately as possible.

Press any key to continue to the next slide.

After the fractal cue has disappeared from the screen, you will receive feedback indicating whether or not you answered correctly on the trial.

If you responded correctly, you will earn one point and the screen will display "**+1**". If you did not respond correctly, you will lose one point and the screen will display "**-1**".

Press any key to continue to the next slide.

At the end of the experiment, your accumulated points over all four blocks will be summed. This total will be multiplied by a conversion factor to determine how much money you earn.

Remember: it is important that you respond as quickly and accurately as possible on each trial, since your performance will affect how much money you earn in the experiment.

Press any key to continue to the next slide.

A fixation cross will appear in the center of the screen after each trial. During this time, you should maintain your gaze on the center of the screen.

Press any key to continue to the next slide.

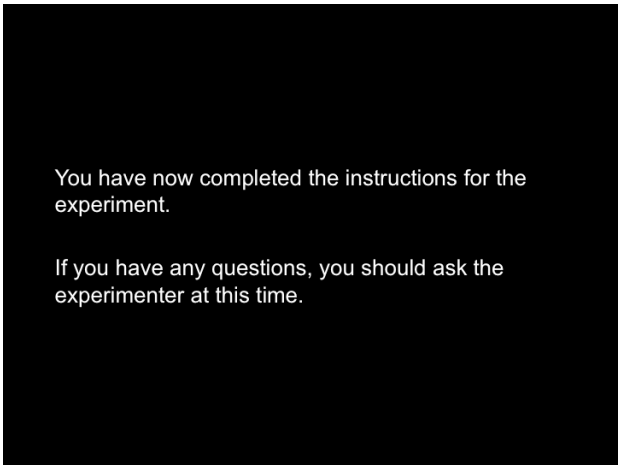
You have now completed the instructions for the experiment.
If you have any questions, you should ask the experimenter at this time.

Appendix B

IMAGINE TASK INSTRUCTIONS

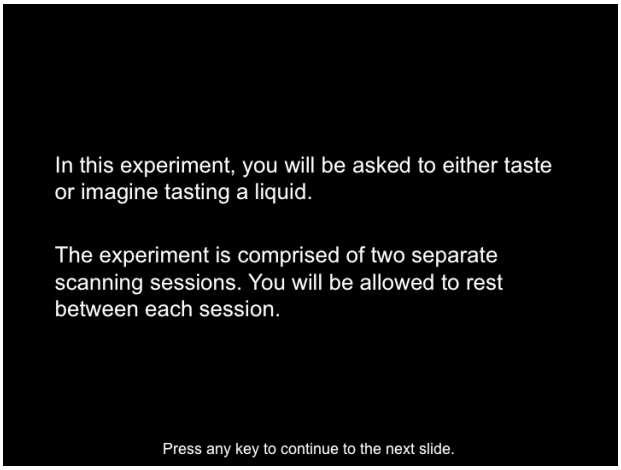

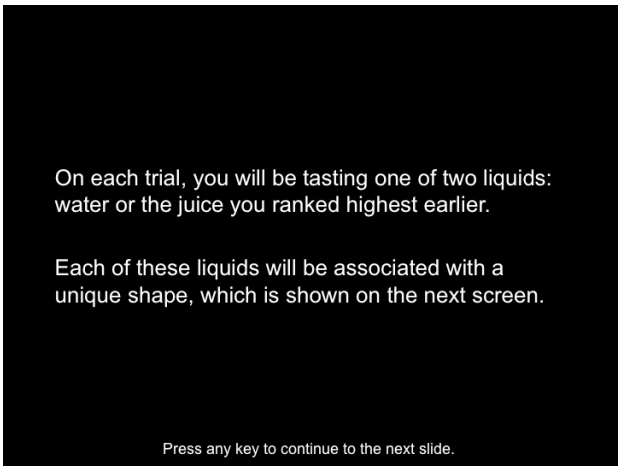

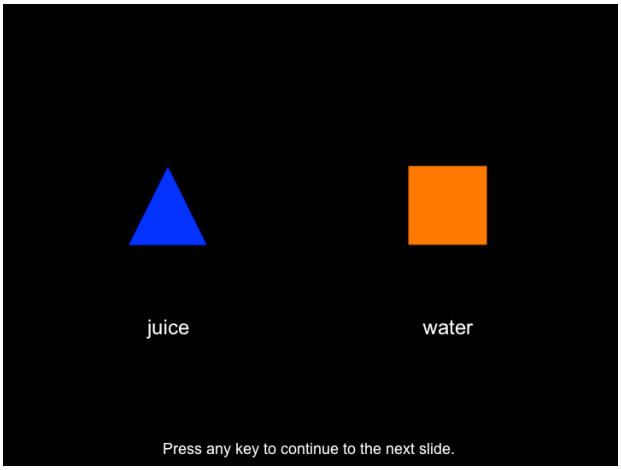

In some trials, you will be instructed to CONSUME the liquid associated with the shape. In these trials, the shape will be surrounded by a rectangle, as shown below:

CONSUME juice

CONSUME water

Press any key to continue to the next slide.

In other trials, you will be instructed to IMAGINE tasting the liquid associated with the shape. In these trials, the shape will be surrounded by a thought bubble, as shown below:

IMAGINE juice

IMAGINE water

Press any key to continue to the next slide.

The appearance of a cue will signal the beginning of a trial.

Whenever you see a cue appear on the screen, you should press either the left or right button. The button you press will depend on the type of cue you see.

Press any key to continue to the next slide.

You should press the
LEFT button for WATER trials
and the
RIGHT button for JUICE trials.

It is important that you make the appropriate response for each cue as soon as you see it appear onscreen.

Press any key to continue to the next slide.

If the trial is a CONSUME trial, the tube will deliver either juice or water to your mouth. The cue will remain onscreen for several seconds, allowing you to fully taste the liquid. During this time you should hold the liquid in your mouth and swish it around, as if you were tasting a drink.

Press any key to continue to the next slide.

After several seconds of tasting, the shape cue will disappear from the screen and the word 'swallow' will appear. This is your cue to swallow the liquid.

You should swallow the liquid normally. This means you should feel liquid moving down your throat.

It is very important that you do not swallow the liquid before you have been instructed to do so.

Press any key to continue to the next slide.

IMPORTANT: Do not suck on the tubing!

Let the liquid squirt into your mouth without sucking. Sucking will create air pockets in the tubing and disrupt future juice delivery.

Press any key to continue to the next slide.

If the trial is an IMAGINE trial, the tube *will not* deliver liquid to your mouth. In these trials, the shape cue will be a signal for you to *imagine* that you are tasting either the juice or water. Like in the CONSUME trials, you should act as if you were tasting a drink by swishing the imaginary liquid in your mouth.

Again, you should "taste" the liquid for the entire time the cue remains onscreen.

Press any key to continue to the next slide.

Just as in the CONSUME trials, the word 'swallow' will appear onscreen after several seconds of "tasting." You should physically swallow the imaginary liquid just as you would a real drink.

Again, it is very important that you do not swallow until you have been instructed to do so.

Press any key to continue to the next slide.

At the end of each trial – whether it is a CONSUME or IMAGINE trial – a fixation cross will appear in the center of the screen. You should maintain your gaze on the center of the screen during this time.

Press any key to continue to the next slide.

The brain signal that we will use to compare the two trial types is extremely sensitive to motion.

Therefore, it is very important that you try and remain as still as possible during the experiment. This means that you should try to keep your head very still while tasting and swallowing.

Moreover, as you will see on the next slide, the less you move, the more likely you are to earn extra money!

Press any key to continue to the next slide.

Your compensation for this task will depend, in part, on your ability to fully imagine the experience of tasting the liquids.

At the end of the experiment, we will compare your brain activation during the IMAGINE trials to the activation during the CONSUME trials. The more similar the brain activations are, the more money you will earn.

Therefore, it is very important that you try and make the experience of imagining tasting the liquid as similar as possible to actually tasting it.

Press any key to continue to the next slide.

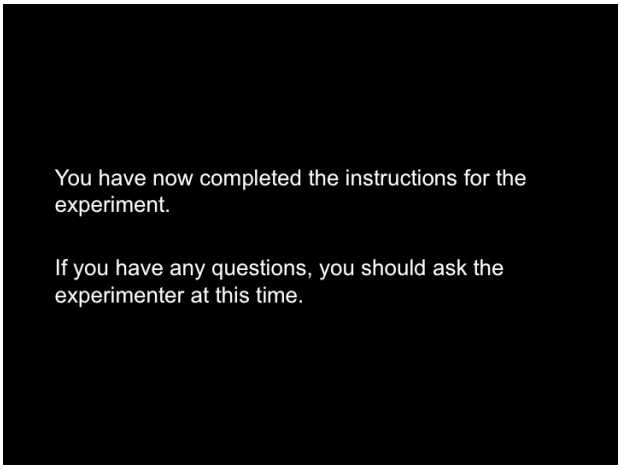
You have now completed the instructions for the experiment.
If you have any questions, you should ask the experimenter at this time.

Appendix C

IMAGINE POST-TASK QUESTIONNAIRE

Subject ID: _____

IMACON Post-Task Questionnaire

1. Overall, how ***successful*** were you at imagining tasting the liquid? Please rate your success on the scale below, where 1 is "not successful at all," 5 is "somewhat successful," and 10 is "extremely successful." Please use the intermediate ratings if you fall between those categories.

not at all				somewhat					extremely
1	2	3	4	5	6	7	8	9	10

2. Was there a difference in your ability to imagine tasting the juice and the water?

YES NO

3. If yes, please indicate your ***success*** (using the same scale as above) for both juice and water:

JUICE:

not at all				somewhat					extremely
1	2	3	4	5	6	7	8	9	10

WATER:

not at all				somewhat					extremely
1	2	3	4	5	6	7	8	9	10

4. If you did succeed at imagining the taste of the liquids, how ***similar*** was your imaginary taste experience to the real experience of tasting the liquids? Please rate the similarity on the scale below, where 1 is "not similar at all," 5 is "somewhat similar," and 10 is "extremely similar." Please use the intermediate ratings if you fall between those categories.

not at all				somewhat					extremely
1	2	3	4	5	6	7	8	9	10

5. Was there a difference in between the juice and the water for how ***similar*** the imaginary experience was to the actual tasting experience?

YES NO

Subject ID: _____

6. If yes, please indicate the ***similarity*** (using the same scale as in question 4) for both juice and water:

   JUICE:

   not at all somewhat extremely

   1 2 3 4 5 6 7 8 9 10

   WATER:

   not at all somewhat extremely

   1 2 3 4 5 6 7 8 9 10

7. Is there anything else you'd like to tell us about your experience?